Development of two-dimensional EUV spectroscopy for study of impurity behavior in ergodic layer of LHD

Erhui WANG

Doctor of Philosophy

Department of Fusion Science

School of Physical Sciences

The Graduate University for Advanced Studies

2013

Abstract

The impurity plays an important role in the fusion research based on magnetically confined toroidal devices from the points of view of the impurity radiation loss at plasma core, fuel dilution due to the impurity contamination and edge plasma cooling by impurity radiation to mitigate the divertor heat flux. The Large Helical Device (LHD) is characterized by the presence of stochastic magnetic field layer called 'ergodic layer' surrounding the core plasma. The ergodic layer therefore consists of open magnetic file lines with fully three-dimensional structure, of which the magnetic field structure is entirely different from the scrape-off layer in plasma edge of tokamaks. The study of impurity behavior in the ergodic layer of LHD is then extremely important for control of the impurity influx, effective utilization of the impurity screening and steady operation of the detached plasma.

In order to study the impurity behavior in the ergodic layer of LHD, the two-dimensional measurement of impurity line emissions is highly requested. For the purpose a space-resolved extreme ultraviolet (EUV) spectrometer has been developed to observe the full vertical profile and two-dimensional distribution of impurity line emissions in LHD. The vertical profile and two-dimensional distribution have been successfully observed with enough spatial resolution for carbon and iron spectra. The two-dimensional edge temperature is measured from impurity line emissions. The vertical profile and the two-dimensional distribution of CIV located in the edge boundary of the ergodic layer are also observed in the vicinity of X-point. These results are compared with three-dimensional edge plasma simulation with EMC3-EIRENE code. The comparison shows a fairly good agreement between the observation and the simulation. It indicates the importance of the parallel transport in the edge boundary of the ergodic layer, in particular, the friction force between bulk and impurity ions and the ion temperature gradient force along magnetic field.

For two-dimensional EUV spectroscopy two stepping motors are newly installed on the space-resolved EUV spectrometer to scan the observation range in horizontal and vertical directions. In the vertical direction, two different vertical observation chords are at least needed to measure the full vertical profile of impurity line emissions because the vertical observation range of the spectrometer only coves half of the plasma length at horizontally elongated plasma cross section. In order to measure the two-dimensional distribution of impurity line emissions, the space-resolved EUV spectrometer is scanned horizontally with a fixed vertical angle during a stable discharge. The scanning speed is usually set to 1-5 mm/s which depend on the length of discharge. The horizontal scanning range at the magnetic axis position is around 800 mm which is limited by a diamond LHD port and a rectangular spectrometer port. The spatial position of observation chord is calibrated by a toroidal slit with rectangular-corrugated edge installed between LHD plasma and space-resolved EUV spectrometer. The working wavelength range is extended from 50-500 Å to 30-650 Å by adding the second CCD stage for enlarging the CCD movement distance. The CCD position is then deviated from an exact focal plane in wavelength ranges of 30-50 Å and 500-650 Å and the spectral resolution is lowered a little in those wavelength ranges. In practical use of the spectrometer, however, any visible problem is not observed through the present study.

Vertical profiles of HeII (303.78 Å, E_i=54 eV) and CIV (312.4 Å, E_i=64 eV) have been measured at different plasma cross sections by scanning the spectrometer angle toroidally to observe the edge impurity distribution at different poloidal positions. The radial location of HeII reflects the penetration of neutral helium and the radial location of CIV expresses the index of plasma edge boundary in the ergodic layer of LHD. The result indicates that the radial location of HeII is positioned at inner side compared to that of CIV, whereas the ionization energy of HeII is smaller than that of CIV. The distance between HeII and CIV radial positions is nearly constant, i.e. 4 mm, which is not a function of the poloidal positions. The experimental result is compared with calculated penetration depth of the neutral helium assuming the room temperature of 300 K. The calculation shows a good agreement with the experimental result. The full vertical profile of HeII is also

measured at horizontally elongated plasma cross section. It is found that the HeII intensity at the bottom of plasma is stronger than that at the top of plasma. This asymmetric intensity profile is also observed in the CV vertical profile, while it is disappeared in the CVI vertical profile.

Electron temperature distribution in the ergodic layer is important information for studying the edge impurity behavior. A line intensity ratio for Li-like ions is used to measure the vertical profile and two-dimensional distribution of electron temperature in the ergodic layer. The Li-like CIV is adopted for the temperature measurement, which is located in the edge boundary of ergodic layer because of its low ionization energy. When two CIV lines of 2p-3d (384 Å) and 2p-3s (420 Å) are selected, those can be simultaneously observed in the same CCD position. Therefore, we can exclude the uncertainty based on the absence of reproducibility between two discharges. The line intensity ratio of 2p-3d/2p-3s is sensitive to the electron temperature in the range of 5-40 eV and entirely insensitive to the electron density in the range of $n_e<10^{14}$ cm^{-3}, which are calculated by CHIANTI and ADAS codes. The edge electron temperature estimated from the CIV intensity ratio ranges in 5-23 eV. Since magnetic field lines near the edge boundary are directly connected to the divertor plates with short magnetic field lines around 10 m, the CIV temperature can be correlated with the temperature on the divertor plates. The electron temperature on divertor plates is measured by Langmuir probe. The measured divertor temperature distributing around 10 eV shows a good consistency with the edge temperature evaluated from the CIV intensity ratio. The electron temperature is also measured from NeVIII intensity ratio of 3p-2s/3s-2p (88 Å/103 Å) for Li-like Ne^{7+} ion, which is located near last closed flux surface (LCFS) in the edge plasma of LHD. The vertical profiles of electron temperature evaluated from ADAS and CHIANTI codes range in 100-130 eV and 120-230 eV, respectively. The electron temperature at LCFS measured from Thomson Scattering is determined to be 120 eV, while the temperature at LCFS is 110 eV for ADAS and 170 eV for CHIANTI. The electron temperature profile is also simulated with three-dimensional edge transport code. The result shows a good agreement with the ADAS result. As a result it is found that the ADAS code is applicable to the edge

temperature measurement. The two-dimensional distribution of electron temperature in the ergodic layer is measured using NeVIII intensity ratio in discharges with electron cyclotron resonance heating (ECH) discharges. The electron temperature at the top edge of plasma shows a higher temperature of 210-220 eV in all toroidal locations, whereas the electron temperature in the vicinity of X-point shows a lower temperature around 150-180 eV.

The CIV vertical profiles near X-point at horizontally elongated plasma cross section are studied with magnetic field structure in the ergodic layer. In low-density range less than $2x10^{13}$ cm^{-3}, the CIV profile near X-points is almost flat. When the density increases, two peaks newly begin to appear near X-points in addition to usual edge peaks, whereas such peaks do not appear in the profile of CVI located near LCFS. Those peaks become very clear at high-density range of $n_e \geq 8x10^{13}$ cm^{-3}. This phenomenon can be also observed at different magnetic axis positions. The vertical profile of CIV is analyzed using three-dimensional edge transport code. In the low-density case, the C^{3+} ions move upstream and widely expand in the ergodic layer due to dominant thermal force, which leads to the flat CIV profile. With increasing the density, the friction force becomes dominant and the impurity ions start to move downstream. The C^{3+} ions stay in the vicinity of the X-point, where magnetic field lines are directly connected to divertor plates. Thus, the two peaks near X-point are clearly formed by increase in the C^{3+} density. The two-dimensional distributions of HeII, CIV and CVI are observed for different plasma axis positions. It is found that the impurity emission becomes considerably strong along the poloidal trajectory of X-points and the poloidal trace is moved from inboard X-point trajectory to outboard X-point trajectory when the plasma axis is changed from 3.60 m to 3.90 m.

Contents

Chapter 1

Introduction

1.1 Nuclear fusion research

Nuclear fusion is the primary energy source maintaining most of stars. In fusion reactions, low-mass nuclei combine or fuse to form more massive nuclei, releasing energy in the form of radiation and in the kinetic energy of the fusion products. When we consider the nuclear fusion as the energy source on earth, the most promising fusion reaction is D-T reaction because of its lower energy threshold and bigger cross-section compared with other fusion reactions [1]. The D-T reaction is expressed by

$$D + T \rightarrow {}^4He + n + 17.6MeV\,, \tag{1.1}$$

where D, T, ^{4}He and n are the deuterium, the tritium, the alpha particle and the neutron. The kinetic energy of 17.6 MeV is divided into 3.5 MeV for the alpha particle and 14.1 MeV for the neutron. In the fusion reactor the alpha particle with energy of 3.5 MeV is utilized for maintaining the fusion reactor through collisions with bulk ions and electrons and the energy is basically gained through the neutron.

In order to realize the controlled fusion reactor, many types of fusion devices for magnetic confinement have been developed in the past several decades, such as tokamak, stellarator, reversed-field pinch and magnetic mirror. The tokamak was invented in the

1950s by Soviet physicists, Igor Tamm and Andrei Sakharov. After confirming a good performance of the tokamak, many tokamaks have been constructed in many countries. At present, ASDEX Upgrade, DIII-D, EAST, JET and KSTAR [1] have been operated in the world, and JT-60SA [2] and ITER [3] are under construction as the next-generation tokamak. In particular, the ITER is the world's largest tokamak aimed at the D-T operation. The ITER project is basically supported by seven member entities, i.e., China, the European Union (EU), India, Japan, Korea, Russia and United States. Compared with the tokamak, the stellarator has a special character of having no plasma current, which can exhibit a good performance in the viewpoint of steady state operation of the fusion reactor. At present, Large Helical Device (LHD) is the largest stellarator having heliotron-type magnetic configuration in which the superconducting magnet is used for all the coil system [4]. A detailed explanation of LHD is made in section of 1.3. Wendelstein 7-X is another large superconducting stellarator device having modular coil system, which has been developed in Germany and will be completed in 2015 [5].

For a D-T plasma, the power balance is given by

$$P_H + \frac{1}{4}\overline{n^2\langle\sigma v\rangle}\xi_a V = \frac{3\overline{nT}}{\tau_E}V \tag{1.2}$$

where P_H is the external heating power, n and T the ion density and temperature, respectively, $<\sigma v>$ the rate coefficient of D-T reaction, ξ_α the α-particle energy released per reaction, τ_E the energy confinement time and V the plasma volume. In this equation, the left second term and the right term indicate the total α-particle heating power and the rate of plasma energy loss, respectively.

The requirement for the plasma burn to be self-sustaining is then written by

$$n\tau_E > \frac{12}{\langle\sigma v\rangle}\frac{T}{\xi_a}. \tag{1.3}$$

When parabolic density and temperature profiles are assumed in the fusion reactor, the ignition requirement at the peak value is given by a relation of

$$\hat{n}\hat{T}\tau_E > 5\times10^{21} m^{-3} keVs \tag{1.4}$$

Figure 1.1 illustrates the progress of $nT\tau_E$ condition obtained in the different magnetic confinement fusion devices [6]. The fusion device is now close to the breakeven condition indicating that the fusion output is equal to the power input. However, several physics subjects to be resolved are still remained to realize the fusion reactor with steady state operation such as the plasma-wall interaction, removal of helium ash, α-particle confinement and so on in addition to the steady maintenance of plasma current in the tokamak. Further effort has to be paid to the fusion experiment.

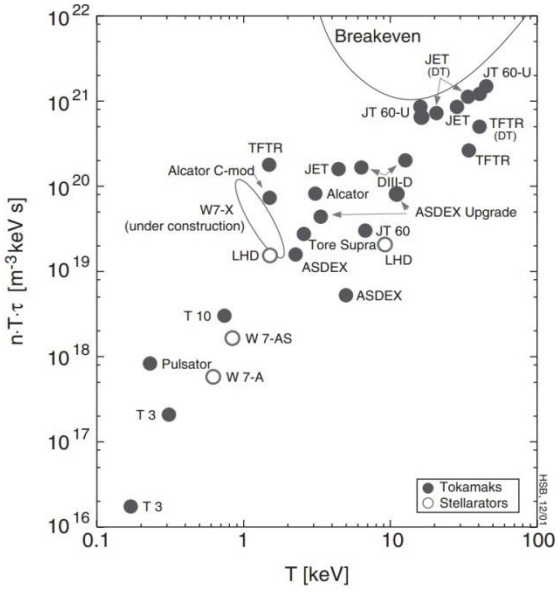

Fig.1.1 Diagram of $nT\tau_E$ values versus ion temperature, T, obtained in different magnetically confined fusion devices.

1.2 Role of the impurity in fusion plasmas

Fusion plasmas magnetically confined in a toroidal vacuum vessel always contain the impurity through the plasma-wall interaction. The impurities, e.g., carbon and iron, come in the plasma as the source of first wall, divertor plates, mechanical limiters and antennas for high-frequency wave heating through the physical and chemical sputtering in addition to helium used for discharge cleaning. Noble gases and solid impurity pellet are frequently used for the transport study [7]. The light impurity such as carbon dilutes the fuel ions and the heavy impurity enhances the radiation loss. In the beginning of fusion study, the radiation loss from heavy impurities was found to be half to the input power [8].

The impurity ions in fusion plasmas are now classified as low-, medium- and high-Z elements. The most common low-Z impurities are lithium, boron, carbon and oxygen. The lithium and boron are brought into the plasma as the result of lithium and boron coating to the first wall which are carried out to reduce the oxygen and metallic impurity influxes originating with the plasma-facing materials. The source of carbon is the graphite tiles being used for protection of the vacuum vessel. Typical medium-Z impurities are chromium, iron and nickel which are the composition element of the vacuum vessel made of stainless steel. On the other hand, the high-Z impurity was not common in the fusion experiment during past several decades. Recently, however, molybdenum and tungsten materials are begun to use instead of the graphite tiles. In particular, the use of high-Z materials is important for ITER in relation to tritium retention, carbon dust and mitigation of divertor heat load.

The impurity concentration in fusion plasmas has been maintained in a low level with the technical development on wall cleaning and edge plasma control. A typical density of medium- and high-Z impurities is 0.1% or less to the electron density, while the carbon density is a few percent [9].

The density of impurity ions at certain radial location of plasma can be written by an impurity continuity equation of

$$\frac{\partial n_z}{\partial t} = -\nabla \bullet \Gamma_z + n_z[n_{z-1}S_{z-1} - n_z S_z + n_{z+1}a_{z+1} - n_z a_z], \tag{1.5}$$

where n_z is the density of impurity ions in the ground state of ionization state z, Γ_z the impurity flux in ionization state z, S_z and α_z the ionization and recombination rate coefficients, respectively. When $\frac{\partial n_z}{\partial t} = 0$ and $\Gamma_z = 0$ for all z, the equation expresses the coronal equilibrium condition.

The ion motion along magnetic field lines is much more rapid than the radial transport perpendicular to magnetic field lines. The radial distribution of impurity ions can be then treated as a one-dimensional transport. It is usually expressed as a function of flux surface coordinate. The impurity flux is represented by

$$\Gamma_z = -D_z(r)\nabla n_z(r) + V_z(r)n_z(r), \tag{1.6}$$

where $D_z(r)$ and $V_z(r)$ are the diffusion coefficient and the convective velocity, respectively. Typical values observed in the experiment range in $0.1 \le D \le 1.0$ m^2/s and $-10 \le V \le +5$ m/s with an assumption that the transport does not depend on the ion charge. The diffusion coefficient is often expressed as a function of plasma radius, whereas the convective velocity should be V=0 at plasma center and V<0 at plasma edge in usual discharges.

Typical profiles of electron temperature and density in JET are shown in Fig. 1.2(a) [9]. The radial impurity distribution in each ionization stage takes a shell structure as a function of plasma radius, as seen in the carbon radial profile in Fig. 1.2(b). Here, a spatially constant value of D_z=1.0 m^2/s and V=0 is assumed in the impurity transport calculation for simplicity. The radial location of C^{6+} ion is shifted to inner position in plasma radius compared to the coronal model without transport.

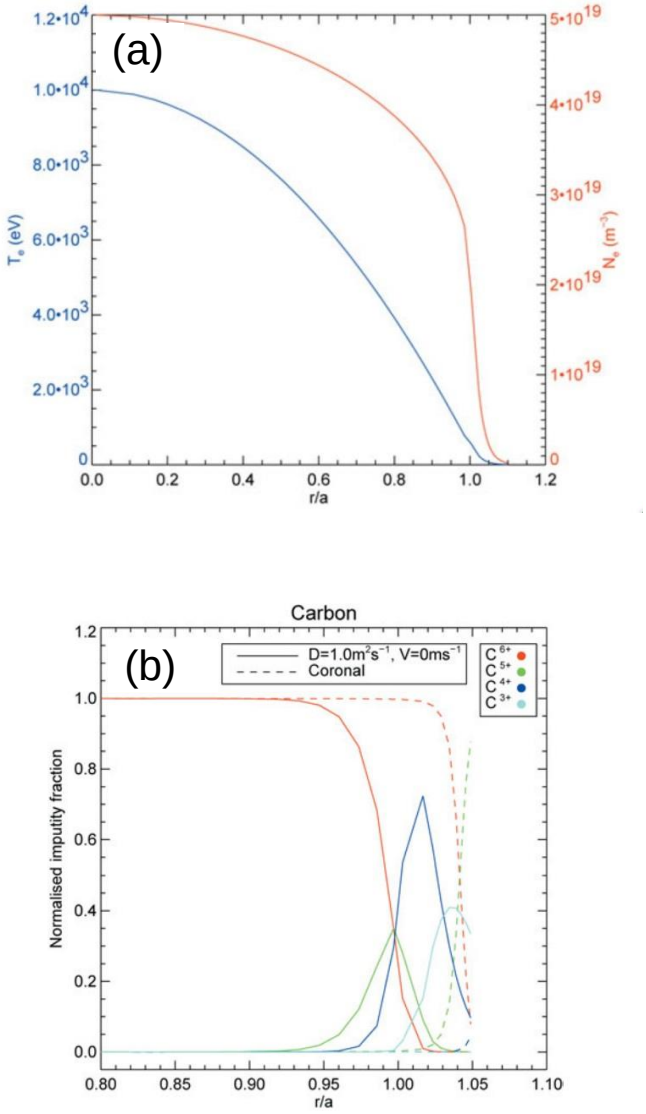

Fig. 1.2 (a) Profiles of electron temperature, T_e, and electron density, N_e, in JET and (b) radial profiles of carbon ions in different ionization stages (solid lines). The dashed line indicates the result from Coronal equilibrium.

The spectral line of impurities in fusion plasmas is emitted in a wide wavelength range from near infrared to soft X-ray, i.e. 1-12000 eV, as listed in Table 1.1. The molecular spectra such as hydrocarbon exist in the near infrared and visible wavelength ranges and the spectra from low-ionized impurity ions including neutral impurity are emitted in the visible, UV and VUV ranges. Such impurity emissions are located in the plasma edge. In the EUV range, on the other hand, the measurement of highly ionized impurity ions is possible in addition to the low-ionized impurities, whereas only helium- and hydrogen-like impurity ions located in the plasma center are observed in the soft X-ray range. Therefore, the EUV spectroscopy can cover a wide range of impurity charge states.

A lot of information on the plasma behavior can be obtained from the impurity spectroscopy. The ion temperature and the plasma rotation are measured from Doppler broadening and shift of the spectral line, respectively. The electron temperature and density can be measured from the line intensity ratio. The impurity density and impurity influx are determined from the analysis on absolute intensity of spectral line influx. The impurity transport is usually studied by measuring the temporal behavior of spectral lines based on laser blow-off and impurity pellet injection techniques. The measurement of bremsstrahlung continuum is also possible if the stray light of the spectrometer and electric noise of the detector are entirely reduced. This is a noble method to obtain the effective charge, Z_{eff}, of the fusion plasma.

Table 1.1 Spectral ranges for spectroscopy

Spectral Region	**Wavelength/ Energy Region**
Near Infrared	7000-12000 **Å**/1-2 eV
Visible	4000-7000 **Å**/2-3 eV
Ultraviolet (UV)	2000-4000 **Å**/3-6 eV
Vacuum ultraviolet (VUV)	500-2000 **Å**/6-24 eV
Extreme ultraviolet (EUV)	10-500 **Å**/24-1200 eV
Soft X-ray	1-10 **Å**/1200-12000 eV

1.3 Large Helical Device

Large Helical Device (LHD) is the world largest superconducting fusion device. The magnetic field for plasma confinement is basically produced by a pair of helical coils (HC) with poloidal pitch number of l=2 and toroidal pitch number of m=10. The elliptical magnetic flux surfaces are produced by HC coils. Three pairs of poloidal coils shown in Fig. 1.3, i.e., inner vertical (IV), inner shaping (IS) and outer vertical (OV) coils are used for cancelation of the vertical field produced by HC coils, horizontal shift of the magnetic axis and the shaping of elliptical plasma with the quadruple field of IS coils. The main parameters of LHD are listed in Table 1.2. In LHD, a helical double-null divertor intrinsically exists by the presence of HC coils and the divertor layer is twisted poloidally and toroidally reflecting the shape of the HC coils.

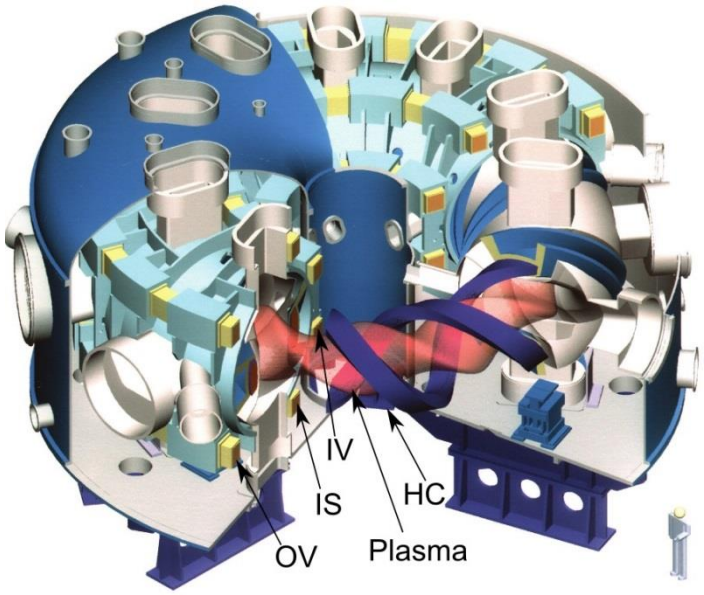

Fig. 1.3 Cut-away drawing of LHD.

Table 1.2 Main parameters of LHD

Major radius R	3.5-4.0 m
Minor radius <a>	0.546-0.65 m
Plasma volume V_p	20-30 m^3
Magnetic field B_t	3 T
NBI	28 MW
ECH	3.7 MW
ICRF	2 MW

In LHD, the discharge is performed with three heating methods of electron cyclotron resonance heating (ECH) [10], ion cyclotron range of frequency (ICRF) heating [11] and neutral beam injection (NBI) heating [12]. The ECH is used to initiate the plasma discharge and to achieve high electron temperature plasmas. Recently it is also used for maintenance of long pulse discharges. The ICRF is mainly used for demonstrating a steady state operation of the LHD discharge. The NBI heating is carried out using five beams, i.e., three tangential negative-ion-source-based NBI beams with energy of 180 keV and two perpendicular positive-ion-source-based NBI beams with energy of 40 keV. The total heating power of NBI heating is now about 28 MW.

Many kinds of diagnostic systems have been installed on LHD and many plasma parameters have been measured. Although all the diagnostics are giving valuable information for understanding the behavior of LHD plasmas, the electron temperature and density profiles are especially important and the basis for analyzing many LHD data including spectroscopic data. Those are measured in LHD by YAG Thomson scattering (TS) system along the major radius at the mid plane of horizontally elongated plasma cross section [13]. The spatial and temporal resolutions are 12-25 mm and 10-100 ms, respectively. Three sets of interferometer systems of multichannel far infrared (FIR) laser interferometer [14], two-color millimeter-wave interferometer [15] and a CO_2 laser imaging interferometer [16] are also used for the electron density measurement.

Table 1.3 Passive spectrometers in LHD

Name	Type	Grating (grooves/mm)	λ range (Å)	Spatial resolution
1.33-m visible	Czerny-Turner	1800	2000-8000	26 mm (entire plasma)
0.5-m visible	Czerny-Turner	100	2000-10000	26 mm (entire plasma)
0.3-m visible	Czerny-Turner	1200	2000-9000	26 mm (entire plasma)
3-m VUV	Normal incidence	1200	500-3100	20 mm (entire plasma)
EUV_L1	Grazing incidence	1200	30-650	No
EUV_L2	Grazing incidence	1200	30-650	15 mm (entire plasma)
EUV_S1	Grazing incidence	2400	10-130	No
EUV_S2	Grazing incidence	2400	10-130	15 mm (half of plasma)
X-ray crystal	Johann	4 crystals	1.7-4.0	No (core plasma)
XICS*	Johann	Quartz(110)	3.94-3.96	20 mm (entire plasma)

*X-ray Imaging Crystal Spectrometer

In order to study the impurity behavior, many kinds of spectrometers working in different wavelength ranges have been developed and installed on LHD. The specifications of these spectrometers are listed in Table 1.3 [17]. The two visible spectrometers with focal length of 1.33 m and 0.5 m are used for study of edge hydrogen and helium behaviors. Another visible spectrometer with a short focal length of 0.3 m is used for the measurement of bremsstrahlung continuum profile. The absolute intensity calibration of all other EUV spectrometers is carried out based on the visible bremsstrahlung profile. Two EUV spectrometers named EUV_L2 and EUV_S2 working in different wavelength ranges of 30-650 Å and 10-130 Å are installed for the profile measurement of impurity lines, respectively, whereas other two EUV spectrometers named EUV_L1 and EUV_S1 are only used for the impurity monitor with high-time resolution of 5 ms. In the present study the EUV_L2 has been mainly used for two-dimensional measurement of impurity line emissions. The details of the spectrometer are explained in Chapter 2.

1.4 Edge magnetic field structure of LHD and impurity transport in ergodic layer

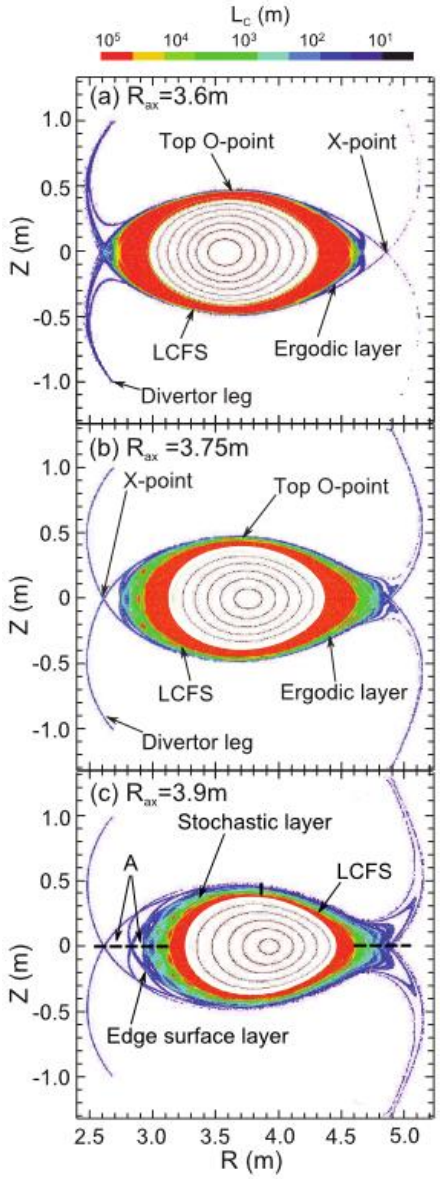

Fig. 1.4 Magnetic field structure at horizontally elongated plasma cross section of (a) R_{ax}=3.6 m (b) R_{ax}=3.75 m and (c) R_{ax}=3.9 m. The connection length of magnetic field lines, L_c, is indicated with color.

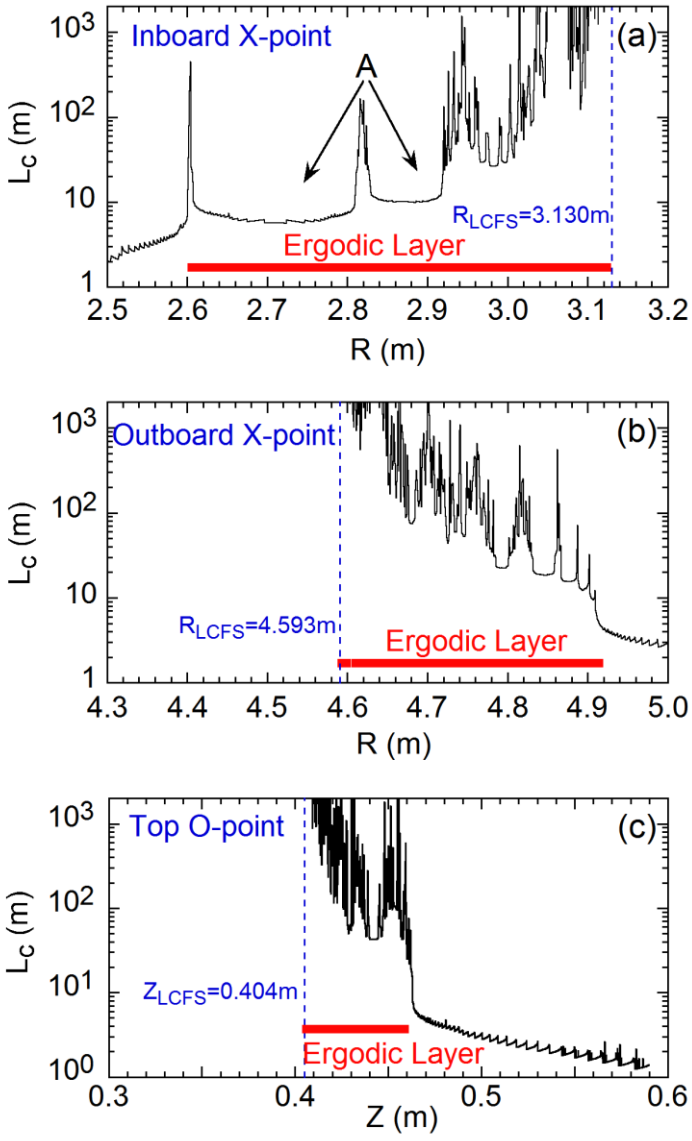

Fig. 1.5 Connection length of magnetic field lines, L_c, at (a) inboard X-point (b) outboard X-point and (c) top O-point at R_{ax}=3.9 m (see Fig. 1.4(c)).

In tokamak, the scrape-off layer (SOL) locating outside the last closed flux surface (LCFS) is composed of open flux surfaces. In LHD, the edge magnetic field structure is much more complicated compared to the tokamak edge. The edge magnetic structure of LHD is illustrated in Fig. 1.4. There intrinsically exists a thick ergodic layer outside the LCFS consisting of stochastic magnetic field lines. The stochastic magnetic field is formed by the higher order Fourier components which are involved in the magnetic field produced by the helical coils. The thickness of the ergodic layer, λ_{erg}, increases as the magnetic axis position is outwardly shifted from R_{ax}=3.6 m to R_{ax}=3.9 m. The thickness of ergodic layer in the poloidal cross section is minimal at the two O-points near the helical coils, e.g., λ_{erg}=2 cm for R_{ax}=3.6 m and λ_{erg}=10 cm for R_{ax}=3.9 m. The thickness is maximal at the two X-points, e.g., λ_{erg}=10-20 cm for R_{ax}=3.6 m. The connection length of magnetic field lines in the ergodic layer ranges in 10-2000 m which corresponds to 0.5-100 toroidal turns of the torus.

The ergodic layer is composed of two layers, i.e., stochastic layer and edge surface layer. Those are indicated in Fig. 1.4(c). The LCFS in LHD is defined as the outmost flux surface on which the deviation of magnetic field lines is less than 4 mm while it travels about 1000 m along the torus. Outside the stochastic layer region, there exists a region with multiple thin curved layers called edge surface layer which is created by radial movement of the X-point and high local shear based on large rotational transform. In the edge layer region, several island layers are embedded together with a poloidal mode number of 10 in the open flux surface. With increasing the minor radius, the poloidal mode numbers of the natural island layers decrease and the widths of islands increase. Eventually, the island layers overlap each other and the stochastic field layer is formed at the edge region of the LHD plasma. There is no clear separatrix in the edge plasma region of LHD. The field lines from stochastic region enter the edge surface layer and finally arrive at divertor plates passing through the vicinity of X-points after many toroidal circulations. The connection length from X-points to divertor plates is very short, e.g. order of plasma minor radius. Figure 1.5 shows the connection length of magnetic field

lines at inboard and outboard X-points and top O-point in R_{ax}=3.9 m. The horizontal range in the figures is indicated with dashed lines in Fig. 1.4(c). From the figures we understand that the thicknesses of ergodic layer and the profile of connection length are completely different in the three poloidal positions. In the region denoted with 'A' in Figs. 1.4(c) and 1.5(a), the connection length is very short and the field lines are directly connected to the divertor plates, but not to the stochastic layer.

The particle and heat fluxes diffuse out of the core plasma through the LCFS and enter the SOL in tokamaks or the ergodic layer in LHD. Those are finally conducted to the divertor plates. However, the particle and heat transports in the ergodic layer are entirely different from those in the tokamak SOL because the magnetic field structure in the ergodic layer is fully stochastic and the magnetic field connection length is much longer compared to the SOL. Based on such a background in the edge plasma of LHD, 3-D edge plasma transport code, EMC3-EIRENE, has been developed in LHD to study the particle and heat transports in the ergodic layer [18]. The EMC3 code solves a set of Braginskii equations of mass, momentum and energy in arbitrarily magnetic field geometry. The EIRENE code solves a kinetic model of the neutral transport by simulating the recycling neutral at divertor plates.

The fluid equation of momentum balance parallel to magnetic field lines for impurity is given by

$$m_z \frac{\partial V_{z//}}{\partial t} = -\frac{1}{n_z}\frac{\partial T_i n_z}{\partial s} + m_z \frac{V_{i//} - V_{z//}}{\tau_s} + ZeE_{//} + 0.71\mathrm{Z}^2 \frac{\partial T_e}{\partial s} + 2.6\mathrm{Z}^2 \frac{\partial T_i}{\partial s}, \qquad (1.7)$$

where z, i, and s denote the impurity with charge state Z, the bulk plasma ion and the coordinate along magnetic field line. The variables of $V_{i//}$, $V_{z//}$, τ_s and $E_{//}$ denote the parallel velocities of background ion and impurity, impurity-ion collision time and parallel electric field, respectively. In this equation, T_z=T_i is assumed. The terms on the right hand side represent the impurity pressure gradient force, the friction force exerted by the

background parallel plasma flow, electrostatic force, electron and ion thermal forces called temperature gradient force. The dominant terms in the equation are the friction force at the second term and the ion thermal force at the fifth term. For the steady condition, therefore, the equation can be written by

$$V_{z//} = V_{i//} + 2.6Z^2 \frac{\tau_s}{m_z} \frac{\partial T_i}{\partial s}. \tag{1.8}$$

The ratio of the friction force to the thermal force in eq.1.7 is thus given by

$$\frac{friction force}{thermal force} \sim \frac{(5/2) n_i T_i V_{i//}}{k_i^0 T_i^{2.5} \nabla_{//} T_i} \propto \frac{n_i |M|}{T_i \nabla_{//} T_i}, \tag{1.9}$$

where k_i^0 and M are the parallel heat transport coefficient and the Mach number, respectively. The numerator and denominator represent convective and conductive energy fluxes, respectively. Since the background plasma flow is usually directed towards the downstream, i.e., from plasma edge to diverter plates, the friction force pushes the impurity to the divertor region, which enhances the impurity screening. On the contrary, the thermal force pushes the impurity to the upstream because the temperature gradient changes the collisionality along the magnetic field. Therefore, the impurity transport in the ergodic layer dominantly depends on the ratio of the friction force to the thermal force. In LHD, the carbon transport in the ergodic layer has been studied based on EMC3-EIRENE code. Results on the carbon density distribution and the force balance between friction and thermal forces are shown in Fig. 1.6 [19]. In the low-density discharge, the thermal force is dominant and pushes the carbon ion to the upstream. In the high-density discharge, however, the friction force becomes dominant instead of the thermal force and changes the force balance. As a result, the carbon ion moves to the downstream

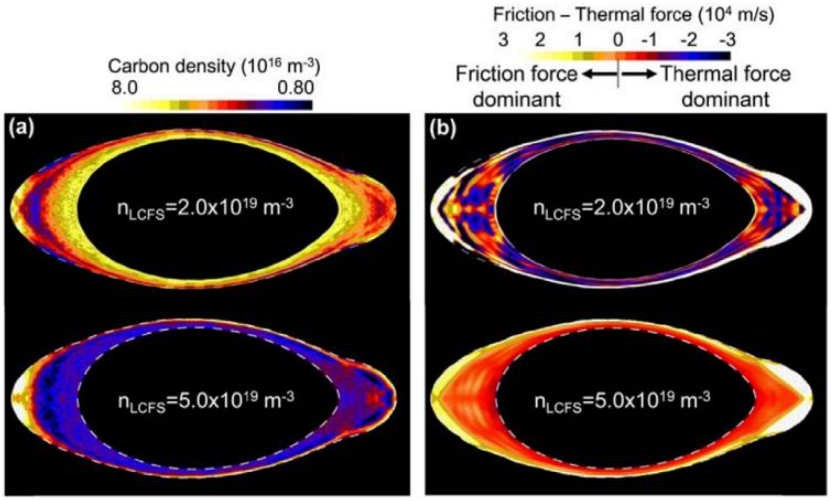

Fig. 1.6 (a) Carbon density distributions in ergodic layer at low ($2x10^{19}$ m^{-3}) and high ($5x10^{19}$ m^{-3}) electron densities defined at LCFS and (b) balance between friction and thermal forces.

1.5 Objective and structure of the thesis

In order to study the impurity behavior in the ergodic layer with three-dimensional magnetic field structure, it is necessary, at least, to measure the two-dimensional distribution of impurity line emissions. Since the impurity line emissions emitted in the ergodic layer are mainly in the EUV wavelength range, a space-resolved EUV spectrometer measuring upper half of the full vertical impurity profile is upgraded to the two-dimensional spectroscopic system. The two-dimensional EUV spectroscopy can be possible if the observation chord of the space-resolved EUV spectrometer is scanned vertically and horizontally. Therefore, two stepping motors are additionally installed on the EUV spectrometer system to change the view angle of space-resolved EUV spectrometer along vertical and horizontal directions. The two-dimensional distribution of

impurity line emissions can be measured by horizontally scanning the spectrometer observation chord during single discharge at a fixed vertical spectrometer angle. In addition, the working wavelength of the space-resolved spectrometer is extended from 50-500 Å to 30-650 Å to measure further impurity spectral lines. For the purpose the second stage for moving the CCD position is added to the original stage to make the CCD movement distance wider. Details of the upgrade on the space-resolved EUV spectrometer are explained in Chapter 2.

In Chapter 3, the full vertical profile and two-dimensional distribution are shown for typical impurity line emissions observed in LHD. In Chapter 4, the vertical profiles of HeII and CIV are analyzed at different toroidal and poloidal angles. It is found that the HeII is located at inner radial position compared to the CIV, whereas the ionization energy of HeII (E_i=54 eV) is lower than that of CIV (E_i=65 eV). The distance between HeII and CIV radial locations is nearly constant, i.e. $\Delta Z \approx 4$ mm, for different poloidal positions.

Two-dimensional measurement of electron temperature in the ergodic layer is of crucial importance to study the transport in the edge plasma of helical devices. However, there was no diagnostics to measure such the two-dimensional edge temperature distribution in the fusion research. A diagnostic method based on the intensity ratio between two line emissions is attempted to measure the two-dimensional electron temperature distribution in the ergodic layer of LHD. In Chapter 5, the vertical profile and two-dimensional distribution of electron temperature in the ergodic layer are measured using the line intensity ratio. The intensity ratio between two spectral lines with significant different excitation energy is given by

$$\frac{I_{g,j}}{I_{g,k}} = \frac{\Delta E_{g,j}\gamma_{g,j}}{\Delta E_{g,k}\gamma_{g,k}} \exp\left(\frac{\Delta E_{g,k} - \Delta E_{g,j}}{kT_e}\right) = F(T_e), \qquad (1.10)$$

where $\gamma_{g,j}$ is the collision strength. The ratio is sensitive to the change in electron temperature, if $\frac{\Delta E_{g,k} - \Delta E_{g,j}}{kT_e} >> 1$. Here, it is assumed that the two lines are emitted from the same plasma volume. The most common line ratio for the temperature measurement is 2s-2p/2s-3p for Li-like ions. However, these line pairs have considerably different wavelengths, e.g., CIV 2s-2p (1550 Å)/2s-3p (312 Å). Then, the line ratio of CIV 2p-3d (384 Å)/2p-3s (420 Å) is used to measure the electron temperature profile in the edge boundary of ergodic layer. The result is compared with the temperature at divertor plates measured by Langmuir probe. NeVIII line ratio of 2s-3p (88 Å)/2p-3s (103 Å) is also adopted to measure the two-dimensional distribution of electron temperature near LCFS in the ergodic layer. The measured electron temperature profile is compared with the simulation.

The analysis of two-dimensional distribution of impurity line emissions brings us extremely important information on the impurity behavior in the ergodic layer. In Chapter 6, the vertical profile structure of impurity emissions near X-points are studied at different electron densities. Two-dimensional distribution of impurity line emissions is analyzed at different plasma axis positions and the line intensity near X-point is compared between inboard and outboard X-points. The experimental result is analyzed with 3-D edge transport code, EMC3-EIRENE. In Chapter 7, the thesis is summarized and the conclusion is given.

References

[1] J. Wesson, Tokamaks, 4th edition, Oxford University press, (2012).

[2] S. Ishida, et al., Nucl. Fusion **51**, 094018 (2011).

[3] R. Aymar, et al., Plasma Phys. Control. Fusion **44**, 519 (2002).

[4] A. Iiyoshi, et al., Nucl. Fusion **39**, 1245 (1999).

[5] L. Wegener, Fusion Eng. Des. **84**, 106 (2009).

[6] H.S. Bosch, Nucl. Fusion Lect. Notes Phys. **670**, 445 (2005).

[7] S. Morita, et al., Plasma Sci. Technol. **13**, 290 (2011).

[8] E. Hinnov, et. al., Nucl. Fusion **18**, 1305 (1978).

[9] B.C. Stratton, et. al., Fusion Sci. Technol. **53**, 431 (2008).

[10] T. Shimozuma. et al., Fusion Eng. Des. **53**, 525 (2001).

[11] T. Mutoh, et al., Fusion Eng. Des. **26**, 387 (1995).

[12] M. Fujiwara, et al., Plasma Phys. Control. Fusion **41**, B157 (1999).

[13] K. Narihara, et. al. Rev. Sci. Instrum. **72**, 1122 (2001).

[14] K. Kawahata, et al., Rev. Sci. Instrum. **70**, 707 (1999).

[15] K. Kawahata, et al., Rev. Sci. Instrum. **70**, 695 (1999).

[16] K. Tanaka, et al., Rev. Sci. Instrum. **72**, 1089 (2001).

[17] M. Goto, et al., Fusion Sci. Technol. **58**, 394 (2010).

[18] M. Kobayashi, et al., Contrib. Plasma Phys. **48**, 255 (2008).

[19] M. Kobayashi, et al., Nucl. Fusion **53**, 033011 (2013).

Chapter 2

Development of EUV spectrometer system for 2-D measurement

2.1 Introduction

Impurities play an important role for the experimental study of magnetic confinement fusion research in the viewpoint of radiation loss included bremsstrahlung continuum in addition to fuel dilution. The plasma performance is influenced by the impurities not only in the plasma core but also in the plasma edge including the scrape-off layer. Therefore, the study of impurity behavior is important to improve the plasma performance. The line emissions from impurities are frequently used for the impurity diagnostics. For the purpose many kinds of impurities are used by injecting an solid impurity pellet and puffing a noble gas instead of intrinsic impurities such as carbon and iron [1,2]. Since the electron temperature in current magnetic fusion devices is significantly high, most of the impurity line emissions are radiated in vacuum ultraviolet (VUV: 500-2000 Å) and extreme ultraviolet (EUV: 10-500 Å) wavelength ranges [3].

A number of EUV spectrometers have been developed for the impurity diagnostics of fusion plasmas. A survey poor resolution extended domain spectrometer (SPRED) has been widely used with an aberration-corrected holographic toroidal grating [4]. The emission lines from both the light and heavy impurities in the wavelength range of 100-

1100 Å can be monitored with SPRED for the impurity diagnostics in tokamak discharges, while the spectral resolution is considerably poor. Following the same principle, a high efficiency EUV overview spectrometer (HEXOS) covering 25-1600 Å region is developed for Wendelstein (W7-X) stellarator [3]. Recently, two high-resolution grating spectrometers called XEUS (X-ray and EUV spectrometer) and LoWEUS (Long-wavelength and EUV spectrometer), which work in the 5-400 Å region, have been installed on National Spherical Tokamak Experiment (NSTX) [5]. Two flat-field EUV spectrometers called EUV_Short and EUV_Long with varied line spacing (VLS) groove holographic grating have been also developed in Large Helical Device (LHD) to measure the wavelength ranges of 10-130 Å and 50-500 Å, respectively [6,7]. All of the EUV spectrometers mentioned above have been mainly used as the simple impurity monitor.

Although most of the EUV spectrometers installed on the fusion devices do not have any spatial resolution, a few EUV spectrometers have the function of the spatial resolution. It is possible to measure one-dimensional distribution of impurity lines using a spherical concave grating with large astigmatism at grazing incidence. In DIII-D tokamak, an EUV spectrometer with spatial resolution has been developed by utilizing the large astigmatism inherent to a concave grating based on the Rowland mounting near-grazing incidence [8,9]. The spatially resolved measurement in the EUV range is also possible for the flat-field VLS grating. A space-resolved EUV spectrometer working in 60-400 Å has been developed using the VLS grating and installed on LHD to observe one-dimensional impurity line emission profile [10]. Such spectrometers have an enough performance to study the impurity transport in the core plasma in which the magnetic surfaces are clearly formed. The observed line-integrated intensity profile can be easily reconstructed into the local emissivity as a function of the magnetic surface based on Abel inversion technique. However, if the plasma has no poloidal and toroidal symmetries, the impurity transport can not be sufficiently studied from the radial profile measured only at some toroidal position.

The magnetic configuration for plasma confinement in LHD has three-dimensional structure which characterizes one of typical features in helical devices with external coil

system. In particular, the three-dimensional effect is remarkably emphasized in the edge magnetic structure consisting of stochastic magnetic field lines, so called 'ergodic layer', which are caused by higher orders of Fourier components in helical coils and overlapping of natural islands due to the presence of radial magnetic fields. A two-dimensional measurement with good spatial resolution is therefore required to study the impurity transport in the ergodic layer with three-dimensional structure. However, an optical spectroscopy using visible light is not applicable to the edge plasma diagnostics of LHD because the edge temperature is considerably high. Typical edge electron temperature of LHD plasmas range in ~20 eV at the edge boundary of ergodic layer and 100-500 eV at the last closed flux surface (LCFS) mainly as a function of electron density and magnetic filed strength. The two-dimensional measurement of impurity line emissions in the EUV range is strongly desired to study the impurity transport in the ergodic layer. For the purpose the space-resolved EUV spectrometer for vertical profile measurement is improved by adding a new mechanism to observe the two-dimensional distribution of impurity line emissions in edge plasma of LHD. In this chapter the instrumentation of the space-resolved EUV spectrometer for two-dimensional measurement is presented with typical examples of two-dimensional distributions of EUV line emissions observed from LHD edge plasma. The present result shows the first attempt for the two-dimensional measurement in the EUV wavelength range to study plasmas with stochastic magnetic field.

LHD coil system consists of continuous superconducting helical coils with poloidal pitch number of ℓ=2 and toroidal pitch number of m=10 and three pairs of superconducting poloidal coils. The magnetic surfaces have three-dimensional structure due to the absence of toroidal symmetry in the helical coils. The pair of helical coils creates a toroidal plasma with elliptical poloidal cross section. The elliptical plasma poloidally rotates quickly when it moves toroidally. A schematic view of the LHD plasma within LCFS is shown in Fig. 2.1. The major and average minor radii in the standard configuration of LHD with maximum plasma volume is R=3.6 m and a=0.64 m, respectively. Here, the diameters in long and short axes of the elliptical plasma cross section are l_{max}=1.81 m and l_{min}=0.89 m,

respectively. The value of φ in the figure denotes the toroidal angle and $\varphi=0^{o}$ is defined at horizontally elongated plasma cross section. The position of LCFS in LHD is defined by the outermost flux surface on which the deviation of the magnetic field line is less than 4 mm while it travels 100 turns along the torus [11].

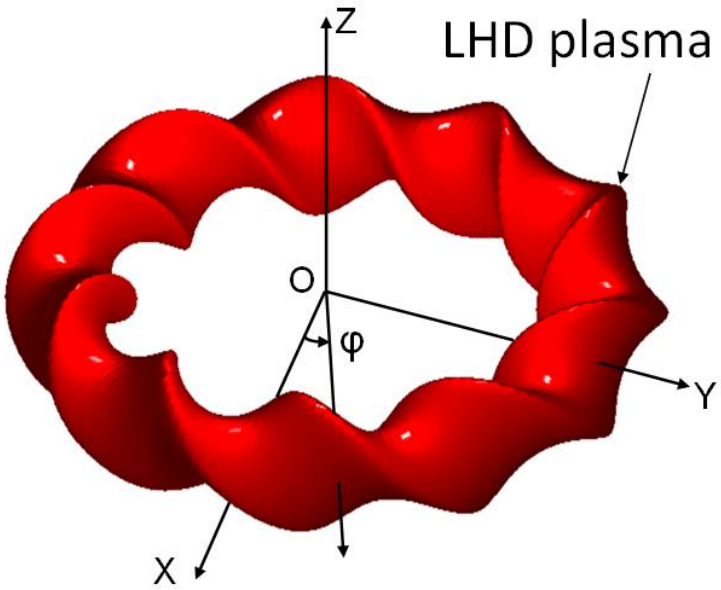

Fig. 2.1 Three-dimensional schematic view of LHD plasma with poloidal pitch number of ℓ=2 and toroidal pitch number of M=10. The symbols of φ and X denote toroidal angle and the coordinate connecting torus center and LHD port center of #10-O.

In LHD the LCFS is surrounded by a thick stochastic magnetic field layer called ergodic layer. The structure of the ergodic layer is shown in Fig. 2.2 at magnetic axis position of R_{ax}=3.9 m. The ergodic layer mainly consists of stochastic magnetic field lines with lengths from 10 to 2000 m, which correspond to 0.5-100 toroidal turns in the LHD. The thickness of the ergodic layer, λ_{erg}, varies with the poloidal and toroidal angles exhibiting a complicated three-dimensional structure. The minimum thickness of the ergodic layer is appeared at two poloidal locations near the helical coils, which are here defined as 'O-point'. The minimum λ_{erg}, which strongly depends on the R_{ax}, are 2 cm for

R_{ax}=3.60 m and 10 cm for R_{ax}=3.90 m at horizontally elongated plasma cross section of φ=0°, while λ_{erg} is different at inboard and outboard sides in vertically elongated cross section of φ=18°, i.e., 12 cm at inboard side and 5 cm at outboard side in R_{ax}=3.90 m as seen in Fig. 2.2(b). In contrast to it, the maximum λ_{erg} is given in poloidal location near X-points at low field sides. The values of λ_{erg} at horizontally elongated plasma cross section range in 10-20 cm at R_{ax}=3.60 m and 30-45 cm at R_{ax}=3.90 m taking different values at inboard and outboard X-points. The λ_{erg} increases with not only R_{ax} but also β value (≡ plasma pressure/magnetic pressure) [11]. The magnetic field lines in the ergodic layer have enough toroidal lengths and radial thickness to confine the edge plasma, whereas they frequently repeat radial movement during toroidal turn. Therefore, the electron temperature and density in the ergodic layer are considerably high and range in 10-500 eV and 1-10x10^{13} cm^{-3}, respectively.

In the outside of ergodic layer, there exist four intrinsic divertor legs connecting X-points region to divertor plates. The whole particles coming out the plasma are transferred through the divertor legs and reach the divertor plates made of carbon. In order to study the three-dimensional edge transport, the carbon line emissions are usually used in LHD because of the high intensity [12].

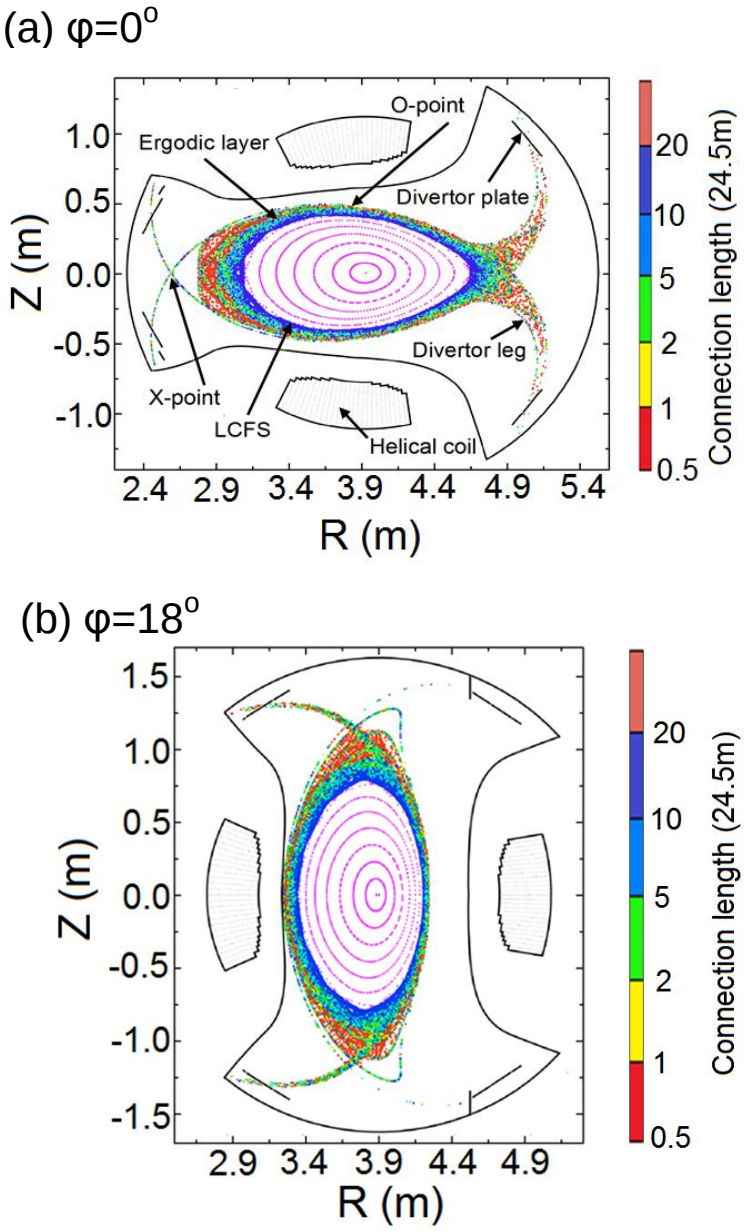

Fig. 2.2 Magnetic field structures of LHD at (a) horizontally elongated plasma cross section (φ=0°) and (b) vertically elongated plasma cross section (φ=18°) in magnetic axis position of R_{ax}=3.9 m. Different colors in ergodic layer mean different magnetic field connection length in unit of one toroidal turn of 24.5 m.

2.2. Space-resolved EUV spectrometer system for 2-D measurement

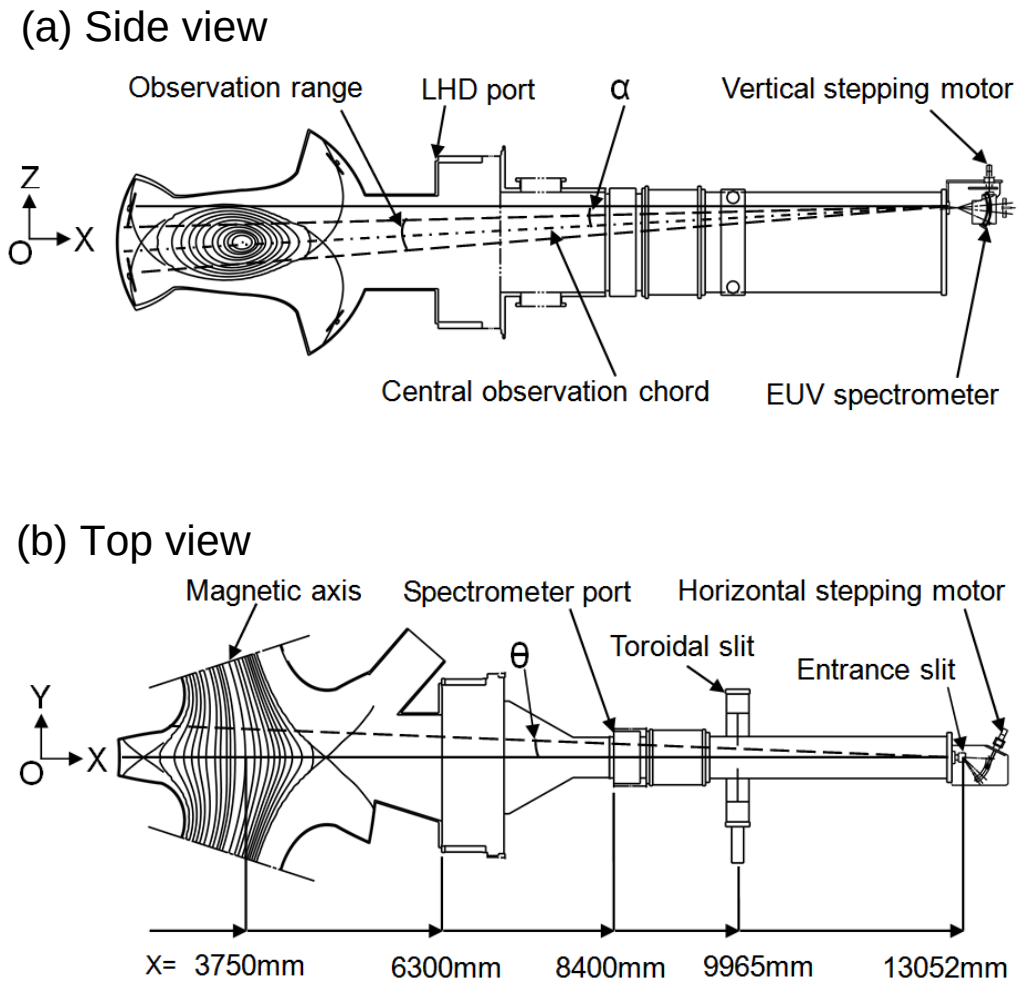

Fig. 2.3 Schematic view of EUV spectrometer system in LHD from (a) side view and (b) top view. The symbols of α and θ denote vertical angle and horizontal angle against central chord of EUV spectrometer, respectively. Distances indicated in the bottom of (b) express X values in Fig. 2.1.

In LHD many kinds of spectrometers working in visible, VUV and EUV ranges have been installed for monitoring the impurities and studying the impurity transport [13]. The space-resolved EUV spectrometer working in 60-400 Å range is also installed on LHD for vertical profile measurement [10]. The spectrometer has been recently improved for the two-dimensional measurement by adding a new mechanism to scan the observation chord horizontally during single discharge. The schematic diagram of the space-resolved flat-field EUV spectrometer system after modification is illustrated in Fig. 2.3. The modified space-resolved EUV spectrometer is also installed on LHD perpendicular to the toroidal magnetic filed at a distance of 9 m from the plasma center to observe the vertical profile at the horizontally elongated plasma cross section ($\varphi=0^{o}$) as well as the former EUV spectrometer. A vertical stepping motor is used to change the vertical observation range in the poloidal plasma cross section, as shown in Fig. 2.3(a). The position of central observation chord for the measurement along vertical direction is expressed as vertical angle, α, which is defined by an angle from the horizontal observation chord of the spectrometer. A horizontal stepping motor is used to change the horizontal angle, θ, of the observation chord, which is defined by an angle from the central chord with $\varphi=0^{\circ}$ at the horizontal elongated plasma cross section, as seen in Fig. 2.3(b). A toroidal slit with a rectangular-corrugated edge, which is used for the angle calibration of all the observation chords, is placed between the plasma and EUV spectrometer [14].

The space-resolved EUV spectrometer mainly consists of an entrance slit, a spatial resolution slit placed in front of the entrance slit, a gold-coated varied-line-spacing (VLS) grating and a charge-coupled device (CCD) detector. The entrance slit of 100 μm is used in the present study, since the spectral width is less than 5 pixels even in such a wider entrance slit. In the binning mode operation of CCD five pixels are summed and converted into one channel. The spectral resolution of 0.22 Å is obtained at 200 Å in the full image mode of CCD. The vertical spatial resolution of 10 mm is obtained when the spatial resolution slit with 0.2 mm width is used. The present width of the spatial resolution slit is suitable for the edge impurity measurement, but a wider spatial slit is better for the core

impurity measurement because good spatial resolution is not necessary in most of the experiments and the spectrometer brightness is of course increased. In practice, it is found that the core impurity line intensity is much weaker than the edge impurity intensity when the intensity per CCD vertical channel is compared between the core and edge impurity lines. In the present experiment the spatial resolution slit of 0.5 mm in width is adopted to measure both the impurity emissions from core and edge plasmas.

A holographic laminar-type VLS grating (Shimadzu 30-002: 1200 grooves/mm) with effective area of 26 mm in groove length and 46 mm in groove distance is used to make the flat focal plane. The radius of the grating curvature is 5606 mm. This large curvature can be treated as a flat plane and guarantees a straightforward reflection of the EUV emission on the whole area of grating. The angle of incidence fixed at 87^{o} covers a wavelength range of 60-400 Å when the flat focal plane is exactly defined in the calculation. However, the practical range of the wavelength interval can be considerably wider than such a calculated range.

A back-illuminated CCD (Andor DO420-BN, 26.6×6.6 mm^2 area) with 1024×255 pixels is adopted as the multi-channel detector with flat surface. An electrical insulator is placed between the detector and the spectrometer, since the spectrometer has to be grounded. A pulse motor is used for the movement of the CCD detector position along the focal plane to change the wavelength range to be measured. The CCD detector can be cooled down to $-70^{o}C$ by a Peltier device to reduce the thermal noise. Generally, it is operated at $-20^{o}C$, at which the thermal noise is sufficiently removed. The sub-image mode is used for the routine measurement on impurity profile diagnostics. The sampling time is usually set to 200 ms when the CCD is operated by the binning mode at 5 pixels. Therefore, the radial profiles with 204 channels are measured for the present space-resolved EUV spectroscopy. The vertical range of about 50 cm can be simultaneously observed, of which the range corresponds nearly half of the whole vertical length at horizontally elongated plasma cross section.

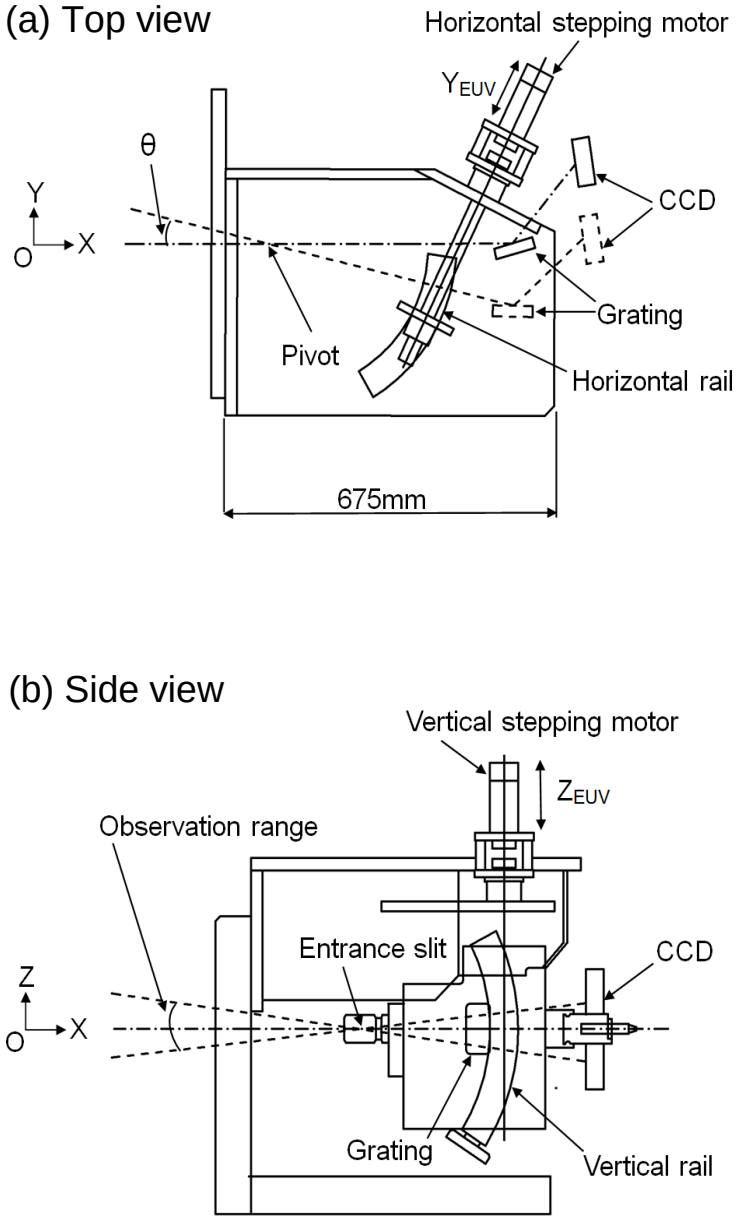

Fig. 2.4 Schematic drawings of EUV spectrometer system in (a) side view and (b) top view. Pivot is scanning center of EUV spectrometer

The EUV spectrometer is connected to a big differential pumping chamber following the LHD port through a small bellows, as shown in Fig. 2.3. The detailed structure of the EUV spectrometer is shown in Fig. 2.4. The EUV spectrometer can be vertically and horizontally moved by vertical and horizontal stepping motors, respectively. The electric motors are covered with 1 mm thick iron plate to avoid the effect of magnetic leakage from the LHD coil system. In order to fix the pivot position during the movement the spectrometer is placed on two circular rails, of which the center is set to the pivot. Therefore, the central observation chord through the grating center always goes through the pivot. The radii of the vertical and horizontal rails are 400 mm and 325 mm, respectively. The vertical and horizontal positions of the spectrometer moved by the two stepping motors are accurately measured by an electric scale as Z_{EUV} and Y_{EUV}, respectively. The vertical and horizontal angles of all the observation chords can be accurately calibrated by the toroidal slit with rectangular-corrugated slit. The details of the calibration are described in ref.14.

The observation ranges in vertical and horizontal directions are limited by both the spectrometer and LHD ports. Schematic view of the ports is shown in Fig. 2.5. The LHD port has a diamond shape with inside vertical size of 1160 mm due to the presence of helical coils. The spectrometer port has a rectangular shape with inside horizontal and vertical sizes of 500 mm and 1300 mm, respectively. Therefore, the observation area is also limited at the top-right and bottom-left corners of the LHD port. Here, it is noticed that the position of the spectrometer port is 2100 mm behind the LHD port, as shown in Fig. 2.3. Considering the positions among the spectrometer, the spectrometer port, the LHD port and the plasma, the horizontal plasma observation length practically ranges from Y=-460 mm to Y=+460 mm at the midplane of Z=0 mm, of which the range is indicated in Fig. 2.5 with two vertical dashed lines. These values correspond to the toroidal angles of $\varphi=\pm 7.0°$ (see Figs. 2.1 and 2.3). In the figure, the projection of plasma edge at LCFS is also traced for the magnetic axis position of 3.75 m. The minimum distance of 430 mm from the plasma edge to the midplane is given at the horizontally elongated plasma cross

section of φ=0°. Then, the detailed information on the plasma edge near the X-points can be observed at top-left and bottom-right corners.

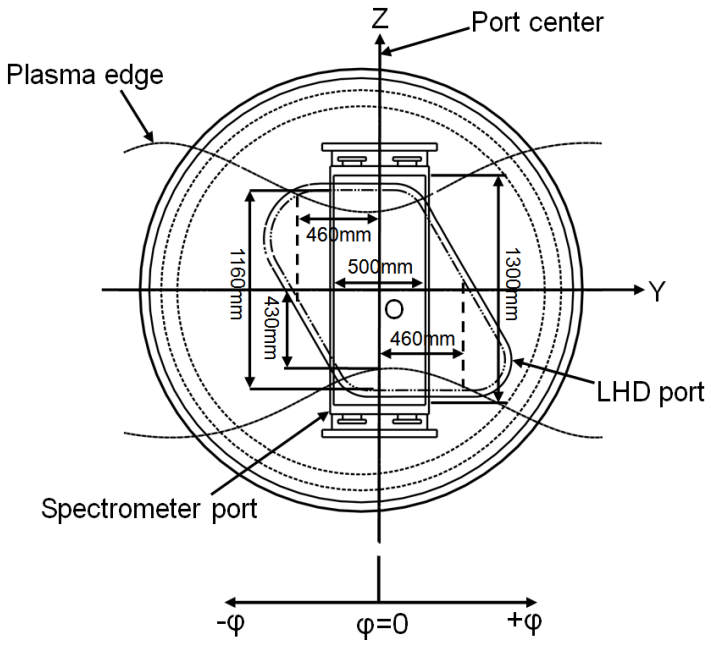

Fig. 2.5 Structures of rectangular EUV spectrometer port and diamond LHD port. The projection of LHD edge plasma boundary is plotted as 'Plasma edge'.

The vertical observation ranges in different poloidal cross sections are shown in Fig. 2.6 against the magnetic configuration with plasma axis position of R_{ax}=3.75 m. Before improving the performance of the space-resolved EUV spectrometer the vertical profile of EUV line emissions has been only observed at the horizontally elongated plasma cross section with the toroidal angle of φ=0°, as shown in Fig. 2.6(b). In this profile measurement most of the observation chords pass through both the X-point regions at inboard and outboard sides, while a few edge observation chords can measure the radial profile at both the top and bottom O-points with enough spatial resolution (see also Fig.

2.2(a)). The magnetic field structure near the inboard and outboard X-points in LHD is considerably different. It is difficult for the original space-resolved spectrometer to study the edge impurity behavior at the X-point region in details because the line emissions from inboard and outboard sides are overlapped along the same observation chord. Then, the space-resolved EUV spectrometer has been altered in order to improve this situation by adding toroidal scanning mechanism.

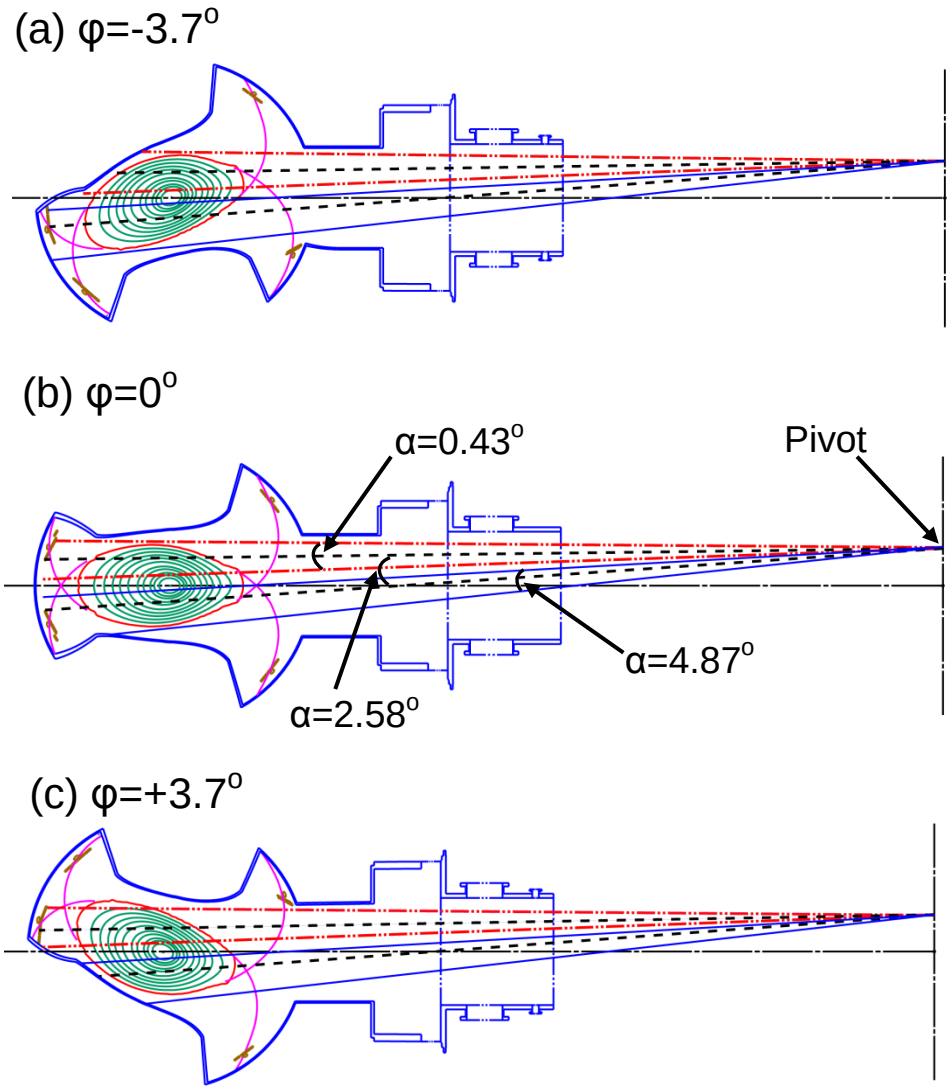

Fig. 2.6 Vertical observation ranges of space-resolved EUV spectrometer at toroidal angles of (a) φ=–3.7° (b) φ=0° (c) φ=+3.7°.

The poloidal cross sections at different toroidal angles of φ=–3.7° and +3.7° are shown in Figs. 2.6(a) and (c) with typical ranges of the observation chord, respectively. It is clearly seen that each observation chord passes through only one side of the two X-point regions. In particular, the spatial resolution for studying the impurity transport at the X-point is fairly improved in the outboard side X-point, i.e., upper observation chords at large negative toroidal angle (see Fig. 2.6(a)) and lower observation chord at large positive toroidal angle (see Fig. 2.6(c)), since the observation chords at the two sections are not limited by the diamond-shaped LHD port (see Fig. 2.5). On the other hand, the measurement of the inboard side X-point region is improved only in the lower observation chords at large negative toroidal angle (see Fig. 2.6(a) because the upper observation chords at large positive toroidal angle is hided by the vacuum vessel (see Fig. 2.6(c)). In the present two-dimensional measurement of the line emissions, the horizontal angle of θ is scanned during single LHD discharge fixing the vertical angle. In order to observe the full vertical image of impurity line emissions we need the toroidal scan at least three times at different positions in vertical angle of α, as the vertical observation range is limited by the size of CCD.

2.3. Positional calibration of observation chords

A toroidal slit consisting of two large plates with sizes of 1 m vertical height and 0.5 m horizontal width is placed between the plasma and the EUV spectrometer at which the position is 9965 mm away from the LHD torus center and 3089 mm away from the entrance slit (see Fig. 2.3). The toroidal slit can be horizontally moved to adjust an opening area defined by the two slit plates. A series of rectangular-corrugated edge with an opening periodically varied along 1010 mm long vertical length is attached to one of the two slit plates. A part of the rectangular-corrugated edge in the toroidal slit is shown in Fig. 2.7. The horizontal width of the rectangular corrugation is 20 mm, and the vertical width of the opening is periodically changed from 2 mm to 9 mm to identify each

observation chord. The projected image of the rectangular-corrugated edge can be observed by the CCD when the opening area of the toroidal slit is adjusted to 20 mm in horizontal width.

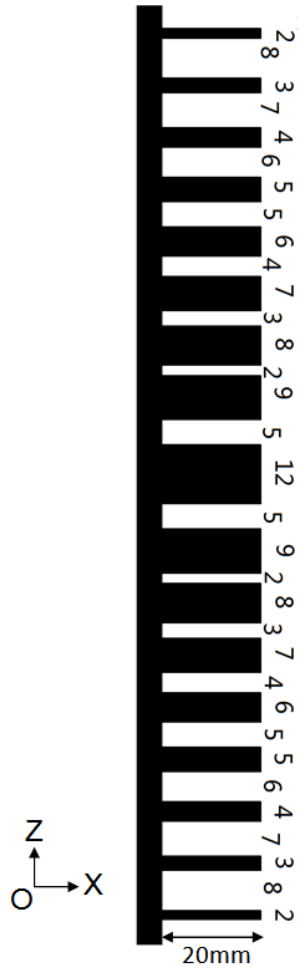

Fig. 2.7 Schematic drawing of toroidal slit with rectangular-corrugated edge installed between LHD plasma and EUV spectrometer.

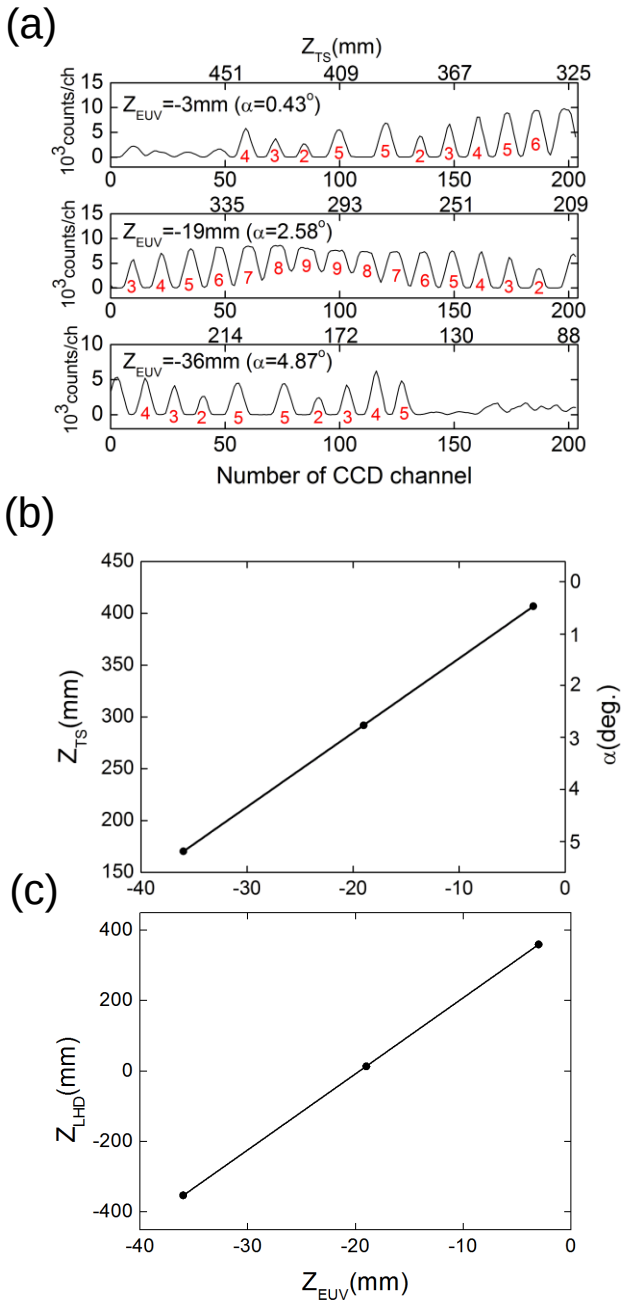

Fig. 2.8 (a) Calibration of vertical angle against observation chords of space-resolved EUV spectrometer and (b) vertical position of central observation chord at toroidal slit, Z_{TS}, and (c) at LHD plasma, Z_{LHD}, with magnetic axis position of R_{ax}=3.75 m as a function of moving distance at vertical screw bolt of EUV spectrometer, Z_{EUV}. Numbers under peak signals in (a) indicate the toroidal slit opening width shown in Fig. 2.7.

Figure 2.8(a) shows the projection of the rectangular-corrugated slit for three different values in vertical position of the EUV spectrometer, Z_{EUV}, i.e., Z_{EUV}=-3 mm (top), Z_{EUV}=-19 mm (middle) and Z_{EUV}=-36 mm (bottom). Here, the vertical position of Z_{EUV} is given by the distance along a vertical screw bolt which is rotated by a stepping motor to scan the vertical angle. The value of Z_{EUV}=0 mm denotes the horizontal position of α=0°. The three different observation ranges in positions of Z_{EUV}=-3, -19 and -36 mm in Fig. 2.8(a) are indicated for the horizontally elongated plasma cross section of φ=0° in Fig. 2.6(b) as α=0.43°, 2.58° and 4.87°, respectively. The numerals denoted at each intensity peak in the three traces of Fig. 2.8(a) indicate the opening width of the rectangular-corrugated slit shown in Fig. 2.7. The CCD channel number at the center of the intensity profile denoted with each numeral corresponds to the center of the opening at each rectangular slit. Thus, the number of CCD vertical channel can be connected with the vertical position of the toroidal slit. There are no enough signals at upper observation chords (#1≤N_{CCD}≤#50) in the top trace and at lower observation chords (#140≤N_{CCD}≤#200) in the bottom trace of Fig. 2.8(a). It should be noticed here that such observation chords are positioned outside the plasma as shown in Fig. 2.6(b). The vertical position of each observation chord at the toroidal slit, Z_{TS}, determined with the rectangular-corrugated slit is shown in the top of three traces. The relation between the Z_{EUV} and Z_{TS} is plotted in Fig. 2.8(b) for central observation chord passing through the CCD channel number of N_{CCD}=#102. The vertical angles of all the observation chords can be calibrated based on the present method. The Z_{EUV} is thus converted to the vertical position in the LHD plasma, Z_{LHD}. The result is plotted in Fig. 2.8(c) for the plasma axis position of R_{ax}=3.75 m.

Horizontal position of the EUV spectrometer is scanned by a horizontal stepping motor, as seen in Fig. 2.3(b). Here, we also define the horizontal position of the spectrometer, Y_{EUV}, with the distance along a horizontal screw bolt as well as the case of vertical position, Z_{EUV}. The toroidal slit is also used to calibrate the horizontal position of observation chord of the EUV spectrometer. In the calibration, the toroidal slit is fixed at

certain horizontal position with a narrow opening, and then the EUV spectrometer is scanned by the horizontal stepping motor during a single discharge. The horizontal angle of the observation chord can be determined by a horizontal position where the spectral intensity reaches the maximum. The relation between the Y_{EUV} and the horizontal position at toroidal slit, Y_{TS}, is examined by changing the toroidal slit position. The result is plotted in Fig. 2.9(a). Since the acceleration and deceleration of the stepping motor are sufficiently fast compared to the CCD sampling time of 200 ms, the horizontal movement of EUV spectrometer can be considered as a linear function of time as seen in Fig. 2.9(a).

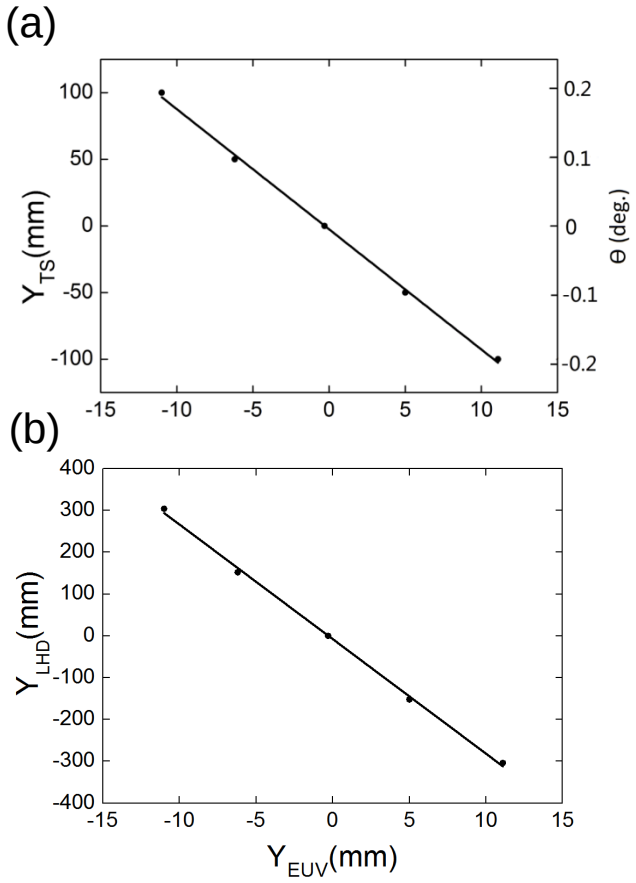

Fig. 2.9 Horizontal position of central observation chord (a) at toroidal slit, Y_{TS}, and (b) at LHD plasma, Y_{LHD}, with magnetic axis position of R_{ax}=3.75 m as a function of moving distance at horizontal screw bolt of EUV spectrometer, Y_{EUV}.

In the present EUV spectrometer a compact He-Ne laser is installed on the backside of grating to check the observation chord. The position of laser light is aligned through the mirror reflection on the grating called zero-th-order light by adjusting two small flat mirrors to visualize the optical axis connecting the grating center and entrance slit. Therefore, we also use the laser light to examine the position of the observation chord. Here, the value of Y_{TS}=0 means the central horizontal chord connecting the LHD port center and the torus center. The relation between the stroke of the horizontal screw bolt and the horizontal distance at LHD plasma, Y_{LHD}, is thus obtained by considering the magnification in the viewing angle determined from geometric relation among the spectrometer, the toroidal slit and the LHD plasma. The result is shown in Fig. 2.9(b).

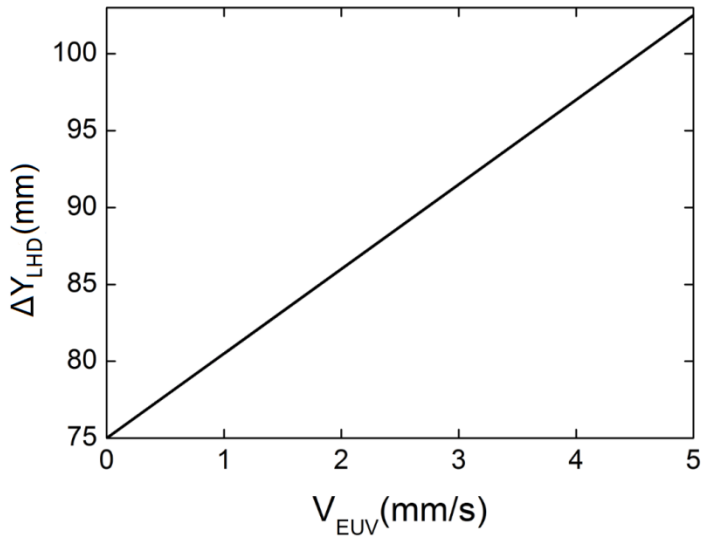

Fig. 2.10 Spatial resolution in horizontal direction, ΔY_{LHD}, as a function of scanning velocity of EUV spectrometer, V_{EUV}.

The spatial resolution in the toroidal direction is a function of the speed in horizontal spectrometer scan, while the original resolution is 75 mm at the plasma center. The spatial resolution at plasma center, ΔY_{LHD}, calculated from the horizontal scanning

speed, V_{EUV}, is plotted in Fig. 2.10. The spectrometer is usually scanned at relatively high speed of V_{EUV}=3-5 mm/s, which is basically determined by the length of discharges. The spatial resolution is then lowered by 10-30% from the original resolution.

2.4 Experimental results

In LHD, the discharge is generally initiated by electron cyclotron heating (ECH), while it can be started up by tangentially injected negative-ion-source based neutral beam (N-NBI) with high energy of 180 keV through the ion collision ionization. The LHD discharges in density range of 10^{13}-10^{15} cm^{-3} are mainly sustained and heated by three N-NBIs with total input power up to 20 MW. The ECH with injection power up to 4 MW and perpendicularly injected 40 keV positive-ion-based neutral beams (P-NBI) with total input power up to 10 MW are used for electron and ion heating in low-density range less than 10^{13} cm^{-3}, respectively. The pulse length of N-NBI is normally limited to 3 s due to the high heat load of several components in the ion source. As a special case the N-NBI operation can be extended up to 10 s with reduced input power. The present space-resolved EUV spectrometer, on the other hand, requires at least a stable discharge during 6 s for scanning the whole toroidal angle, even if it is scanned with the maximum horizontal speed of V_{EUV}=5 mm/s, because the toroidal distance longer than ΔY=600 mm has to be moved in a single discharge (see Fig. 2.9(b)).

In order to make the discharge length longer, therefore, the N-NBI is connected tandem, as shown in Fig. 2.11. Each of two N-NBIs is mainly operated at 4 s pulse length after plasma initiation by ECH. The discharge is made at magnetic axis position of R_{ax}=3.75 m and toroidal magnetic field strength of B_t=2.64 T. However, the maintenance of stable discharge is not easy in the tandem operation, in particular, at the period in which two N-NBIs are overlapped at the middle of discharges. The line-averaged electron density, n_e, measured by far infrared interferometer gradually increases in the second N-

NBI phase, while the central electron temperature, T_e, measured by YAG laser Thomson scattering gradually decreases in the same period. After turning off the second N-NBI at t=7.8 s the third N-NBI is injected during short time interval of 1.5 s. The EUV spectrometer is horizontally scanned from t=1.4 s to 7.4 s. During the toroidal scan the density and the temperature are ranged in $4.5\text{x}10^{13} \le n_e \le 7.5\text{x}10^{13}$ cm^{-3} and $1.0 \le T_e \le 1.5$ keV, respectively. The full two-dimensional distribution of edge impurity line emissions are measured with three different discharges in which upper (α=0.43°), middle (α=2.58°) and lower (α=4.87°) parts of LHD plasmas are observed with three different vertical angles. Fig. 2.12 and 2.13 show the two-dimensional distributions of CIV (312.4 Å) and HeII (303.78 Å), respectively (see Figs. 2.6 and 2.8). The images from upper, middle and lower halves of plasmas are obtained by scanning the EUV spectrometer in ranges of Y_{EUV}=-20 mm - 10 mm, -16 mm - 14 mm and -14 mm - 16 mm, respectively. All the images are plotted as the projection on X=3.75 m plane which is equal to the magnetic axis position of R_{ax}=3.75 m.

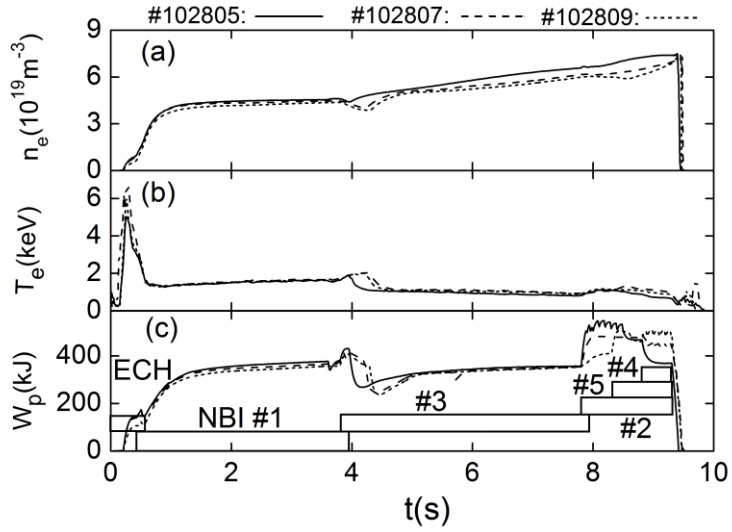

Fig. 2.11 Waveform of LHD discharges with tandemly connected NBIs; (a) line-averaged electron density, (b) central electron temperature and (c) plasma stored energy.

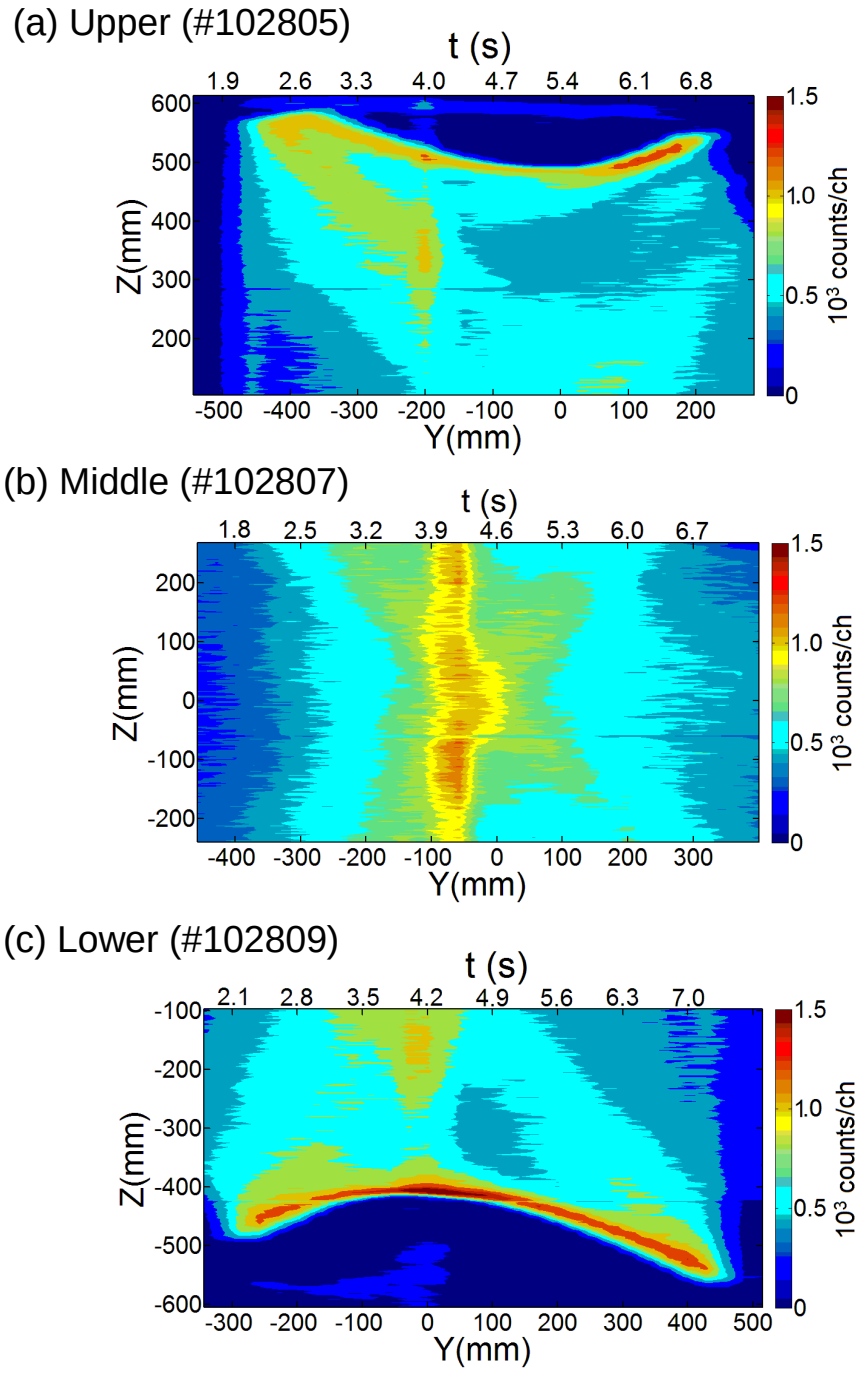

Fig. 2.12 Two-dimensional images of CIV (312.4 Å: 3p-2s); (a) upper position (α=0.43°), (b) middle position (α=2.58°) and (c) lower position (α=4.87°).

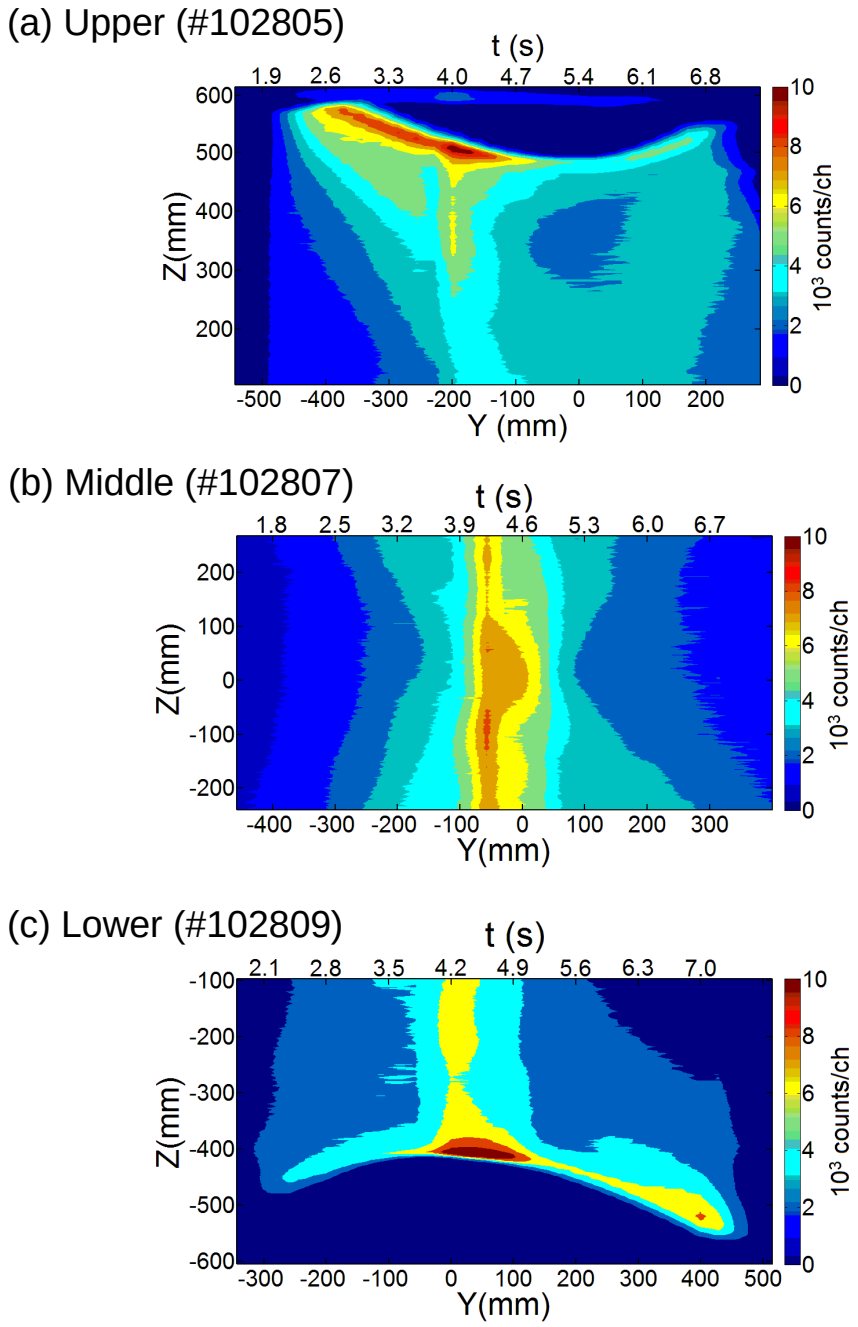

Fig. 2.13 Two-dimensional images of HeII (303.78 Å: 2p-1s); (a) upper position (α=0.43°), (b) middle position (α=2.58°) and (c) lower position (α=4.87°).

When the NBI is switched from #1 beam to #3 beam, the plasma parameters are considerably changed during the switching phase, as seen in Fig. 2.11. The intensity of CIV at t=3.9-4.2 s apparently increases in all the three figures of Fig. 2.12, in particular, it is enhanced in Fig. 2.12(b). Therefore, the strong CIV intensity seen at the NBI switching phase involves the effect of changed plasma parameters. In Fig. 2.12(a), the image of CIV is disappeared at upper right (Y≥200 mm) and lower left (Y≤-300 mm) corners due to the diamond shape of the LHD port (see Fig. 2.5). This effect is also seen in Fig. 2.12(c). Weak signals are recorded outside the CIV image, e.g., upper range of Z≥600 mm at Y=–100 mm in Fig. 2.12(a) and lower range of Z≤-430 mm at Y=0 mm in Fig. 2.12(c). These seem to be the reflection light from inner surface of the spectrometer port.

The two-dimensional distribution of HeII (303.78 Å) shown in Fig. 2.13 is entirely different from the CIV image, while the ionization energy of HeII (E_i=54 eV) is very similar to that of CIV (E_i=64 eV). The HeII intensity is much stronger than the CIV intensity, whereas no He gas puffing is done in the present discharges. The He gas has been probably stored in plasma facing components through several He discharges, He-glow discharge cleaning and ICRF long pulse operation with He majority ions. Since the intensity of HeII is strong, the EUV emission reflected from inner surface of the vacuum chamber is disappeared in the plots, whereas the effect of the NBI switching phase is still visible during t=3.9-4.2 s. The strongest HeII emissions are located at upper edge in toroidal position of -500≤Y≤–100 mm (see Fig. 2.13(a) and Fig. 2.6(c)) and at lower edge in horizontally elongated plasma cross section of 0≤Y≤100 mm (see Fig. 2.13(c) and Fig. 2.6(b)). The singly ionized carbon ion released from divertor plates travels along stochastic magnetic field lines in the ergodic layer and ionized to a next charge state during the travel. The CIV emitted from C^{3+} ions is then located in the edge boundary of the ergodic layer. Therefore, the image of CIV indicates the parallel transport in the ergodic layer. In the case of He, however, the HeII image suggests the He pressure distribution in the vacuum vessel of LHD because the radial position of HeII is a little inside compared to that of CIV, while the ionization energy of HeII is smaller than that of CIV [14]. At

present, critical explanation is difficult since the images include considerably large uncertainties based on a temporal change and shot-to-shot difference in discharge conditions.

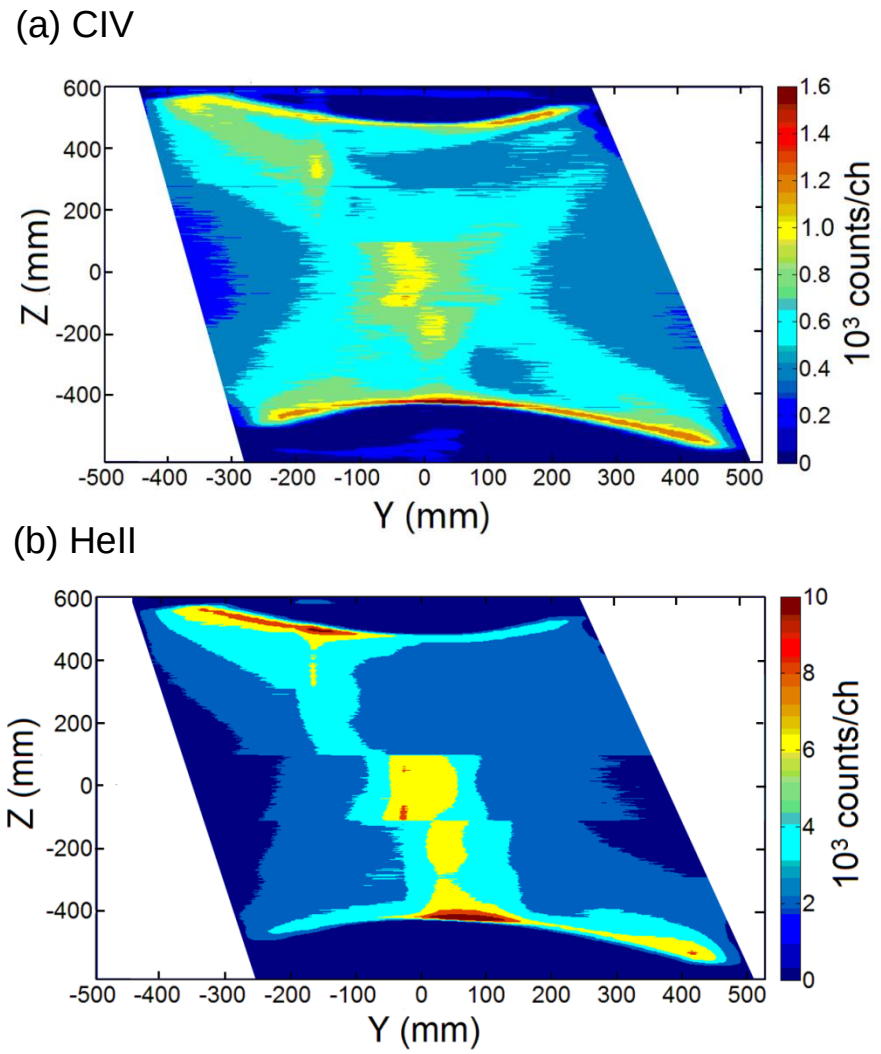

Fig. 2.14 Full two-dimensional images of (a) CIV (312.4 Å: 3p-2s) and (b) HeII (303.78 Å: 2p-1s) combined with three partial images of Figs. 2.12 and 2.13, respectively.

The full image of two-dimensional distribution is reconstructed by connecting three partial images plotted in Figs. 2.12 and 2.13. The reconstructed full images of CIV and HeII are shown in Figs. 2.14 (a) and (b), respectively. The outline of the image shows a fairly good agreement with the diamond-shaped LHD port. In the case of CIV the trace of X-points can be weakly seen from top-left to bottom-right for outboard X-point and from bottom-left to top-right for inboard X-point. In the case of HeII, however, any indication on the X-points can not be entirely seen in the figure.

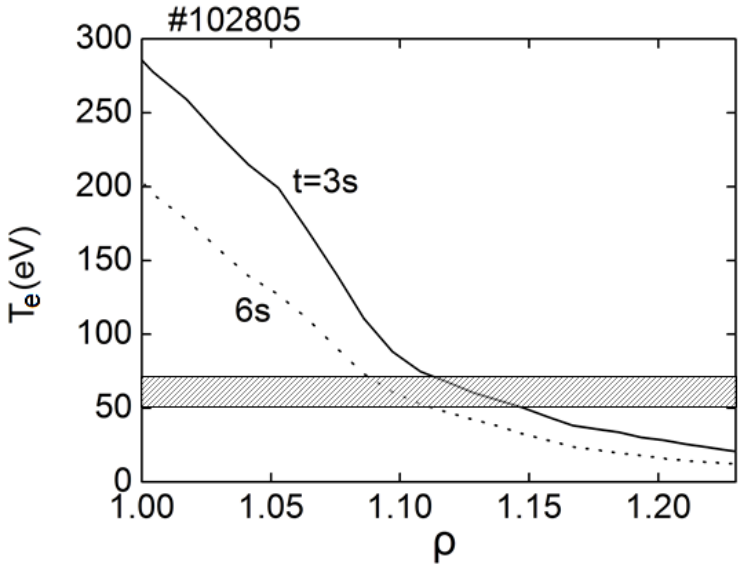

Fig. 2.15 Electron temperature profiles at t=3 s and t=6 s in ergodic layer. Radial location of CIV is suggested with shaded area.

The C^{3+} ion emitting CIV 3p-2s line exists in the farthest edge in the ergodic layer, since the C^{+} and C^{2+} ions are ionized up to the C^{3+} ion before arriving at the edge boundary in the ergodic layer. Therefore, the CIV line is emitted from a narrow edge range in the ergodic layer corresponding to the ionization energy of 64 eV. The edge electron temperature profiles measured by YAG Thomson scattering are plotted in Fig. 2.15 at t=3 s

(solid line) and 6s (dotted line) in discharges shown in Fig. 2.11. The CIV exists in the narrow temperature range of 50 eV≤T_e≤70 eV indicated with shaded area in the figure. It corresponds to the radial range of 1.11≤ρ≤1.15 at 3 s and 1.09≤ρ≤1.11 at 6 s.

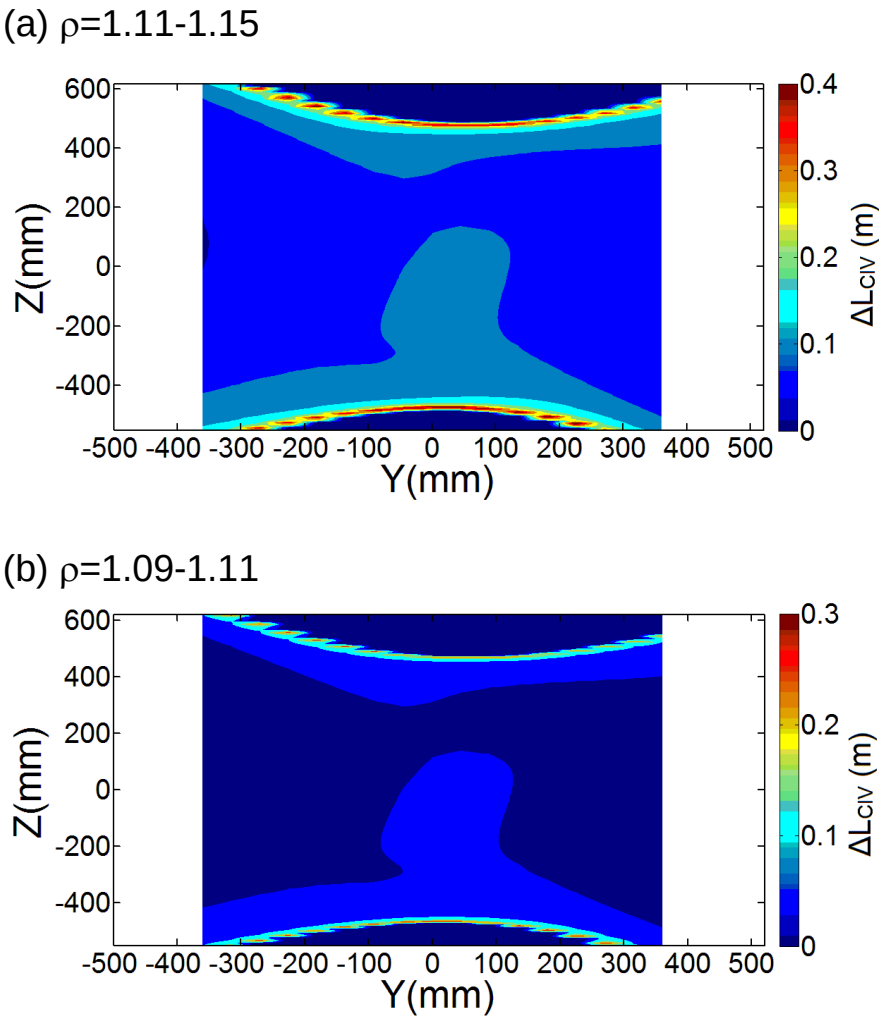

Fig. 2.16 CIV chord length calculated from shaded area in Fig. 2.15 at t=3 s (1.11≤ρ≤1.15) and (b) t=6 s (1.09≤ρ≤1.11).

The chord length of CIV emission, ΔL_{CIV}, is calculated for each observation chord based on the Fig. 2.15 in order to compare with the experimental result. The calculated results are shown in Fig. 2.16. Here, the magnetic surface structure calculated with variation moments equilibrium code (VMEC) and measured pressure profile is simply extended to the outside of LCFS with keeping similar structure. The calculation suggests that the CIV chord lengths along the toroidal direction at upper and lower edges distribute in similar ranges, i.e., ΔL_{CIV}=0.3-0.4 m in Fig. 2.16(a) and ΔL_{CIV}=0.2-0.3 m in Fig. 2.16(b). Therefore, the nonuniform intensity distributions seen in the two-dimensional distributions of CIV and HeII in Fig. 2.14 indicate the nonuniformity of the impurity density in the ergodic layer based on the three-dimensional structure of stochastic magnetic filed in addition to the nonuniformity of the edge plasma parameters.

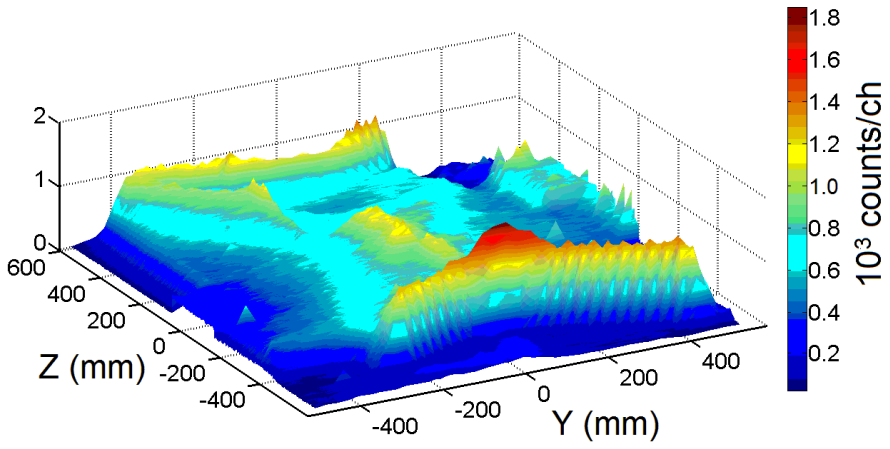

Fig. 2.17 Three-dimensional plot of CIV (312.4 Å: 3p-2s) line emission.

Fig. 2.14(a) is finally re-plotted with three-dimensional axes, as shown in Fig. 2.17. The nonuniformity in the CIV emission is clearly seen at the edge of the ergodic layer in

the three-dimensional plot. The trace of the outboard side X-point is also seen, whereas the trace of the inboard side X-point is very weak. It seems to reflect the difference in the number of magnetic field lines directly connecting inboard and outboard X-points to divertor plates.

2.5 Summary

Two-dimensional diagnostics using a space-resolved EUV spectrometer installed on LHD has been developed by adding a toroidal scanning mechanism of the observation chord. The purpose of the present diagnostics is to study the impurity transport in the ergodic layer consisting of stochastic magnetic filed. The basic function and characteristics on the two-dimensional measurement are examined using a toroidal slit with rectangular-corrugated edge installed between the LHD plasma and EUV spectrometer. The result shows good vertical and horizontal spatial resolutions of 10-15 mm and 75-100 mm, respectively, while the values depend on the spatial-resolution slit width and the horizontal scanning velocity. The two-dimensional measurement is tested using CIV (312.4 Å: 3p-2s) and HeII (303.78 Å: 2p-1s) EUV lines. The two-dimensional images of CIV and HeII with observation area of 1200mm in vertical direction and 1000 mm in horizontal direction are successfully observed from the ergodic layer of LHD with good signal-to-noise ratio showing nonuniform intensity distribution as expected. In LHD, the C^{2+} (E_i=48 eV) and C^{3+} (E_i=64 eV) ions exist in the divertor legs and the ergodic layer, respectively, and the C^{4+} (E_i=392 eV) and C^{5+} (E_i=490 eV) ions with higher ionization energies are located near LCFS. When the two-dimensional image of carbon emissions from all the ionization stages can be measured in steady state discharges of LHD, the study on the impurity transport in the stochastic magnetic filed layer will be much improved, since it was formerly studied using one chord-integrated signal based on a normal EUV spectrometer without any spatial resolution [15].

References

[1] H. Nozato, et al., Rev. Sci. Instrum. **74**, 2032 (2003).

[2] D. M. Thomas, et.al, Fusion Sci. Technol. 53, 487 (2008).

[3] W. Biel, et al., Rev. Sci. Instrum. **75**, 3268 (2004).

[4] R. J. Fonck, et al., Appl. Opt. **21**, 2115 (1982).

[5] J. K. Lepson, et al., At. Mol. Opt. Phys. **43**, 144018 (2010).

[6] M. B. Chowdhuri, S. Morita, and M. Goto, Appl. Opt. **47**, 135 (2008).

[7] M. B. Chowdhuri, et al., Rev. Sci. Instrum. **78**, 023501 (2007).

[8] D. Content, et al., Rev. Sci. Instrum. **57**, 2041 (1986).

[9] A.Nudelfuden, R. Solanki, and H. W. Moos, Appl. Opt. **24**, 789 (1985).

[10] C. Dong, et al., Rev. Sci. Instrum. **81**, 033107 (2010).

[11] T. Morisaki, et al., J. Nucl. Mater. **313**, 548 (2003).

[12] M. Kobayshi, et al., J. Plasma Fusion Res. **3**, 1005 (2008)

[13] M. Goto, et al., Fusion Sci. Technol. **58**, 394 (2010).

[14] C. Dong, et al., Phys. Plasmas **18**, 082511 (2011).

[15] M. B. Chowdhuri, et al., Phys. Plasmas **16**, 062502 (2009).

Chapter 3

1- and 2-D distributions of impurity line emissions

3.1 Introduction

Spectroscopy has been widely used in studies of magnetically confined fusion plasmas as a reliable tool to diagnose impurity species, electron and ion temperatures, plasma rotation, rotational transform and so on [1]. The impurity transport has also been studied using spectroscopic methods. In order to study the impurity transport in both the edge and core plasmas, extreme ultraviolet (EUV) spectroscopy is particularly important because most of the spectral lines emitted from low- and high-Z impurity ions exist in the EUV range with strong intensity [2].

Large Helical Device (LHD) is a superconducting fusion device with poloidal/toroidal period numbers of 2/10, a major radius of 3.6 m and an averaged minor radius of 0.64 m [3]. The magnetic geometry of LHD is a three-dimensional structure due to the absence of toroidal symmetry. Many types of spectrometers working in visible, VUV and EUV ranges are installed on LHD to monitor the impurity behavior and to study the impurity transport [4]. Two flat-field EUV spectrometers called EUV_Short and EUV_Long with a varied line spacing (VLS) groove holographic grating were developed in LHD to monitor the impurity behavior in wavelength ranges of 10-130 Å and 50-500 Å, respectively [5,6]. A space-resolved EUV spectrometer working in 60-400 Å was also

developed for measuring the one-dimensional vertical profile of impurity line emissions at a horizontal elongated cross section in LHD. The vertical profile has been observed with an excellent spatial resolution [7]. Recently, the space-resolved EUV spectrometer has been upgraded to observe the two-dimensional distribution of impurity lines emitted from edge stochastic magnetic field layer, so called ergodic layer, with extension of working wavelength range to 30-650 Å. In this chapter, one and two-dimensional distributions of impurity line emissions are briefly presented.

3.2 Experiment setup

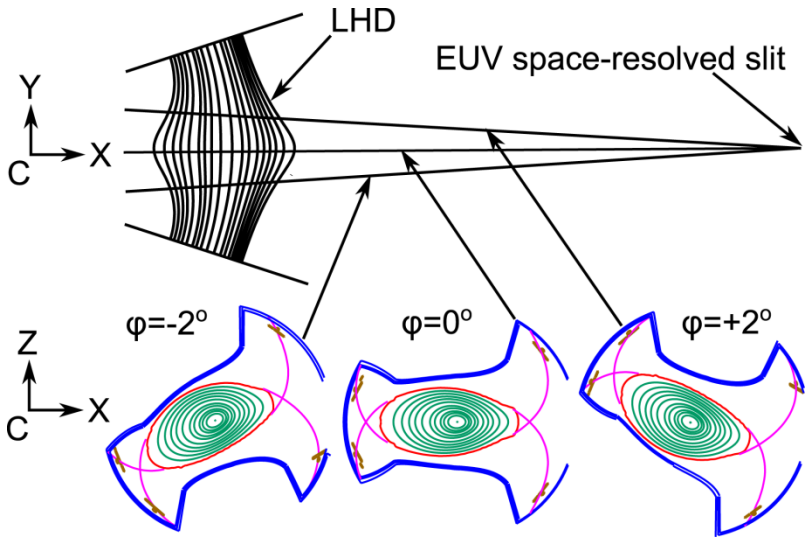

Fig. 3.1 Poloidal cross sections of LHD plasma against three different observation chords of space-resolved EUV spectrometer. Symbol denoted with "C" means torus center.

A schematic drawing of different poloidal cross sections observed by the space-resolved flat-field EUV spectrometer is shown in Fig. 3.1. The EUV spectrometer is placed at distance of X=13052 mm from the torus center along major radius direction (Y=0), denoted with "C". Then, the observation chord with a horizontal angle of φ=0° passes through the toroidal position of horizontally elongated plasma cross section, while the elliptical plasma poloidally rotates five times in one toroidal turn. The spectrometer evacuated by a magnetically floating turbo molecular pump is maintained in the order of 10^{-8} torr. The space-resolved EUV spectrometer has been recently upgraded to the two-dimensional diagnostic by adding a stepping motor, with which the observation chord can be horizontally scanned during a stable discharge. The two-dimensional distribution is recorded by scanning the observation chord between φ=-7° – +7°, of which the angles are limited by the LHD #1-O diamond port and the rectangular port of vacuum vessel extension between the LHD and the spectrometer. Since the elliptical plasma cross section rotates with the horizontal angle, the X-point structures at inboard and outboard sides can be separately observed as seen in the cross sections denoted with φ=-2° and φ=+2° in Fig. 3.1.

The space-resolved EUV spectrometer mainly consists of an entrance slit, a spatial resolution slit placed in front of the entrance slit, a gold-coated varied-line-spacing (VLS) holographic grating and a back-illuminated charge-coupled device (CCD) detector with 1024 × 255 pixels, which is usually operated at -20°C. The reflectivity at shorter wavelength range shorter than 200 Å was increased and the stray light was also reduced together with higher order light by adopting the laminar-type holographic grating with an effective area of 26 mm in groove length and 46 mm in groove distance. The concave VLS grating (1200 grooves/mm) with angle of incidence of 87^{o} creates approximately a flat focal plane in a considerably wider range of the wavelength. A CCD (1024 x 255 pixels) is used as the detector which can be moved along the wavelength dispersion in the focal plane by a stepping motor to cover the wavelength range 60-400 Å. The wavelength range was limited by the inside structure of the spectrometer. Then, a second stage for

scanning the wavelength range is added to the original stage to extend the wavelength range to 30-650 Å. Although the excellent flat focal image is not theoretically guaranteed in the extended wavelength ranges of 30-60 Å and 400-650 Å, no problem appears in the practical use. The EUV line emissions can be measured with sufficient spectral resolution even in the extended wavelength ranges.

The spectral resolution of 0.22 Å is obtained at 200 Å in the full image mode of CCD data acquisition. The vertical spatial resolution of 10 mm is obtained when the spatial resolution slit of 0.2 mm in width is used. It is noticed that a good spatial resolution is necessary for the edge impurity measurement since the plasma parameters quickly change as a function of radial position. In the present study, the spatial resolution slit of 0.5 mm in width is adopted to increase the intensity of impurity line emissions. The vertical spatial resolution is, however, still good, i.e., 15 mm. The sampling time and the binning mode of CCD are set to 200 ms and 5 pixels in the present study, respectively. Although the spatial resolution in the toroidal direction is originally 75 mm at the plasma center, it is also a function of the CCD exposure time and the horizontal scanning speed of EUV spectrometer. The EUV spectrometer is generally scanned at relatively high speed of 3-5 mm/s, which is mainly determined by the discharge duration.

In LHD the core plasma inside last closed flux surface (LCFS) is surrounded by a thick ergodic layer due to the presence of higher-order Fourier components in magnetic fields created by a pair of helical coils. The structure of ergodic layer in horizontally elongated cross section ($\varphi=0^{o}$) at magnetic axis position of R_{ax}=3.6 m is shown in Fig. 3.2. The position of LCFS in LHD is defined by the outermost flux surface on which the deviation of the magnetic field line is less than 4 mm while it travels 100 turns along the torus [8]. The ergodic layer mainly consists of stochastic magnetic field lines with lengths from 10 to 2000 m, which correspond to 0.5-100 toroidal turns of the LHD torus. The thickness of the ergodic layer, λ_{erg}, varies with the poloidal and toroidal angles exhibiting a complicated three-dimensional structure. The minimum thickness of ergodic layer appears at two poloidal locations near the helical coils, which are here defined as "O-point". The

λ_{erg} increases not only with R_{ax} but also with β value (≡plasma pressure/magnetic pressure) [8]. The magnetic field lines in the ergodic region are sufficiently long to confine the edge plasma, although the field lines frequently repeat radial movement during the toroidal turn. Therefore, the electron temperature and density in the ergodic layer are considerably high and range in 10-500 eV and 1-10x10^{13} cm^{-3}, respectively [9]. Outside of the ergodic layer, there exists four intrinsic divertor legs connecting the X-point region to divertor plates. The total number of field lines in the inboard X-point directly connecting to the divertor plates, which does not mean the magnetic field strength, is much larger than that in the outboard X-point, at least, in R_{ax}=3.6 m. Here, it should be pointed out that the total number of field lines near the outboard X-point directly connecting to the divertor plates increases as the R_{ax} shifts outwardly.

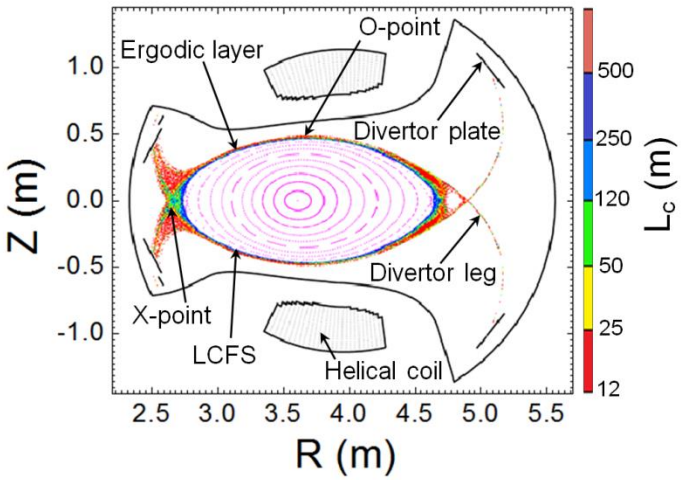

Fig. 3.2 Structures of magnetic surfaces, ergodic layer and divertor legs at R_{ax}=3.6 m in LHD. Magnetic field connection length, L_c, is expressed in different colors.

3.3 1-D distribution of impurity line emissions

The space-resolved EUV spectrometer is usually set to observe the upper half of LHD plasma at horizontally elongated plasma cross section. Fig. 3.3(a) shows a typical CCD image at wavelength range of 280-340 Å with wavelength interval of $\Delta\lambda \approx 60$ Å. The CCD (1024x255 pixels) is operated in the binning mode in which five pixels are converted into one channel. The upper half of HeII (303.78 Å) vertical profile is shown in Fig. 3.3(b). The peak position of vertical profile of HeII around Z=480 mm indicates the radial location of He^{+} (HeII) ions, showing the HeII is located in the ergodic layer. The HeII emission from Z_{LCFS}=400 mm to Z=500 mm reflects a local emission near the top O-point as seen in Fig.3.2. The HeII emission from Z=0 mm to Z=200 mm reflects a local emission in the vicinity of inboard and outboard X-points.

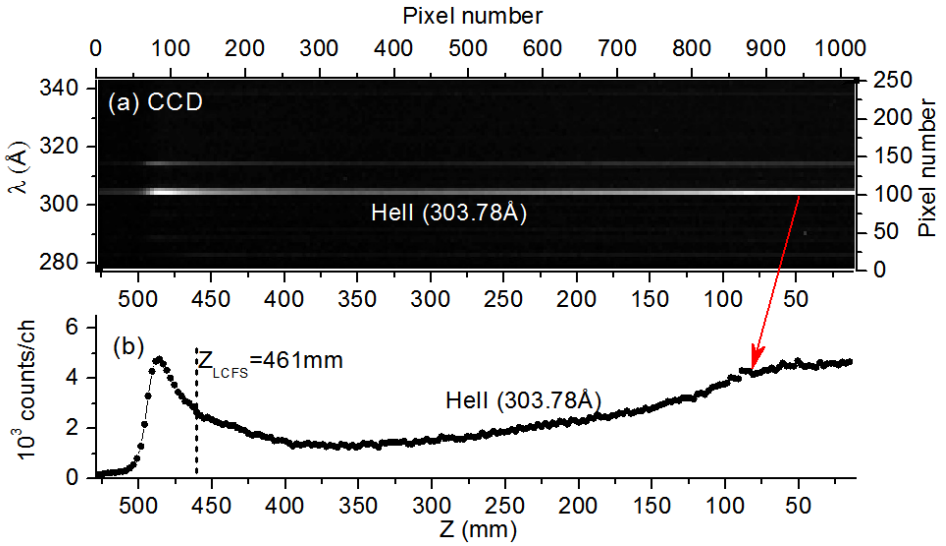

Fig. 3.3 (a) Typical CCD image in wavelength range of 280Å-340 Å and (b) upper half of HeII (303.78 Å) vertical profile. The value of Z_{LCFS}=461 mm indicates the position of last closed flux surface (LCFS) at R_{ax}=3.6 m.

Typical examples on the upper half vertical profile of impurity line emissions are shown in Fig. 3.4. The vertical profiles of HeII (303.78 Å, E_i=54 eV), CIV (312.4 Å, E_i=64 eV) and CVI (33.7 Å, E_i=490 eV) have the intensity peak in the plasma edge because their ionization energies are very small. On the other hand, the FeXX (132.85 Å, E_i=1582 eV) is located in the plasma center due to the relatively high ionization energy. Fig. 3.4(b) shows the vertical profiles of NeVI (122.5 Å, E_i=158 eV), NeVII (106.2 Å, E_i=207 eV) and NeVIII (103.1 Å, E_i=239 eV), which can be simultaneously measured due to their closed wavelengths. The edge profile structure in Fig. 3.4(b) is enlarged as plotted in Fig. 3.4(c). We clearly understand from the figure that radial location of the peak intensities is shifted inside the plasma according to the ionization energy.

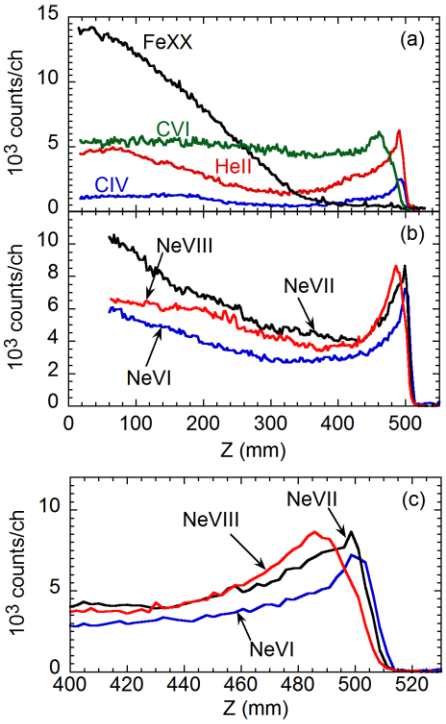

Fig. 3.4 Upper half of vertical profiles for (a) HeII (303.78 Å, E_i=54 eV), CIV (312.4 Å, E_i=64 eV), CVI (33.7 Å, E_i=490 eV) and FeXX (132.85 Å, E_i=1582 eV) and (b) NeVI (122.5 Å, E_i=158 eV), NeVII (106.2 Å, E_i=207 eV) and NeVIII(103.1 Å, E_i=239 eV) and (c) edge profiles enlarged from (b).

When the observation range at horizontally elongated plasma cross section is changed from the upper half to the lower half, the full vertical profile of impurity line emissions can be observed. Then, two discharges are at least needed to measure the full vertical profile. Figure 3.5 shows the full vertical profile of HeII and CVI which are composed of three different discharges. The two profiles of HeII and CVI show an entirely different structure. The profile seems to reflect a different magnetic field structure at radial position where the impurity ion is located. The result also indicates that the vertical profiles are asymmetric, while the HeII and CVI are emitted from different radial location of the edge boundary and the vicinity of LCFS.

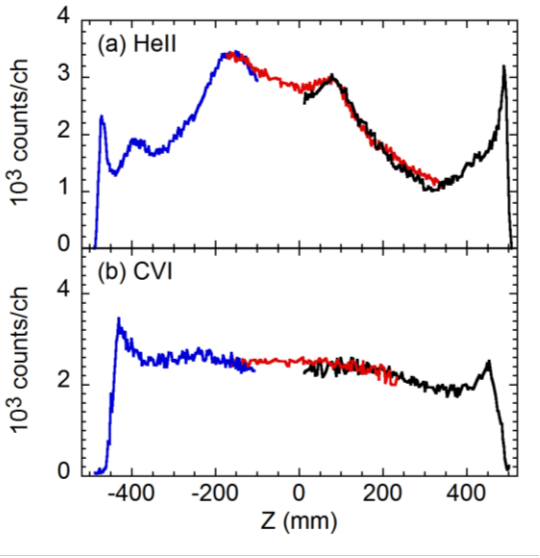

Fig. 3.5 Full vertical profiles of (a) HeII (303.78 Å, Ei=54 eV) and (b) CVI (33.7 Å, Ei=490 eV).

3.4 2-D distribution of impurity line emissions

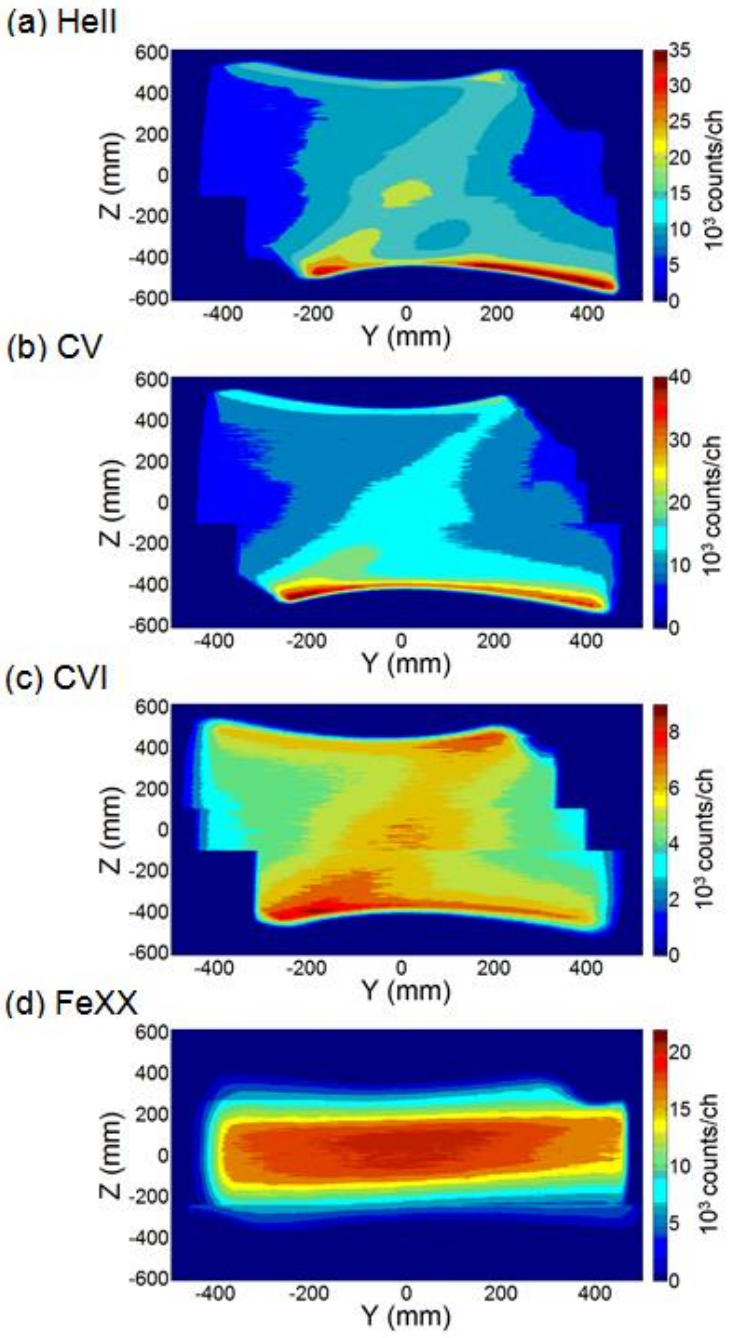

Fig. 3.6 Two-dimensional distributions of (a) HeII (303.8 Å), (b) CV (40.3 Å), (c)CVI (33.7 Å) and (d) FeXX (132.9 Å) line emissions in R_{ax}=3.6 m of LHD. Axes of Z and Y denote vertical and horizontal directions, respectively.

Steady plasmas over 10 seconds heated by the ion cyclotron range of frequency (ICRF) are used for the present measurement. In the discharges the line-averaged electron density and the central electron temperature are maintained at around $2x10^{13}$ cm^{-3} and 2 keV, respectively. The two-dimensional distributions of HeII (303.78 Å: $1s^2\ ^2S_{1/2}$ - $1s2p\ ^2P_{1/2,3/2}$), CV (40.27 Å: $1s^2\ ^1S_0$ - $1s2p\ ^1P_1$), CVI (33.73 Å: $1s\ ^2S_{1/2}$ - $2p\ ^2P_{1/2,3/2}$) and FeXX (132.85 Å: $2s^22p^3\ ^4S_{3/2}$ - $2s2p^4\ ^4P_{5/2}$) are shown in Fig. 3.6. Each figure is a superimposed of three distributions in different vertical ranges, i.e., upper, middle and lower parts of LHD plasma, which are independently recorded in different discharges by changing the vertical angle of EUV spectrometer. The small difference in line intensities among three discharges is corrected using the same line emission measured by other EUV spectrometers. The vertical position in the figure is carefully calibrated using a toroidal slit, which is placed between the LHD plasma and EUV spectrometer [10]. A series of rectangular-corrugated edge with a periodical opening is attached to the side of the toroidal slit. The vertical width of the opening changes between 2 mm and 9 mm to identify each observation chord. An image projected the rectangular-corrugated edge can be observed on the CCD detector, when the toroidal slit opens only 20 mm in horizontal width which corresponds to the size of rectangular opening.

The four impurity ions shown in Fig. 3.6 have different ionization energies of 54 eV (HeII), 392 eV (CV) and 490 eV (CVI) and 1582 eV (FeXX), respectively [11]. Since the electron temperature at LCFS ranges in 200-500 eV in low-density discharges under high-magnetic field of B_t=2.75 T, the HeII emission is located at the outside boundary in the ergodic layer and the CV and CVI emissions are located near LCFS. Seeing three images of Figs. 3.6(a)-(c) we find two important results. One is the strong intensity appeared in the bottom of the image. It seems to express certain impurity transport in the stochastic magnetic field layer. At present the reason is unclear. We need a help of simulation code on the edge plasma transport in order to examine the exact reason. The other is a trace of inboard X-point. It is clearly seen from left-bottom (Y=-200 mm and Z=-400 mm) to right-top (Y=200 mm and Z=500 mm). Compared to Fig. 3.1, one can understand that the trace is originated in the emission from inboard X-point. As mentioned

above, the number of magnetic field lines in the inboard X-point is much larger than that in the outboard X-point (also see Fig. 3.2). The present result strongly suggests the presence of higher density, at least higher impurity density, near the inboard X-point, in which the recycling through the magnetic field directly connecting to the divertor plates can be enhanced. On the contrary, the FeXX emission shows its presence in the central column of plasma. The diagonal trace related to the inboard X-point is of course disappeared from the image of FeXX.

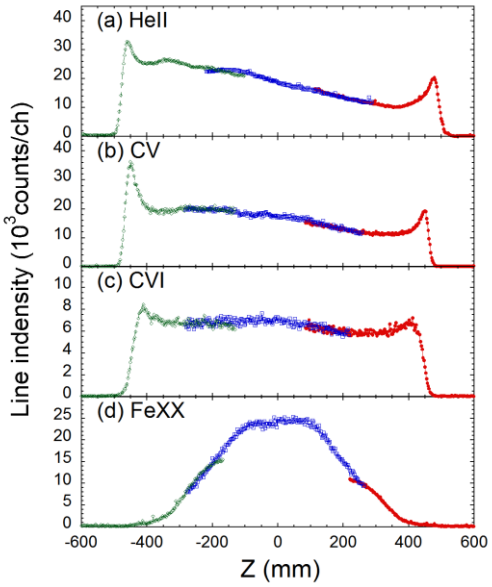

Fig. 3.7 Vertical distributions of (a) HeII, (b) CV, (c) CVI and (d) FeXX line emissions at horizontally elongated plasma cross section (Y=0 mm). Each profile is composed of three discharges traced in different colors. Positions of LCFS are Z=±461 mm at R=3.62 m.

The vertical distributions of HeII, CV, CVI and FeXX are plotted in Fig. 3.7 for observation chord looking at horizontally elongated plasma cross section (Y=0 mm). The profiles of HeII and CV show asymmetric due to the strong emission from the bottom of

LHD plasmas. However, the profile of CVI seems to be symmetric suggesting a function of magnetic surface. The FeXX profile clearly indicates a function of magnetic surface. Detailed analysis on the two-dimensional image is done in the chapter 6 using the edge transport simulation code.

The horizontal distributions of four line emissions at the equatorial plane (Z=0 mm) are also plotted in Fig. 3.8. The horizontal profiles of HeII, CV and CVI have some peaks at the toroidal position of Y=0 mm. It indicates a strong emission from inboard X-point again. The profile of FeXX is nearly constant along the horizontal direction, but the intensity slightly decreases when the horizontal position moves from Y=0 mm to Y=400 mm. It seems to reflect a difference in the plasma length along the observation chord.

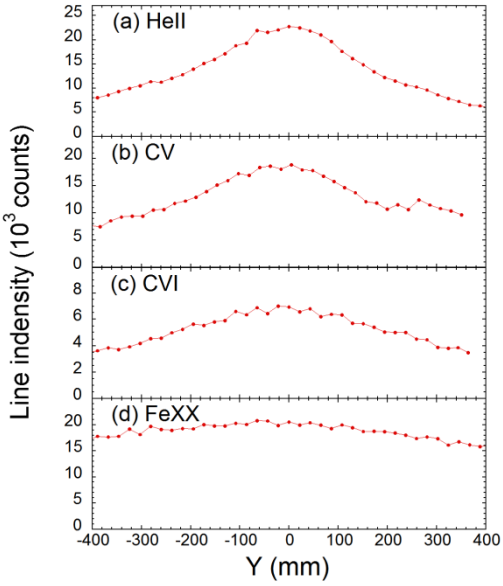

Fig. 3.8 Horizontal distributions of (a) HeII, (b) CV, (c) CVI and (d) FeXX line emissions at equatorial plane (Z=0 mm).

3.4 Summary

A space-resolved EUV spectrometer has been developed to measure the one- and two-dimensional distributions of impurity line emissions ranging in 30-650 Å. The one-dimensional distribution of impurity line emissions have been measured in the full vertical profile by scanning the vertical angle of the spectrometer. The two-dimensional images of HeII, CV, CVI located in the plasma edge and FeXX located in the plasma core are also successfully measured in steady discharges of LHD. It is found that the HeII, CV and CVI are strongly emitted at the inboard X-point, suggesting that the difference in the total number of field lines directly connecting to divertor plates between inboard and outboard X-points.

References

[1] B. C. Stratton, et al., Fusion Sci. Technol. **53**, 431(2008).

[2] N. J. Peacock, Astrophys. Space Sci. **237**, 341 (1996).

[3] A. Komori, et al., Fusion Sci. Technol. **50**, 136 (2006).

[4] M. Goto, et al., Fusion Sci. Technol. **58**, 394 (2010).

[5] M. B. Chowdhuri, et al., Appl. Opt. **47**, 135 (2008).

[6] M. B. Chowdhuri, et al., Rev. Sci. Instrum. **78**, 023501(2007).

[7] C. F. Dong, et al., Rev. Sci. Instrum. **81**, 033107 (2010).

[8] T. Morisaki, et al., J. Nucl. Mater. **313**, 548 (2003).

[9] S. Morita, et al., Plasma Phys. Controlled Fusion **48**, A269 (2006).

[10] C. F. Dong, et al., Phys. Plasma **18**, 082511 (2011).

[11] R. L. Kelly, J. Phys. Chem. Ref. Data, **16**, 1 (1987).

Chapter 4

Radial locations of HeII and CIV line emissions at different poloidal angles

4.1 Introduction

In magnetically confined fusion devices, plasma always contains impurities in addition to working gas of hydrogen isotopes or helium. The impurities usually originate in a variety of plasma facing components such as the first wall on vacuum vessel, poloidal limiter, divertor plates and radio frequency antennas [1]. The energy loss through radiation is enhanced and the fuel is diluted by the presence of impurities. Therefore, it is important to measure the impurity behavior and to understand the transport mechanism of impurities in addition to the study on the influence of impurities giving to the plasma performance.

Spectroscopy is an essential diagnostic to monitor the impurity behavior, providing measurements of ion and electron temperatures, plasma rotation, particle influx and so on [2]. Since the electron temperature in LHD ranges from a few tens of eV at plasma edge to several keV at plasma center, spectral lines from impurities are emitted in wider range of wavelength from visible to X-ray. Various types of spectrometers observing different wavelength ranges have been developed for LHD diagnostics. Recently, a space-resolved extreme ultraviolet (EUV) spectrometer is upgraded to observe the line emission at different toroidal positions of LHD plasma in addition to the extension of observable wavelength

range to 30-650 Å. Two-dimensional image of impurity line emission from several elements such as helium, carbon, neon and iron have been observed from long pulse discharges of LHD by scanning horizontally the observation chord during a discharge. HeII (303.78 Å: E_i=54.4 eV) and CIV (312.4 Å: E_i=64.5 eV) are generally used to study the edge impurity transport because of their low ionization energies, E_i, and strong line emission intensities [3]. In addition, both spectra can be simultaneously measured, since the wavelengths are very close each other. Unfortunately, hydrogen emission can not be measured with present EUV spectrometer.

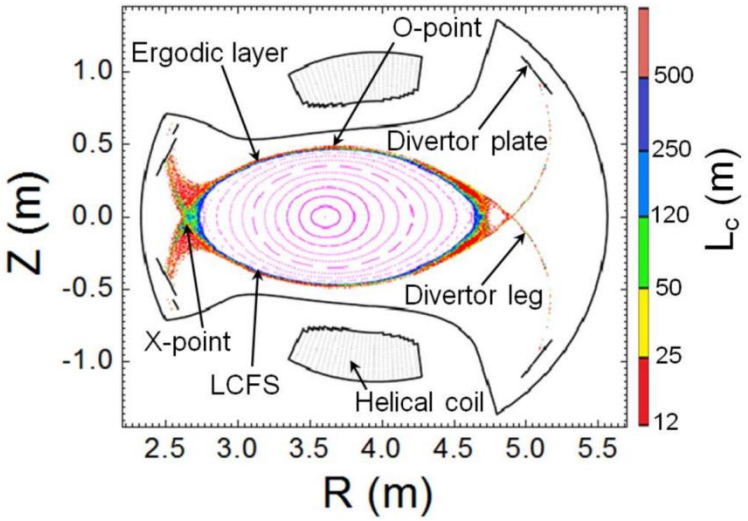

Fig. 4.1Structures of magnetic surfaces, ergodic layer and divertor legs at R_{ax}=3.6 m in LHD.

Magnetic surfaces of LHD have three-dimensional structure due to the absence of toroidal symmetry, and edge magnetic field structure is stochastic due to the presence of higher orders of Fourier component in magnetic field generated by helical coils, forming characteristic topology called ergodic layer. Therefore, the position of last closed flux surface (LCFS) in LHD is defined by the outermost flux surface on which the deviation of the magnetic field line is less than 4 mm while it travels 100 turns along the torus. The

ergodic layer surrounding the LCFS and the magnetic surfaces are shown in Fig. 4.1. The ergodic layer formed by stochastic magnetic field lines with various connection lengths of 10-2000 m becomes thicker as the magnetic axis is outwardly shifted by controlling vertical field or β (≡plasma pressure/magnetic pressure) value increases [4]. The electron temperature inside the ergodic layer typically ranges from 10 to 500 eV [5].

In reference [6], the plasma boundary near upper O-point is studied using HeII and CIV profiles at horizontally elongated plasma cross section. It is found that the peak position of CIV does not change at all in a wide range of electron temperature at LCFS ($100< T_e(\rho=1) <500$ eV) and can be used as the index of edge plasma boundary. In this chapter, the radial position of HeII estimated from the CIV peak position is analyzed against different poloidal positions. Discussion is made with neutral helium behavior.

4.2 Experimental Setup

The space-resolved EUV spectrometer consists of an entrance slit, a spatial resolution slit placed in front of the entrance slit, a varied-line-spacing (VLS) grating and a charge-coupled device (CCD) detector. The vertical spatial resolution is 10 mm when the spatial resolution slit of 0.2 mm width is used. The spectral resolution is 0.22 Å at 200 Å when the CCD is operated in full image mode [7]. In the present experiment, the spatial resolution slit of 0.5 mm is used and the CCD detector is operated in sub-image mode, by which five pixels are converted into one channel, with exposure time of 200 ms. A vertical range of nearly 53 cm can be observed with the present space-resolved spectrometer. The range corresponds to half of the plasma diameter at horizontally elongated plasma cross section (see Fig. 4.1).

A stepping motor is used to change horizontal angle, α, of the observation chord. The horizontal angle is defined by an angle measured from the central observation chord

perpendicular to toroidal magnetic field, which passes through horizontally elongated plasma cross section of LHD plasma, as shown in Fig. 4.2. The space-resolved spectrometer is usually positioned at α=0° to monitor vertical profile at upper half of LHD plasmas. When the horizontal angle is scanned around the pivot, the spectrometer observes different toroidal position. Here, the toroidal angle of φ is defined as the relation seen in Fig. 4.2. The observation chord defined with α intersects the line defined with φ at magnetic axis of plasma, R_{ax}. The relation between toroidal angle, φ, and horizontal angle, α, is plotted in Fig. 4.3. It shows a nearly linear relation because the distance between the pivot of EUV spectrometer and the plasma center is long, e.g., 9241 mm at R_{ax}=3.60 m, and the scanning range of horizontal angle is relatively small.

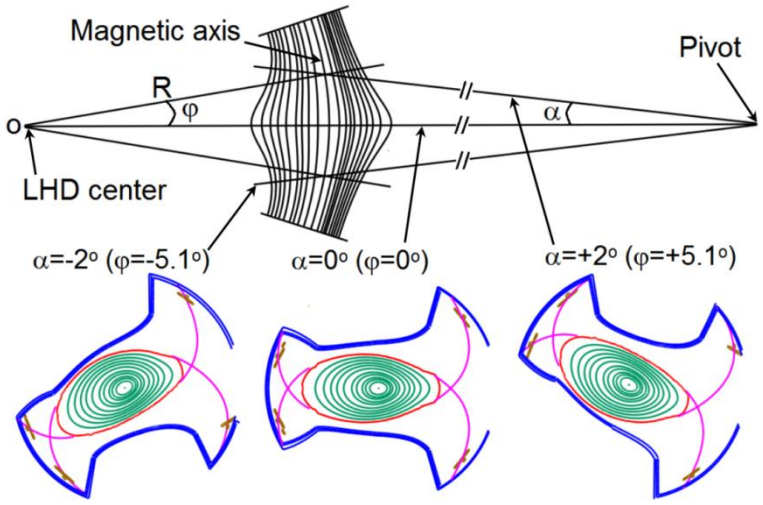

Fig. 4.2 Poloidal cross sections of LHD against three different observation chords of space-resolved EUV spectrometer.

Three cross sections of elliptical LHD plasma are also plotted in Fig. 4.2 at different horizontal angles of α= -2°, 0° and +2°, which correspond to toroidal angles of φ=-5.1°, 0° and +5.1°, respectively. The vertical profile at upper half of LHD plasma can be observed in

range of φ=-7° to +4° which is limited by diamond-shaped LHD port and rectangular spectrometer port. Therefore, the top or the bottom observation chord passing through the plasma edge can measure different poloidal location when the toroidal angle of spectrometer is scanned. In LHD, in particular, edge diagnostics is important at both the X- and O-points because magnetic field structure has a special feature at the two regions, i.e., maximized stochastic region and minimized stochastic region, respectively. When the spectrometer is positioned at $\alpha=0^{o}$, the observation chord has to pass through both of X-points at inboard and outboard sides. The change of toroidal angle in the observation chord is then necessary for individual observation of the two X-points. The spatial resolution in horizontal direction is estimated to be 75 mm.

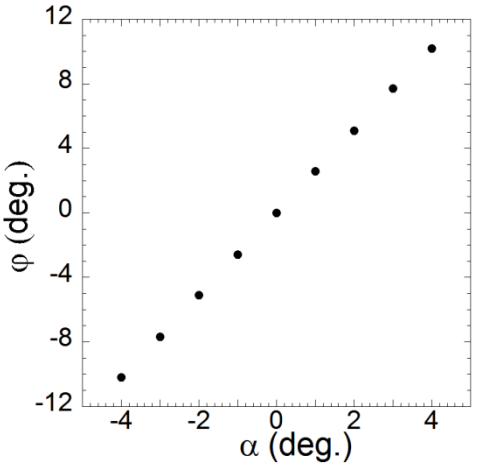

Fig. 4.3 Relation between horizontal angle, α, of observation chord and toroidal angle, φ of LHD.

4.3 Radial location of HeII and CIV line emissions

The impurity profiles are studied in discharges heated by neutral beam injection (NBI). Typical electron temperature and density profiles measured by Thomson scattering system are shown in Figs.4.4 (a) and (b), respectively. The measurement is done along

major radius direction, R, at horizontally elongated plasma cross section of φ=0°. In the NBI discharge of LHD the density profile is flat or hollow, whereas the temperature profile is always peaked except for discharges with hydrogen pellet injection. The central electron temperature ranges in 2-4 keV and the central electron density exceeds 10^{14} cm^{-3} in gas-puffed NBI discharges at high-field operation.

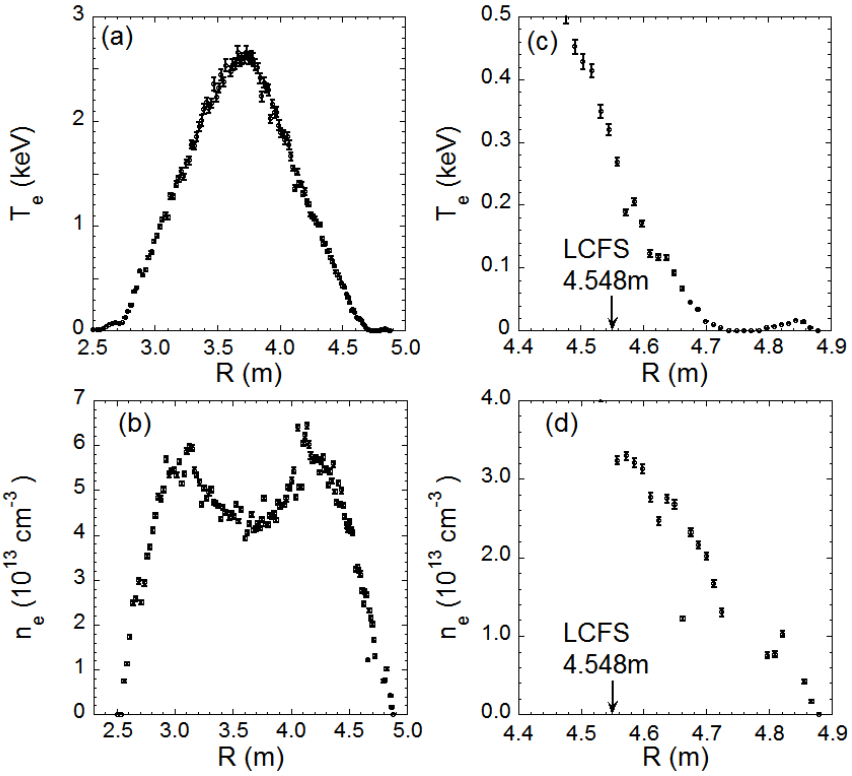

Fig. 4.4 (a) Electron temperature and (b) density profiles and enlarged edge (c) temperature and (d) density profiles at R_{ax}=3.6 m.

Edge temperature and density profiles in the outboard side are shown in Figs.4.4 (c) and (d) as the extension of Figs.4.4 (a) and (b). The position of LCFS calculated by variation moments equilibrium code (VMEC) is 4.548 m [8], which is denoted with arrow in the figure. The electron temperature and density at LCFS are 300 eV and $3.3x10^{13}$ cm^{-3}, respectively. It can be seen that high electron density, which corresponds to 10-50% of the

central density, is maintained even in the ergodic layer located outside the LCFS. Magnetic field lines are enough long to sustain such a high-density edge plasma, although the field lines are accompanied by radial deviation or diffusion in the ergodic region. Therefore, He^{+} (E_i=54.4 eV) and C^{3+} (E_i=64.5 eV) ions, which emit spectral lines of HeII and CIV, respectively, are always located in the outside edge of ergodic layer even in low-magnetic field discharges of LHD, since the ionization energies of HeII and CIV are entirely low compared to electron temperature in the ergodic layer. In LHD, the edge electron temperature profile does not change so much in most of discharges even if the operational density is changed. A few dips or flattening are seen in the edge temperature and density profiles. It is believed that they reflect island structures in the ergodic layer.

The vertical profiles of HeII and CIV in the upper half of LHD plasma are shown in Fig. 4.5 at different horizontal angles. The vertical position is carefully calibrated by a rectangular-corrugated toroidal slit placed between EUV spectrometer and LHD plasma. The profile mainly consists of two parts of edge peaked emission and emission near X-points. The emission structure near X-points is considerably complicated reflecting the presence of many islands in addition to the mixture of long and short magnetic field lines. The analysis of the emission profile near X-points is not simple, and then, the result is presented later in chapter 6. The edge peak emission forms a clear intensity peak due to a long integration of impurity emission along the observation chord. Here, the peak position is defined by the vertical position of the maximum value of HeII and CIV.

Carbon ions originated in the divertor plates made of carbon move upward through the divertor legs as shown in Fig. 4.1. The low charge states of C^{+} (E_i=24.4 eV) and C^{2+} (E_i=47.9 eV) only exist between the divertor plates and X-points because of the short ionization length, e.g., λ_i=1-2 m for C^{+} and λ_i=5-40 m for C^{2+}. The C^{3+} (E_i=64.5 eV) ion has relatively long ionization length of λ_i=40-300 m and it can reach the ergodic layer. It is reported that the peak position of CIV is not sensitive to edge electron temperature at LCFS except for extremely low temperature case [6]. Then, the position of CIV can indicate the index of edge boundary position of LHD plasmas.

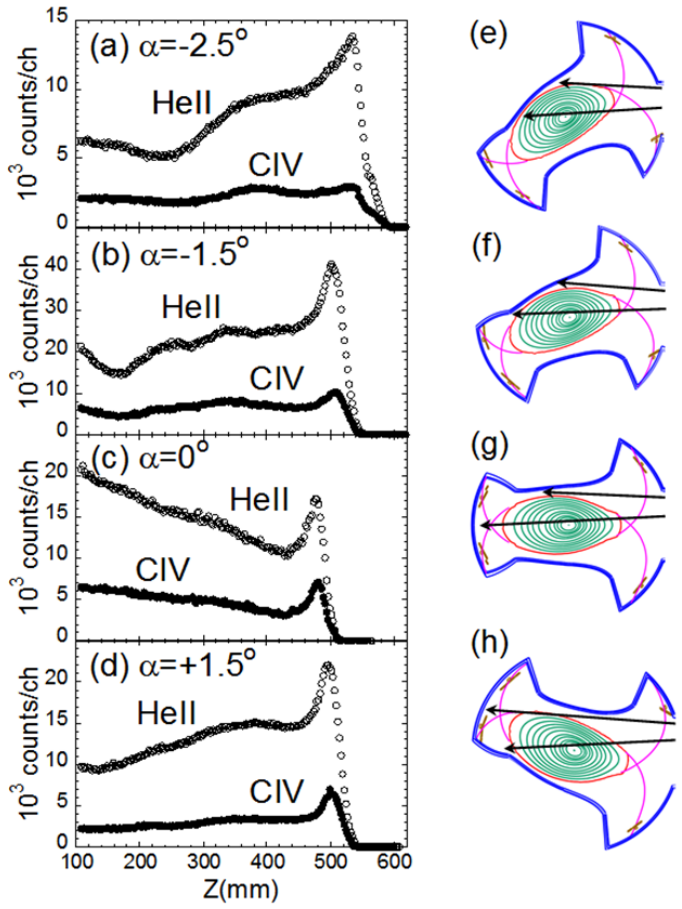

Fig. 4.5 (a)-(d) Vertical profiles of HeII (open circles) and CIV (closed circles) at different horizontal angles, α, and (e)-(h) corresponding plasma cross section. Observation range is indicated with two arrows.

On the other hand, the peak position of HeII reflects the penetration depth of neutral helium because the neutral density decays with the production of He^+ ion. This situation is clear if the peak position is compared between CIV and HeII. The peak position of HeII with lower ionization energy (E_i=54.4 eV) is located at inner side than that of CIV with

higher ionization energy (E_i=64.5 eV). If the He^+ ions originates in the recycling on divertor plates and move to the plasma edge along magnetic field lines, the HeII location should be positioned outside the CIV according to the ionization energy. Therefore, the deeper penetration of the He^+ ions indicates that the neutral helium is directly deposited in the plasma, not coming from the divertor plate. In LHD, high recycling has been observed near X-points [9], in particular, near inboard side X-point. The peak position of HeII is analyzed against different poloidal position to examine the recycling of helium neutral.

Radial location of HeII measured from the peak position of CIV is plotted in Fig. 4.6 against horizontal angle of observation chord. The poloidal position determined by the horizontal angle is also denoted in the figure (also see Fig. 4.4). It is clear from the figure that the position of HeII is located at 4 mm inside compared to the CIV position and seems to be constant against the poloidal location.

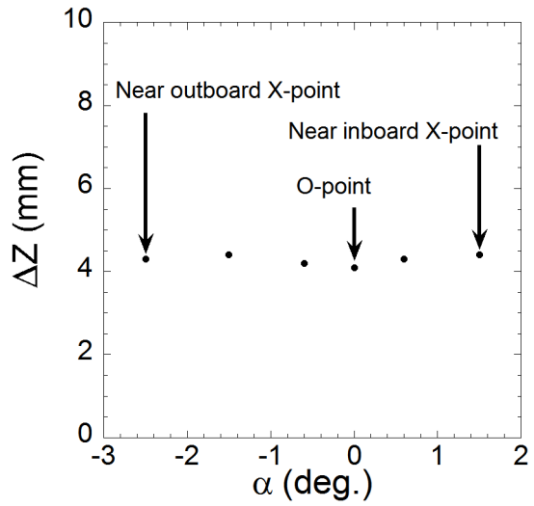

Fig. 4.6 Radial location of HeII measured from peak position of CIV against different horizontal angles.

The neutral helium density at the penetration depth, x, is given by a simple equation of

$$n_0 = n_0(0)\exp[-\int_0^x \frac{n_e\langle\sigma v\rangle_{ioni}}{v_0}dx] \qquad (4.1)$$

where n_0 is the helium neutral density, $<\sigma v>_{ioni}$ the ionization rate coefficient and v_0 the helium velocity. The ionization rate coefficient and v_0 the helium velocity. The helium ion density, $n(He^+)$ is obtained from the neutral density as

$$n(He^+) = n_e \times n_0 \times \langle \sigma v \rangle_{ioni} \tag{4.2}$$

HeII intensity is calculated from the helium ion density considering excitation rate coefficient. When a room temperature (300 K) for the neutral helium and the edge plasma boundary at the foot point of CIV are assumed, we obtain the HeII peak position of a few mm inner side than the CIV peak position, which is similar to the observation. The helium penetration depth at different poloidal locations are nearly the same, as seen in Fig. 6. It means that the neutral helium energy coming into plasmas is equal for all the poloidal location. Then, we conclude that the neutral helium is caused by thermal gas existing in the vacuum vessel, but the recycling is not dominant even in region near the inboard side X-point. The present result is in a good agreement with helium neutral measurement based on Zeeman effect in visible spectroscopy [10].

4.4 Summary

A space-resolved EUV spectrometer is developed to observe impurity line emissions at different toroidal angles of LHD plasmas. The vertical profiles of HeII and CIV are observed at upper half of plasma against different toroidal locations. It is found that the HeII with lower ionization energy of 54.4 eV is located at inner side than the CIV with higher ionization energy of 64.5 eV and the distance between the HeII and CIV peak positions is nearly constant (4 mm) against the poloidal location. The result suggests the source of helium neutral is caused by thermal gas existing in the vacuum vessel, but not by recycling neutral from divertor plates. In order to understand the edge impurity behavior in more details, however, the whole profile including different toroidal locations has to be

analyzed. The analysis is done using three-dimensional edge simulation code in the near future.

References

[1] G. M. Mccracken, et al., Nucl. Fusion **19**, 889 (1979).

[2] B. C. Stratton, et al., Fusion Sci. Technol. **53**, 431 (2008).

[3] S. Morita, et al., J. Plasma Fusion Res. **5**, S2004 (2001).

[4] T. Morisaki, et al., J. Nucl. Mater. **313-316**, 548 (2003).

[5] S. Morita, et al., Plasma Phys. Controlled Fusion **48**, A269 (2006).

[6] C. F. Dong, et al., Phys. Plasma **18**, 082511 (2011).

[7] C. F. Dong, et al., Rev. Sci. Instrum. **81**, 033107 (2010).

[8] S. P. Hirshman, et al., Comput. Phys. Commun. **43**, 143 (1986).

[9] H. Yamazaki, et al., Plasma Fusion Res. **2**, S1115 (2007).

[10] M. Goto, et al., Phys. Rev. E **65**, 026401 (2002).

Chapter 5

1- and 2-D edge electron temperature distributions measured with line intensity ratio

5.1 Introduction

Line intensity ratio between two different transitions in the same ionization stage is an essential tool to measure the electron temperature and density in astrophysical plasmas [1]. In order to measure the electron temperature, the ratio of $2s^2S_{1/2}$-$3p^2P_{3/2}$ to $2s^2S_{1/2}$-$2p^2P_{3/2}$ transitions for Li-like ions is generally used because both lines are very strong and the ratio is sufficiently sensitive to the electron temperature, e.g. CIV (312.4 Å/1548 Å) and NeVIII (88.1 Å/770.4 Å) [2]. However, it is difficult to measure the line pair simultaneously using a single spectrometer. It may introduce a large uncertainty if the intensity ratio is measured with two different types of spectrometers having a different observation volume and a different accuracy in the absolute sensitivity calibration. Therefore, the intensity ratio using closely existing two lines is desired to analyze the data accurately because those lines can be simultaneously measured with a single spectrometer and the spectrometer sensitivity is practically the same between the two lines.

For the purpose the line ratios of Li-like CIV 2p-3d ($^2P_{1/2}$-$^2D_{3/2}$: 384.03 Å, $^2P_{3/2}$-$^2D_{5/2}$: 384.18 Å) to 2p-3s ($^2P_{1/2}$-$^2S_{1/2}$: 419.53 Å, $^2P_{3/2}$-$^2S_{1/2}$: 419.71 Å) transitions and NeVIII 2s-3p ($^2S_{1/2}$-$^2P_{3/2}$: 88.09 Å, $^2S_{1/2}$-$^2P_{1/2}$: 88.13 Å) to 2p-3s ($^2P_{1/2}$-$^2S_{1/2}$: 102.91 Å, $^2P_{3/2}$-$^2S_{1/2}$: 103.09 Å)

are selected in the present experiment. These lines can be simultaneously measured using a space-resolved extreme ultraviolet (EUV) spectrometer installed in LHD and the line ratios are only sensitive to the electron temperature at $n_e \leq 10^{14}$ cm^{-3} in which the electron density of ergodic layer in LHD ranges. CIV line ratio 2p-3d/ 2p-3s and NeVIII line ratio 2s-3p/ 2p-3s are used to measure the electron temperature at edge boundary of ergodic layer and near LCFS of ergodic layer, respectively. In order to analyze the edge electron temperature from line intensity ratio, atomic computer codes of ADAS and CHIANTI v6.02 with collisional-radiative (CR) model are used. ADAS has its origins at the Joint European Tokamak (JET) experiment programmed for maintaining a common approach to analyzing the radiating properties of plasmas. At present it is commonly used for fusion study, in particular, for the edge plasma study in several fusion institutes along with other astrophysics and university groups [3]. CHIANTI is a database of assessed atomic parameters and transition rates necessary for the calculation of the emissivity. It is available for optically thin emissions in the 1–2000 Å range [4].

In LHD, the magnetic field for plasma confinement is basically produced by a pair of helical coils with poloidal and toroidal pitch numbers of l=2 and m=10, respectively. The ergodic layer consisting of stochastic magnetic field lines with lengths from 10 to 2000 m is formed surrounding the main plasma with elliptical poloidal cross section defined by the LCFS. The heat and particle transports in the ergodic layer are strongly affected by the ergodicity of stochastic field lines [5]. The elliptical plasma poloidally rotates five times during one toroidal turn. The plasma cross section is traced in Fig. 5.1 with different toroidal angles denoted by φ, which is defined as horizontal angle of the EUV spectrometer. The space between the two arrows in each figure indicates the observation range for vertical profile measurement.

The thickness of ergodic layer is a function of the magnetic axis position, R_{ax}, and poloidal angle. The minimum thicknesses of ergodic layer is given at the O-point, e.g., 2 cm for R_{ax}=3.60 m and 10 cm for R_{ax}=3.9 m. Typical plasma parameters of the ergodic layer range in 10^{13} cm^{-3}< n_e <10^{14} cm^{-3} and 10 eV< T_e <500 eV. Four divertor legs connecting to

divertor plates made of carbon are also intrinsically formed as a specific character of LHD. Carbon is therefore the most dominant impurity in LHD.

The space-resolved EUV spectrometer working in 30-650 Å is set with horizontal dispersion to observe the vertical profile at horizontally elongated plasma cross section, as seen Fig. 5.1. The spectrometer is recently graded up by adding a horizontal scanning mechanism with a stepping motor to measure the two-dimensional distribution of line emissions. It is then possible to scan the spectrometer horizontally during a stable discharge. The minimum time interval necessary for the horizontal scan is 6 s. The horizontal range for the scanning is limited by the rectangular spectrometer port and diamond LHD diagnostic port [6].

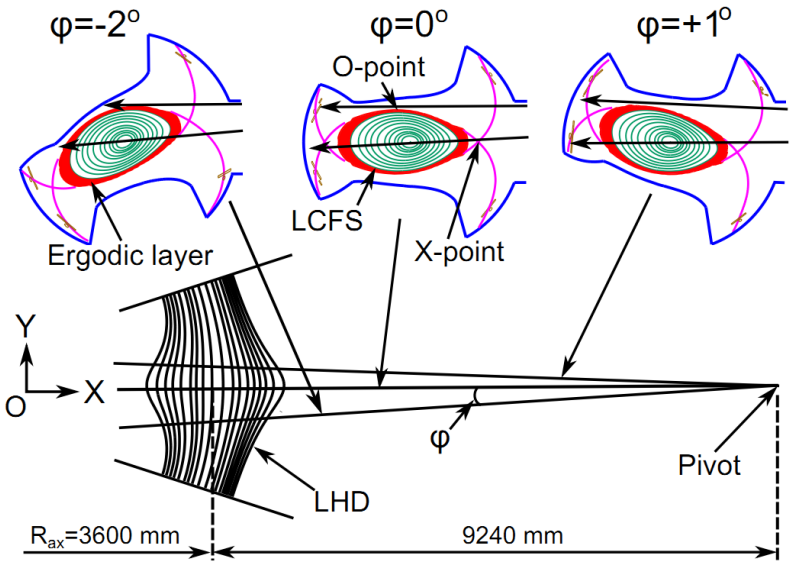

Fig. 5.1 Cross sections of LHD plasma at toroidal angles of φ=-2°, φ=0° and φ=+1°. Two arrows indicate the observation range of space-resolved EUV spectrometer. The toroidal angle is defined as an angle from X-axis at the pivot of spectrometer. The vertical and horizontal spatial resolutions are ΔZ=10 mm and ΔY=80 mm, respectively.

A back-illuminated charge-coupled detector (CCD) with 1024 x 255 pixels (26.6 x 6.6 mm^2) is used for the spectrometer. The vertical profile of line emissions is measured along the long axis of CCD, while the short axis is given as the wavelength dispersion. Therefore, the observable wavelength interval, $<\lambda>$, defined by the short axis size (6.6 mm) of CCD is narrow at present, e.g., $<\lambda>$=40 Å at λ=100 Å and $<\lambda>$=60 Å at λ=300 Å. We then select the line pairs for the temperature measurement having a wavelength difference within the wavelength interval such as CIV 2p-3d/2p-3s (384 Å/420 Å) and NeVIII 2s-3p/2p-3s (88 Å/103 Å) in order to delete the uncertainty based on shot-to-shot reproducibility. The CCD position can be moved by a stepping motor along the wavelength dispersion to change the wavelength. The spectral resolution is $\Delta\lambda$=0.22 Å at λ=200 Å in full image mode of CCD which corresponds to 4-5 pixels at the foot position of spectral line. In practice, the CCD is operated in the binning mode to shorten the sampling time. Five pixels are usually summed into one channel and the sampling time is set to 200 ms. The spectrometer sensitivity is absolutely calibrated using bremsstrahlung continuum [7].

Since the CCD is operated in the binning mode of 5 pixels, the number of vertical observation chords is 204. Several tens of upper observation chords can observe only the region near upper O-point in all different poloidal cross section, as shown in Fig. 5.1, while lower observation chords observe the region near both inboard and outboard X-points. The vertical position of all observation chords is calibrated using a toroidal slit with rectangular-corrugated edge installed between LHD and EUV spectrometer [6].

5.2 Vertical profile of electron temperature in edge boundary of ergodic layer

5.2.1 Vertical electron temperature profile measured from CIV line ratio

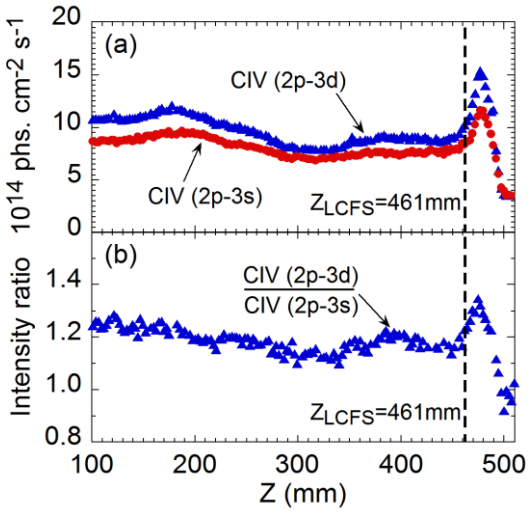

Fig. 5.2 Vertical profiles of (a) CIV 2p-3d (384 Å) and 2p-3s (420 Å) at φ=0° and (b) CIV line intensity ratio of 2p-3d/2p-3s. Position of LCFS is denoted with dashed line.

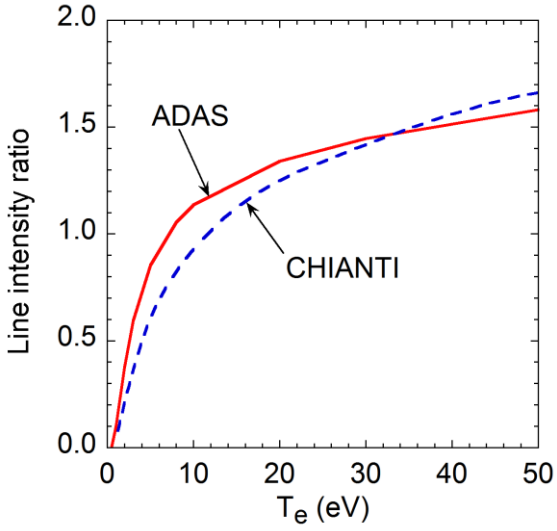

Fig. 5.3 Line intensity ratio of CIV 2p-3d/2p-3s calculated from ADAS (solid line) and CHIANTI (dashed line) codes as a function of electron temperature.

The line intensity ratio of 2p-3d/2p-3s (384 Å/420 Å) in Li-like CIV is observed to measure the electron temperature profile in edge boundary of the ergodic layer. It is examined that the C^{3+} ions with ionization energy of E_i=64 eV are located in the farthest edge in LHD plasmas [8]. The vertical profiles of CIV emissions are shown in Fig. 5.2(a) measured from a discharge heated by NBI. It is clear that the two CIV emissions have a very similar profile both in the vicinities of X- and O-points. In particular, the profile near X-point changing its intensity along vertical direction reflects the structure of stochastic magnetic field in the ergodic layer. The vertical profile of CIV line intensity ratio calculated from Fig. 5.2(a) is shown in Fig. 5.2(b). The CIV intensity ratio ranges from 0.9 to 1.4.

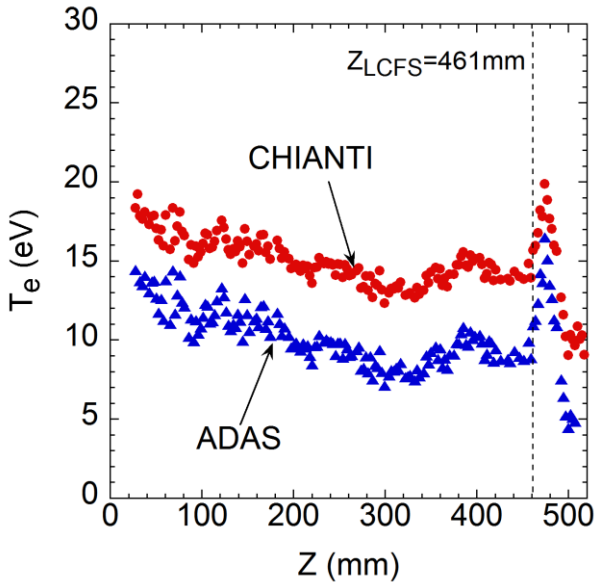

Fig. 5.4 Vertical profile of electron temperature at edge boundary of ergodic layer evaluated from ADAS (triangles) and CHIANTI (circles) codes. Position of LCFS is denoted with dashed line.

The line intensity ratios are calculated by ADAS and CHIANTI codes as a function of electron temperature, as plotted in Fig. 5.3. The line intensity ratio from the ADAS

code gives lower temperature compared to the CHINTI code in range of $T_e \leq 32$ eV, whereas it gives higher temperature in the range of $T_e \geq 32$ eV. The vertical profiles of electron temperature evaluated from the ratio in Fig. 5.2(b) and Fig. 5.3 are shown in Fig. 5.4. The electron temperature ranges in 5-15 eV for ADAS code and 10-19 eV for CHIANTI code.

5.2.2 Comparison with electron temperature on divertor plates

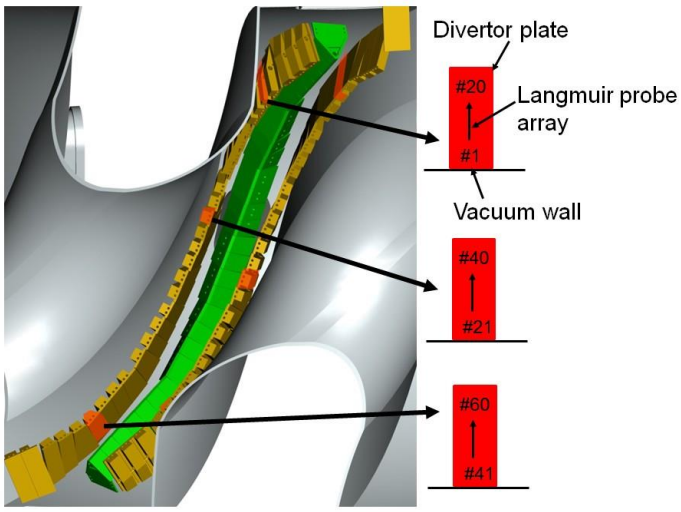

Fig. 5.5 Langmuir probe arrays installed in divertor plates of LHD. Langmuir probe array of #21-#40 is installed in horizontally elongated cross section.

Since the edge boundary at the O-point near Z=480 mm where the CIV is located is connected to the divertor plate with short magnetic field lines around 10 m, the CIV temperature at the O-point can be correlated with the temperature on the divertor plate. The electron temperature on divertor plates is measured by the Langmuir probe embedded in the divertor plate. The position of Langmuir probes at inboard divertor plates is

illustrated in Fig. 5.5. The Langmuir probe arrays of #1-20, #21-40 and #41-60 are located at upper, middle and lower divertor plates in the inboard side of horizontally elongated plasma cross section. The temperature profile on divertor plates is shown in Fig. 5.6. The Langmuir probe array of #1-20 was not operated due to a technical problem. The electron temperature on divertor plates distributes around 10 eV for both the divertor positions of #21-40 and #41-60. The CIV temperature at O-point evaluated with ADAS and CHIANTI codes distributes around 15 eV and 19 eV, respectively. Therefore, the temperature measured with CIV line ratio, 2p-3d/2p-3s, is quite reasonable.

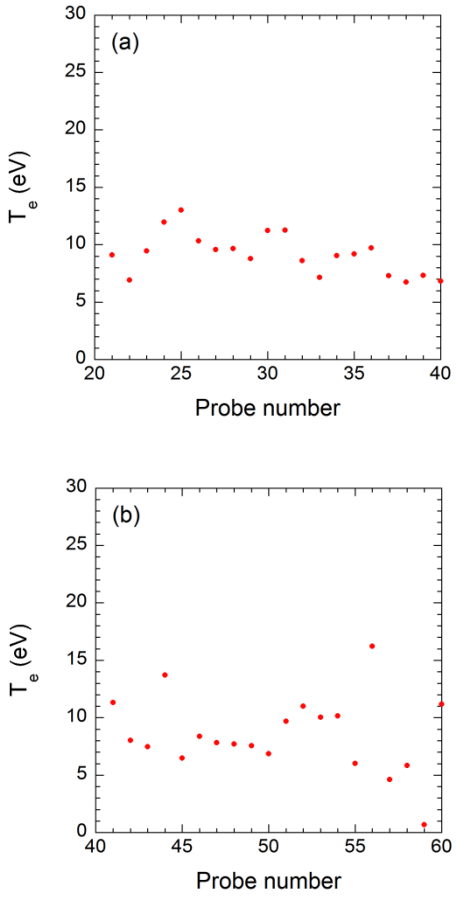

Fig. 5.6 Electron temperature profiles on divertor plates measured by Langmuir probe arrays of (a) #21-#40 and (b) #41-#50, as seen in Fig. 5.5.

5.3 Vertical profile and 2-D distribution of electron temperature near LCFS of ergodic layer

5.3.1 Observation of neon lines

Neon lines are surveyed in neutral-beam-heated discharges by puffing neon gas using a flat-field EUV spectrometer named EUV-Long, which is mainly used to monitor the impurity line emissions with a wide wavelength observation range, e.g., $<\lambda>$=150 Å at λ=100 Å and $<\lambda>$=240 Å at λ=300 Å. The working wavelength ranges from 50 to 500 Å with good spectral resolution, e.g., $\Delta\lambda$=0.22 Å at λ=200 Å. A back-illuminated charge-coupled device (CCD) is used for the detector and the EUV spectrum is sequentially measured with time interval of 5 ms. Typical neon spectra observed from LHD plasmas are shown in Fig. 5.7. The neon lines are mainly emitted in the wavelength ranges of 50-150 Å and 350-450 Å. Several neon line emissions from NeV-X are identified in the figure, whereas some of the neon lines are blended with other lines.

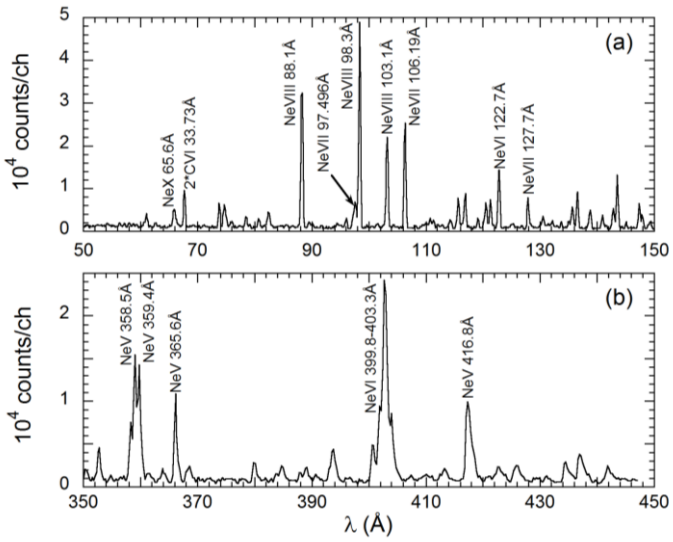

Fig. 5.7 Typical neon line emissions in wavelength ranges of (a) 50-150 Å and (b) 350-450 Å observed in LHD.

Table 5.1 Line pairs of neon for edge electron temperature measurement.

Ionization stages	Line pairs	
	Line 1	Line 2
Ne VII (Be-like)	465.220 Å: $2s^2\ ^1S_0$ - $2s2p\ ^1P_1$	*97.496 Å: $2s^2\ ^1S_0$ - $2s3p\ ^1P_1$
Ne VIII (Li-like)	770.410 Å: $1s^22s\ ^2S_{1/2}$ - $1s^22p\ ^2P_{3/2}$ 780.325 Å: $1s^22s\ ^2S_{1/2}$ - $1s^22p\ ^2P_{1/2}$	88.082 Å: $1s^22s\ ^2S_{1/2}$ - $1s^23p\ ^2P_{3/2}$ 88.120 Å: $1s^22s\ ^2S_{1/2}$ - $1s^23p\ ^2P_{1/2}$
	*98.116 Å: $1s^22p\ ^2P_{1/2}$ - $1s^23d\ ^2D_{3/2}$ *98.260 Å: $1s^22p\ ^2P_{3/2}$ - $1s^23d\ ^2D_{5/2}$ *98.275 Å: $1s^22p\ ^2P_{3/2}$ - $1s^23d\ ^2D_{3/2}$	88.082 Å: $1s^22s\ ^2S_{1/2}$ - $1s^23p\ ^2P_{3/2}$ 88.120 Å: $1s^22s\ ^2S_{1/2}$ - $1s^23p\ ^2P_{1/2}$
	102.911 Å: $1s^22p\ ^2P_{1/2}$ - $1s^23s\ ^2S_{1/2}$ 103.086 Å: $1s^22p\ ^2P_{3/2}$ - $1s^23s\ ^2S_{1/2}$	88.082 Å: $1s^22s\ ^2S_{1/2}$ - $1s^23p\ ^2P_{3/2}$ 88.120 Å: $1s^22s\ ^2S_{1/2}$ - $1s^23p\ ^2P_{1/2}$
	102.911 Å: $1s^22p\ ^2P_{1/2}$ - $1s^23s\ ^2S_{1/2}$ 103.086 Å: $1s^22p\ ^2P_{3/2}$ - $1s^23s\ ^2S_{1/2}$	*98.116 Å: $1s^22p\ ^2P_{1/2}$ - $1s^23d\ ^2D_{3/2}$ *98.260 Å: $1s^22p\ ^2P_{3/2}$ - $1s^23d\ ^2D_{5/2}$ *98.275 Å: $1s^22p\ ^2P_{3/2}$ - $1s^23d\ ^2D_{3/2}$

*NeVII 97.496 Å is blended with NeVIII 98.116-98.275 Å.

The line emissions of NeI-VI are usually located in outer side of the ergodic layer because their ionization energies, E_i, are relatively small, e.g., E_i=158 eV for NeVI. In addition, NeIX (helium-like, E_i=1196 eV) and NeX (hydrogen-like, E_i=1362 eV) emissions are located inside the LCFS due to the high ionization energy. Taking into account the temperature range of the ergodic layer, the use of NeVII (beryllium-like, E_i=207 eV) or NeVIII (lithium-like, E_i=239 eV) seems to be the best choice in the present purpose. Possible candidates of the line pair for NeVII and NeVIII are listed in Table 5.1. The best line pair for the electron temperature measurement is to use the ratio of 2s-3p to 2s-2p transitions because the energy difference between the two transitions is large. That is, the ratios of I(97.496 Å)/I(465.220 Å) for NeVII and I(88.082 Å+88.120 Å)/I(770.410 Å+780.325 Å) for NeVIII can give the best solution. However, the wavelengths of these line pairs are too much separated each other. In particular, the NeVIII 2s-2p resonance transition is completely out of the wavelength range in the present EUV spectrometer. Although the NeVII 2s-2p resonance transition can be measured, two different discharges are necessary to measure the line ratio due to the limited wavelength observation range of

the space-resolved EUV spectrometer. In practice, the measurement of line intensity ratio based on the NeVII 2s-2p transition is already attempted using two discharges, but the resultant electron temperature shows a large uncertainty. It is caused by a little different edge condition between the two discharges with neon puff in addition to the problem on line blending as mentioned below.

On the other hand, the NeVII 2s-3p transition at 97.496 Å is blended with NeVIII 2p-3d transitions at 98.116-98.275 Å, as seen in Fig. 5.7(a). It is also difficult to measure the line ratio using such transitions. At present, therefore, the only choice for the edge temperature measurement using neon is to use the line intensity ratio of NeVIII 2s-3p (88.082 Å+88.120 Å) to 2p-3s (102.911 Å+103.086 Å) transitions. Fortunately, no other lines are blended with these lines and both lines closely exist in wavelength. It enables us to measure the line ratio in a single discharge. The electron temperature is previously measured in solar plasmas from lithium-like CIV line intensity ratio among $\Delta n=1$ transitions of 2s-3p, 2p-3s and 2p-3d transitions, of which the transition is the same as the present study, showing a good agreement with theory [9].

5.3.2 Vertical electron temperature profile measured from NeVIII line ratio

The vertical profile of the NeVIII line emissions is measured at horizontally elongated plasma cross section in R_{ax}=3.75 configuration. One of the results is plotted in Fig. 5.8(a). The position of LCFS calculated by variation moments equilibrium code (VMEC) is indicated with dashed line as Z_{LCFS}=437 mm. It is then clear that the NeVIII emissions are located inside the ergodic layer. The vertical profile of the intensity ratio of NeVIII 2s-3p to 2p-3s transitions calculated from Fig. 5.8(a) is shown in Fig. 5.8(b). The ratio starts to decrease with increase in the vertical range near the top of O-point ($400 \leq Z \leq 485$ mm), while it roughly keeps a constant value close to unity in the vertical range near X-point ($100 \leq Z \leq 300$ mm).

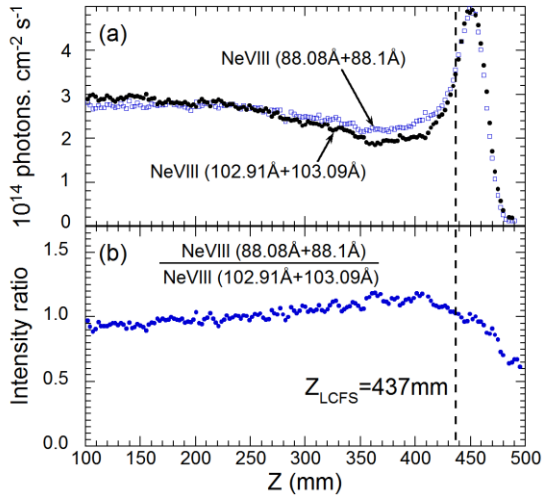

Fig. 5.8 (a) Vertical profiles of NeVIII lines observed from horizontally elongated plasma cross section in R_{ax}=3.75 m configuration and (b) intensity ratio calculated from (a). Position of LCFS is denoted with Z_{LCFS} (dashed line).

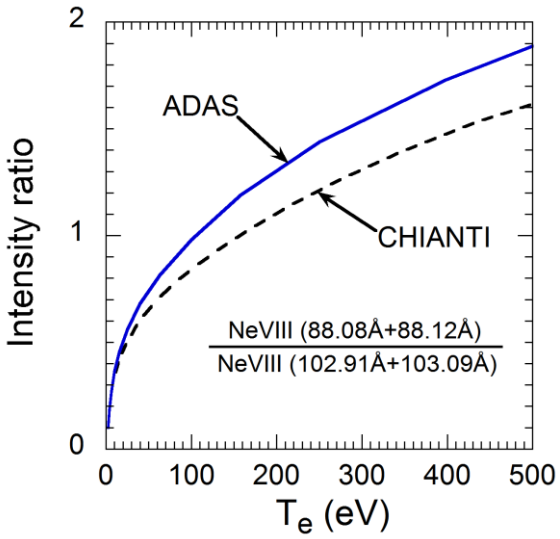

Fig. 5.9 Line intensity ratio of NeVIII (3p-2s)/(3s-2p) calculated from ADAS (solid line) and CHIANTI (dashed line) as a function of electron temperature.

The intensity ratios calculated by ADAS and CHIANTI at electron density $n_e=10^{13}$ cm^{-3} are shown in Fig. 5.9 as a function of electron temperature. The line intensity ratio calculated by ADAS shows a larger value in the whole temperature range compared to that calculated by CHIANTI. Discrepancy in the ratio between the two different results is 15% at T_e=50 eV and 17% at T_e=239 eV which corresponds to the ionization energy of Ne^{7+} ion. The ratio is entirely insensitive to the electron density, at least, below $n_e=10^{14}$ cm^{-3}.

The vertical profiles of electron temperature in the ergodic layer calculated from Figs. 5.8(b) and 5.9 are shown in Fig. 5.10(a). Since the peak position of NeVIII is located near Z=450 mm (see Fig. 5.8(a)), the electron temperature from Z=100 to Z=450 mm in Fig. 5.10(a) indicates the chord-integrated edge temperature in a narrow radial region where the Ne^{7+} exists in the ergodic layer. Therefore, the radial profile in the ergodic layer can be expressed in the range of 450≤ Z ≤490 mm. As seen in the figure the CHIANTI gives higher temperature than the ADAS. The spatial resolution in the measurement is 10 cm and 2.5 cm in the toroidal and vertical directions, respectively.

The edge temperature profile is simulated with three-dimensional edge transport code, EMC3-EIRENE. The result is shown in Fig. 5.10(b). In the simulation the effect of NeVIII radial distribution as chord-integrated signal is considered by multiplying the weight to each emission rate. Therefore, the present transition of NeVIII 2s-3p or 2p-3s ($\Delta n=1$) gives a little higher temperature around 10 eV compared to the NeVIII 2s-2p resonance transition ($\Delta n=0$) because the emission rate of $\Delta n=1$ transition is still large at higher temperature range. The edge temperature simulated here indicates roughly 90 eV at X-point region of 100≤ Z ≤300 mm. This value shows a reasonably good agreement with the temperature from ADAS. The electron temperature at LCFS obtained from the present method is compared with that from Thomson scattering diagnostics, i.e., 110 eV for ADAS, 170 eV for CHIANTI and 120 eV for Thomson. The comparison is also in a good agreement with the temperature from ADAS. Therefore, it seems that the ADAS can give accurate emission rate at least in the present transition.

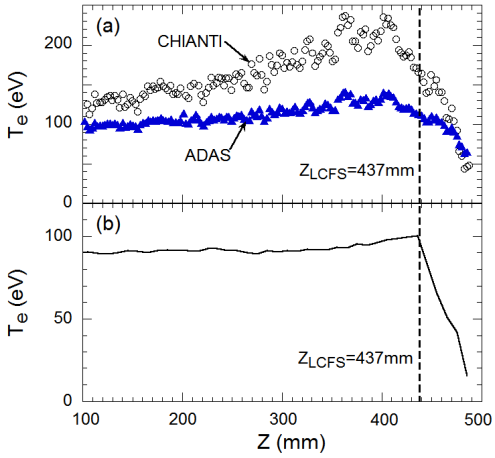

Fig. 5.10 Vertical profiles of edge electron temperature obtained from (a) measurement (ADAS: solid triangles and CHIANTI: open circles) and (b) simulation from three-dimensional edge transport code. Position of LCFS is denoted with Z_{LCFS} (dashed line).

Magnetic field connection length in the ergodic layer at the top of O-point is shown in Fig. 5.11. It forms a complicate structure due to the appearance of many small and large island chains in the ergodic layer. At Z≥485 mm the magnetic field changes the direction by circulating the helical coil and the connection length of magnetic field lines is shorter. The plasma can not be therefore sustained in such a region. A temperature shoulder is appeared near Z=470 mm in Fig. 5.10(b). It reflects a sudden change in the connection length (see Fig. 5.11). A similar shoulder can be also observed in the temperature profile from the present measurement (see Fig. 5.10(a)). However, the peak position in the temperature profile is clearly different between the measurement and simulation, whereas the same spatial resolution as the present measurement is adopted in the simulation. The reason is not clear at present. The measured edge boundary temperature at Z=485 mm is larger than the simulated one. It suggests that a smaller cross-field transport coefficient is required to explain the transport in the ergodic layer.

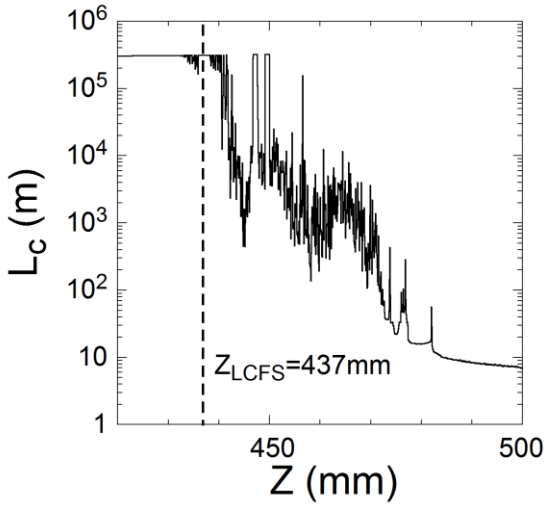

Fig. 5.11 Vertical profile of magnetic field connection length, L_c, in ergodic layer at the top O-point of horizontally elongated plasma cross section in R_{ax}=3.75 m configuration.

5.3.3 2-D electron temperature distribution measured from NeVIII line ratio

Two-dimensional distribution of impurity line emissions is generally measured from long pulse discharges maintained by electron cyclotron heating (ECH) and ion cyclotron resonance heating (ICRH). In the present study the two-dimensional distributions of NeVIII 2s-3p (88 Å) and 2p-3s (103 Å) are obtained from the ECH discharge in magnetic axis position of R_{ax}=3.6 m. The pulse length is 10 s with sufficient steady phase and neon gas is supplied through gas puffing during 30 ms at the beginning phase of discharges, as seen in Fig. 5.12. The electron temperature at LCFS measured by Thomson scattering changes a little during the discharge over 10 s, i.e., from 300 eV at t=1 s to 350 eV at 10 s. The space-resolved EUV spectrometer is horizontally scanned from 1 s to 10 s, i.e., from Y=210 mm to Y=-520 mm with a pivot point near the entrance slit, as seen in Fig. 5.13. The total scanning time to record the full two-dimensional distribution is 9 s at the speed of 80 mm/s.

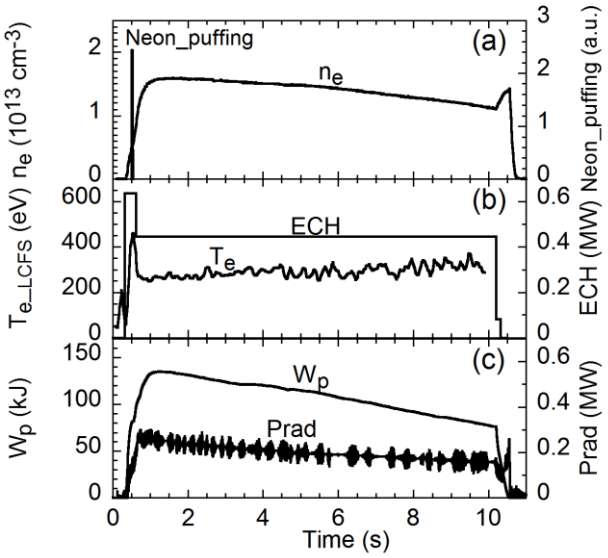

Fig. 5.12 Waveforms of plasma parameters: (a) line-averaged density and neon puff, (b) T_e at LCFS and ECH power and (c) W_p and P_{rad}.

The line intensities shown in Figs. 5.13 (a) and (b) decrease as a function of time during the scan from Y=200 mm to -400 mm, since the electron density gradually decreases during the discharge (see Fig. 5.12). The plasma range in the two-dimensional distribution is indicated by dash line. The observation chord from Y=-400 mm to -520 mm is hidden by the spectrometer port and the plasma is absent at upper region above roughly Z=500 mm. The strong intensity of NeVIII near Y=200 mm and Z=500 mm is due to the Ne gas puffing at the beginning of ECH discharges. The NeVIII is located near the LCFS at all poloidal positions. The two-dimensional distribution of line intensity ratio, NeVIII 2s-3p/2p-3s, calculated from Figs. 5.13(a) and (b) is shown in Fig. 5.13(c). Although a considerably large nonuniformity is seen in the two-dimensional intensity distribution (see Figs. 5.13 (a) and (b)) based on the parameter change during the discharge, it can be deleted when the intensity ratio is calculated.

The line intensity ratio of NeVIII 2s-3p (88 Å) to 2p-3s (103 Å) is not sensitive to the electron density. The intensity ratios calculated by ADAS at electron densities of n_e=1x10^{11} cm^{-3} and n_e=1x10^{13} cm^{-3} are shown in Fig. 5.14. The line intensity ratios calculated at different densities are nearly the same in the temperature range of 10-400 eV.

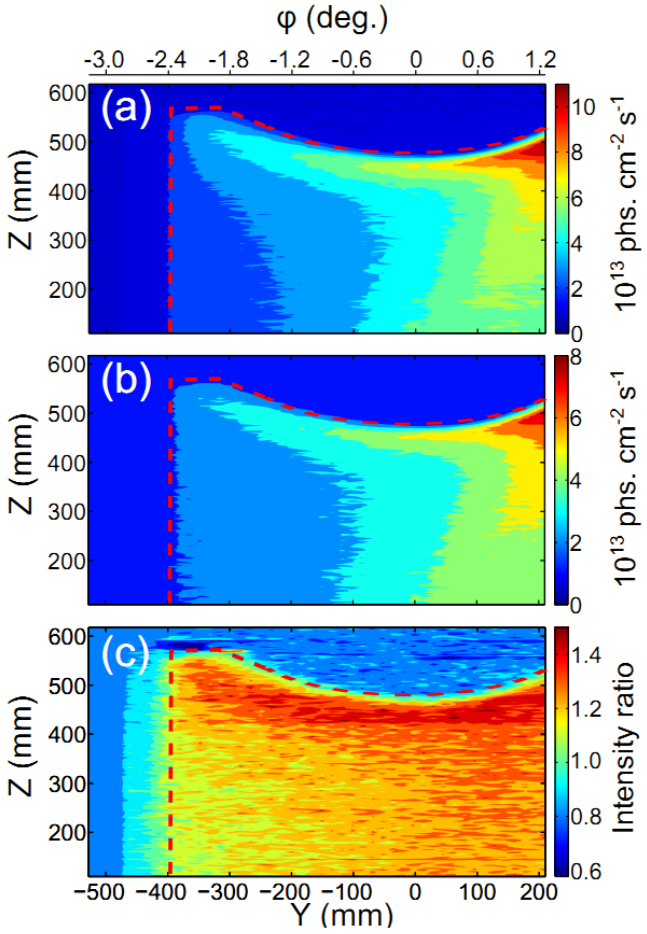

Fig. 5.13 2-dimensional distributions of NeVIII (a) 2s-3p: 88 Å, (b) 2p-3s: 103 Å and (c) line intensity ratio of 2s-3p/2p-3s.

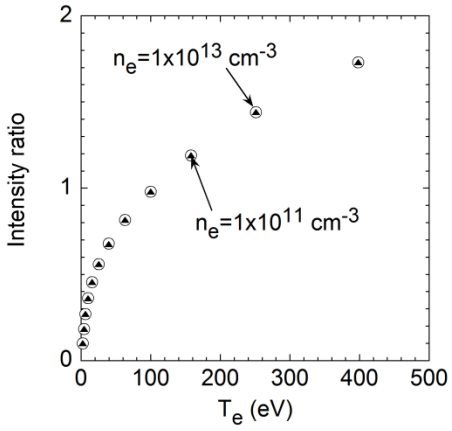

Fig. 5.14 Line intensity ratio of NeVIII 2s-3p (88 Å) to 2p-3s (103 Å) calculated by ADAS at electron densities of n_e=1x10^{11} cm^{-3} (solid triangles) and n_e=1x10^{13} cm^{-3} (open circles).

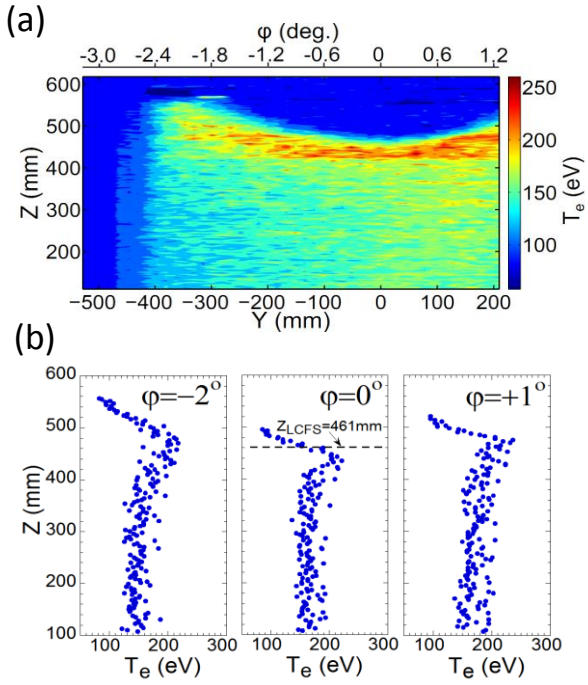

Fig. 5.15 (a) 2-dimensional distribution of edge T_e measured from NeVIII line intensity ratio and (b) vertical profiles of edge T_e at different toroidal positions of φ=-2°, 0° and +1°. Position of LCFS is denoted with dashed line at φ=0°.

The two-dimensional distribution of electron temperature is calculated from Fig. 5.13 (c) and Fig. 5.14. The result is shown in Fig. 5.15(a). Although the electron temperature evaluated from NeVIII intensity ratio distributes in range of 130–170 eV in most of the region, it tends to increase when the radial position moves to the region near O-point. In order to make clear the temperature distribution in the edge plasma, the vertical profiles are plotted in Fig. 5.15(b) at three different toroidal positions of φ=-2^{o}, 0^{o} and +1^{o}. The observation chord of three toroidal positions is indicated in Fig. 5.1. The temperature profile in the ergodic layer can be clearly seen at the region near O-point, i.e., 480≤Z≤560 mm at φ=-2°, 440≤ Z ≤500 mm at φ=0° and 480≤ Z ≤520 mm at φ=+1°. We can understand from the profile that the temperature gradient in the ergodic layer is steeper depending on the thickness of the ergodic layer, when the observation chord moves from X-point to O-point. It also indicates that the temperature in the ergodic layer has a similar value even if the poloidal position is different, at least in the vicinity of O-point. The temperature profile at O-point gives the maximum value at the radial location where the observation chord positions a little inside the LCFS. On the contrary, the temperature in the vicinity of X-point, i.e., 100≤Z≤400 mm at φ=-2°, 0° and+1°, is constant against the vertical position whereas the structure of stochastic magnetic field entirely different along the vertical observation chord. Therefore, a clear toroidal structure of the electron temperature is not seen in the vicinity of X-point at present. The result may suggest that the ergodic layer has a poloidal temperature contour similar to the core plasma with magnetic surfaces.

5.4 Summary

Electron temperature profiles in the ergodic layer of LHD have been measured using line intensity ratio from Li-like CIV and NeVIII. The electron temperature profile in the edge boundary of ergodic layer is measured from the line intensity ratio of CIV 2p-3d/2p-3s, which is around 5-15 eV from ADAS and 10-19 eV from CHIANTI. The result

is compared with the electron temperature on divertor plates measured by Langmuir probe. It shows a similar value because of the short connection length of magnetic field lines between edge boundary of ergodic layer and divertor plates. The electron temperature profile near LCFS of ergodic layer is measured from the line intensity ratio of NeVIII 2s-3p/2p-3s, which ranges in 60-130 eV from ADAS code and 50-230 eV from CHIANTI code. The electron temperature profile is also simulated with three-dimensional edge transport code, EMC3-EIRENE, and the result indicates the electron temperature ranges in 20-100 eV. The electron temperature at LCFS is 170 eV for CHIANTI, 110 eV for ADAS, 100 eV for simulation, and 120 eV for Thomson scattering. Therefore, ADAS code gives reasonable result. Two-dimensional electron temperature distribution near LCFS also has been obtained from NeVIII line ratio in stable discharges heated by ECH in LHD. The electron temperature at the top plasma edge shows a higher temperature of 210-220 eV in all toroidal locations, whereas the electron temperature in the vicinity of X-point shows lower temperature around 150-180 eV.

References

[1] H. E. Mason and B. C. Monsignori Fossi, Astron. Astrophys. Rev. **6**, 123 (1994).

[2] L. Heroux, Proc. Phys. Soc., **83**, 121 (1964).

[3] H. P. Summers, JET-IR **06**, (1994)

[4] K. P. Dere et al., Astron. Astrophys. Suppl. **498**, 915 (2009).

[5] T. Morisaki et al., J. Nucl. Mater. **313**, 548 (2003).

[6] E.H. Wang et al., Rev. Sci. Instrum. **83**, 043503 (2012).

[7] C.F. Dong et al., Rev. Sci. Instrum. **82**, 113102 (2011).

[8] C.F. Dong et al., Phys. Plasmas **18**, 082511 (2011).

[9] F.P. Keenan et al., Solar Phys. **144**, 69 (1993).

Chapter 6

Structure of impurity line emissions near X-point in the ergodic layer

6.1 Introduction

The study of impurity behavior is one of the most important subjects in the magnetic confinement fusion research [1]. The impurities are mainly produced by the interaction between plasma facing components and peripheral plasma, which is called plasma-wall interaction [2]. The impurity released from the plasma facing component is ionized in the edge plasma or divertor region and penetrates to the core plasma through transport in the edge plasma. At the beginning of fusion research a mechanical limiter was used to separate the vacuum vessel from the core plasma. The last closed flux surface (LCFS) is then defined by the limiter position. The impurity released from the limiter easily enters the core plasma. In order to reduce the impurity content in the core plasma, the divertor configuration has been adopted in tokamaks. The LCFS in the divertor configuration can well separate a closed magnetic surface region in which the plasma is confined and an open magnetic surface region called scrape-off layer (SOL) which is connected to the divertor plates through the field lines. The impurities released from the divertor plates are firstly transferred in the divertor region and scrape-off layer, and then reach the LCFS before entering the core plasma. However, a part of the impurities turn back towards the divertor plates by the presence of friction force working between the

impurities and the plasma ions. This impurity screening effect is dominant when the operational density increases [3]. The divertor configuration can also improve the energy confinement. In particular, it is effective for the transition to the H-mode [2].

The poloidal field divertor has been widely used in many tokamaks such as JET, DIII-D and EAST [1]. Magnetic field required is produced by toroidal conductors. In the LHD, on the other hand, the divertor configuration is intrinsically created by a set of helical coils [4]. The magnetic field lines in the edge region are usually stochastic and the separatrix between the closed and open surface regions is not as clearly as that defined in tokamaks. The heat and particle behaviors in the ergodic layer are much complicated compared to those in the scrape-off layer (SOL) in axisymmetric divertor tokamaks.

In the edge region of LHD, the core plasma confined with magnetic surfaces is surrounded by a thick "ergodic layer" consisting of three-dimensional stochastic field lines. There exist four divertor legs connecting to the divertor plates outside the ergodic layer. The edge particle and heat fluxes are removed at the divertor plates made of graphite. Therefore, the plasma-wall interaction is mainly dominant on the divertor plates based on the physical and chemical sputtering. The carbon ionized near the divertor plates are transferred upstream through the divertor legs and the ergodic layer. In LHD, carbon line emissions have been then used to study the impurity behavior in the ergodic layer. The C^{2+} (E_i=48 eV) and C^{3+} (E_i=65 eV) ions are always located at the outer side of ergodic layer, while the C^{4+} (E_i=392 eV) and C^{5+} (E_i=490 eV) ions exist near the LCFS. The line intensity ratio of CV (40.27 Å: $1s^2\ ^1S_0 - 1s2p\ ^1P_1$) + CVI (33.73 Å: $1s\ ^2S - 2p\ ^2P$) to CIII (977.03 Å: $2s^2\ ^1S_0 - 2s2p\ ^1P_1$) + CIV (1550 Å: $2s\ ^2S - 2p\ ^2P$) represents the degree of the impurity screening. It is found that the line intensity ratio decreases by two orders of magnitude when the electron density increases from $n_e=1\times10^{13}$ cm^{-3} to $n_e=8\times10^{13}$ cm^{-3}. The result indicates that the impurity screening in the ergodic layer is enhanced at higher electron density [5].

The experimental result was analyzed with the three-dimensional edge transport code, EMC3-EIRENE. The simulation showed a good agreement with the experiment. It

also suggested that the impurity screening can be explained by the force balance between the ion thermal force and the friction force in the ergodic layer. In low electron density range, the carbon ions are moved upstream due to the presence of strong ion thermal force. In high electron density range, on the contrary, the direction of the plasma flow changes and the carbon ions are moved downstream due to the enhanced friction force [6].

In LHD, the magnetic field structure near X-point in the ergodic layer is much complicated compared to other poloidal location. The impurity behavior near O-point has not been studied until now, while the carbon behavior near O-point was studied well based on the upper-half vertical profile measurement of impurity line emissions [7]. Therefore, in this chapter, the impurity behavior near X-point is studied using the space-resolved EUV spectrometer with which the full vertical profile and 2-D distribution of impurity line emissions can be measured.

6.2 Magnetic field structure near X-point in LHD

Magnetic field structures at horizontally elongated plasma cross section are illustrated in Fig. 6.1 for different magnetic axis positions. In LHD, the LCFS (ρ=1) is defined as the outermost flux surface on which the radial deviation of magnetic field line is less than 4 mm while it travels about 1000 m along the torus [8]. The stochastic field lines are appeared outside the LCFS, which are caused by higher orders of Fourier components involved in the helical magnetic field. The ergodic layer is then formed by overlapping of natural islands due to the presence of radial magnetic fields. The thickness of ergodic layer, λ_{erg}, is a function of poloidal angle. Maximum thickness of the ergodic layer is appeared at inboard or outboard X-points, e.g. λ_{erg}=18 cm at inboard and λ_{erg}=30 cm at outboard for R_{ax}=3.6 m, and minimum thickness is appeared at the top and bottom O-points, e.g. λ_{erg}=2 cm for R_{ax}=3.6 m and λ_{erg}=10 cm for R_{ax}=3.9 m. The thickness basically increases when

the magnetic axis is outwardly shifted, i.e., from R_{ax}=3.6 m to R_{ax}=3.9 m as seen in Fig. 6.1. It also increases with β value (≡ plasma pressure/magnetic pressure) [9].

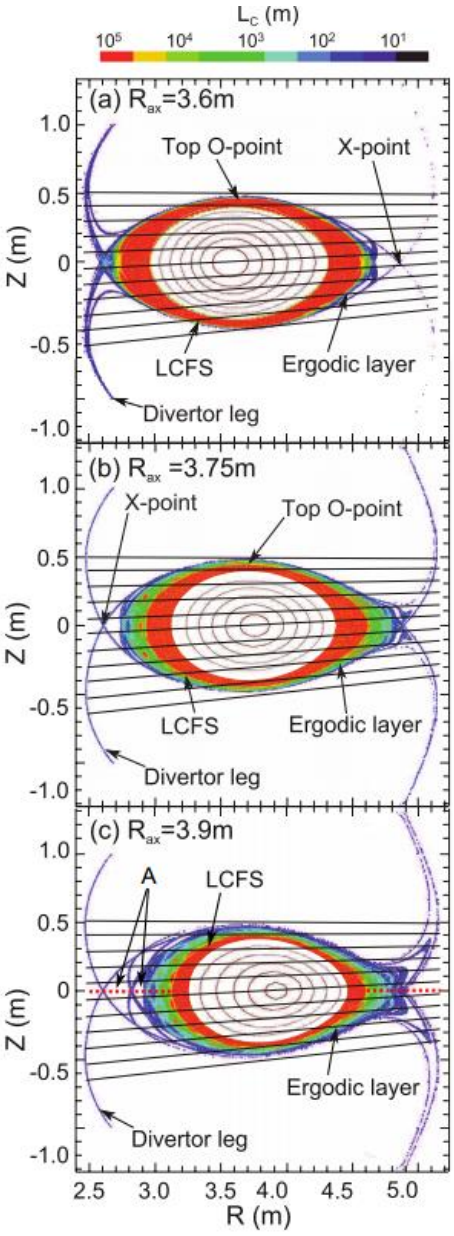

Fig. 6.1 Observation chords of space-resolved EUV spectrometer in each interval of ΔZ=100 mm from Z=-500 mm to Z=+500 mm at horizontally elongated plasma cross section for magnetic axis position of (a) R_{ax}=3.6 m, (b) R_{ax}=3.75 m and (c) R_{ax}=3.9 m. Connection length of magnetic field lines, L_c, is expressed in different color.

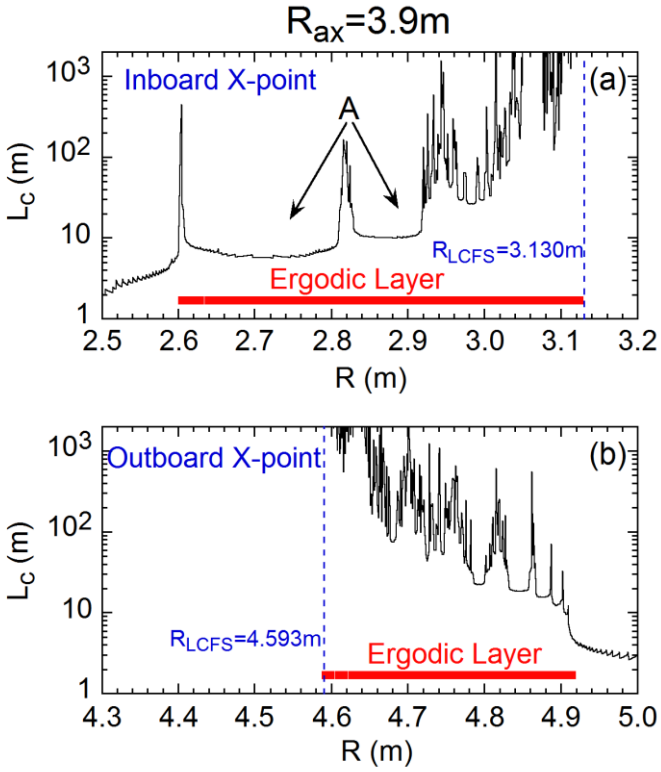

Fig. 6.2 Structure of connection length of magnetic field lines, L_c, at inboard and outboard X-point regions at magnetic axis position of R_{ax}=3.9 m.

In the figures two X-points and four divertor legs are seen outside the ergodic layer, which are intrinsically created by the helical coils. The distribution of magnetic field connection length, L_c, along the major radius direction is shown in Fig. 6.2 for R_{ax}=3.9 m configuration. The range of major radius plotted in Fig. 6.2 is indicated with two dotted lines in Fig. 6.1(c). We understand from the figures that the magnetic field structure near X-points is quite complicate and the magnetic field connection length ranges in 10-2000 m. The notation of "A" in Fig. 6.2 indicates a region with shorter connection length of around 10 m. The region is also indicated in Fig. 6.2 (a) with the notation of "A". The thickness of ergodic layer becomes large with increase in the plasma axis position because the plasma volume defined by the LCFS decreases.

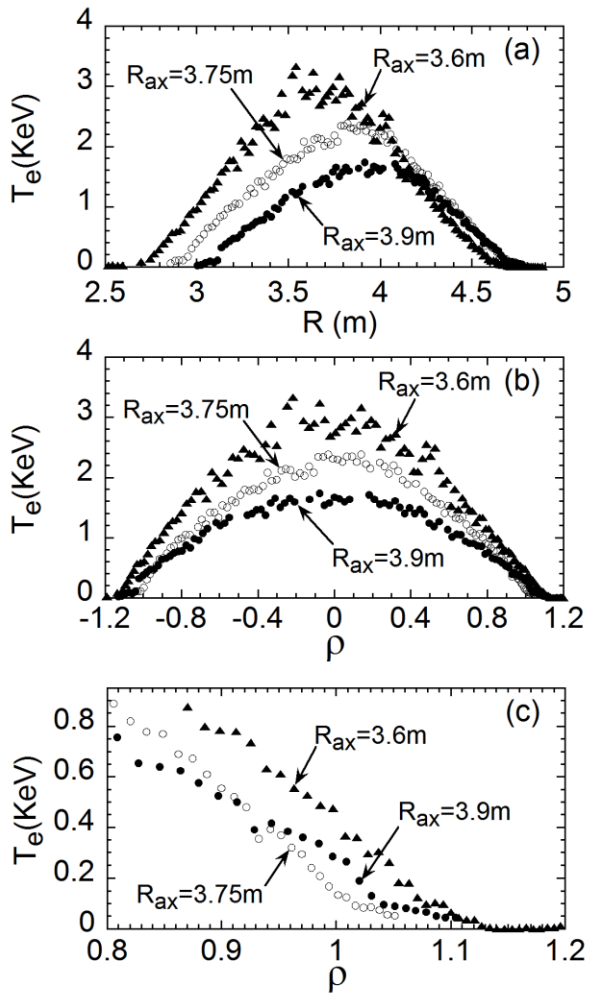

Fig. 6.3 Typical electron temperature (T_e) profiles as a function of (a) major radius, R, (b) normalized minor radius, ρ, at magnetic axis positions of R_{ax}=3.6 m (closed triangles), R_{ax}=3.75 m (open circles) and R_{ax}=3.9 m (closed circles) in LHD. Enlarged electron temperature profiles at outboard side are shown in (c).

In LHD, the electron temperature profile is measured by the Thomson scattering system along the major radius at horizontally elongated plasma cross section [10]. Typical electron temperature profiles at different magnetic axis positions are plotted in Fig. 6.3 under the same input power condition. The plasma volume defined by the LCFS is the

biggest at magnetic configuration of R_{ax}=3.6 m, as seen in Fig. 6.3(a). The highest central temperature is then obtained in the R_{ax}=3.6 m configuration. The edge electron temperature profile at outboard side is shown in Fig. 6.3(c) with enlarged horizontal scale. The electron temperature at LCFS is 400 eV for R_{ax}=3.6 m, 150 eV for R_{ax}=3.75 m and 300 eV for R_{ax}=3.9 m. Here, the value of LCFS in vacuum is used for analyzing the data. Electron temperature and density in the ergodic layer usually range in T_e=10-500 eV and $n_e<10^{14}$ cm^{-3}, respectively. Although such parameters are lower compared to those in the plasma core, the ergodic layer exhibits somewhat a sufficient confinement against the edge plasma.

6.3 Vertical profile of impurity line emissions in the vicinity of X-point

6.3.1 Vertical profiles of CIV and CVI near X-point

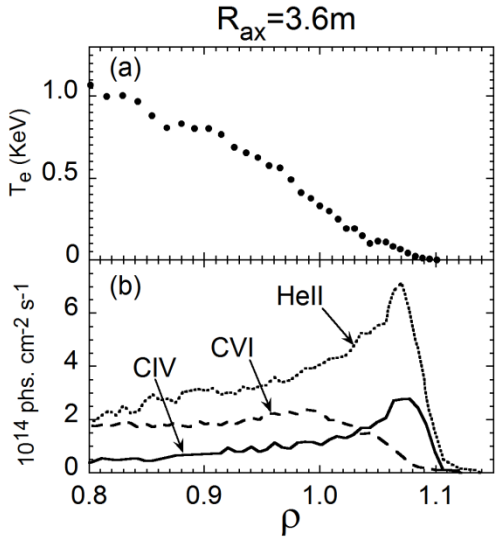

Fig. 6.4 (a) Radial electron temperature profile as a function of normalized minor radius, ρ and (b) radial profiles of HeII (303.78 Å, 2p $^2P_{1/2,3/2}$ -1s $^2S_{1/2}$, E_i=54 eV), CIV (312.4 Å, $1s^2$3p $^2P_{1/2,3/2}$ -$1s^2$2s $^2S_{1/2}$, E_i=65 eV), and CVI (33.73 Å, 2p $^2P_{1/2,3/2}$ – 1s $^2S_{1/2}$, E_i=490 eV) as a function of normalized minor radius, ρ.

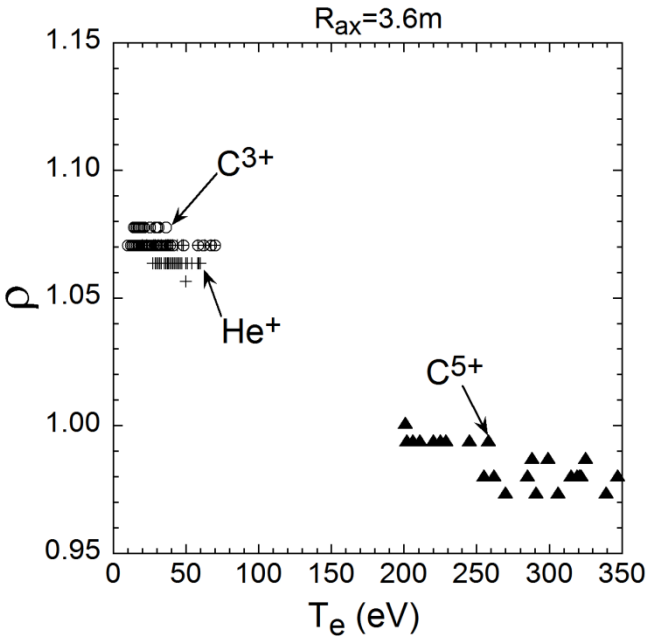

Fig. 6.5 Typical radial locations of He^{+} (E_i=54 eV), C^{3+} (E_i=65 eV) and C^{5+} (E_i=490 eV) ions as a function of electron temperature, T_e, at radial location where the impurity ion exists.

Vertical profiles of HeII (303.78 Å, 2p $^2P_{1/2,3/2}$ -1s $^2S_{1/2}$, E_i=54 eV), CIV (312.4 Å, $1s^2$3p $^2P_{1/2,3/2}$ -$1s^2$2s $^2S_{1/2}$, E_i=65 eV) and CVI (33.73 Å, 2p $^2P_{1/2,3/2}$ – 1s $^2S_{1/2}$, E_i=490 eV) are shown in Fig. 6.4(b). In the figure the vertical position is converted into the normalized plasma minor radius, ρ. Then, the peak position of the radial profiles indicates the radial location of impurity ions. The peak positions of HeII and CIV profiles are located around ρ=1.07 at which the electron temperature is T_e=50 eV, and the peak position of CVI profile is located around ρ=0.98 at which the electron temperature is T_e=400eV. The radial locations of He^{+}, C^{3+} and C^{5+} are analyzed for several discharges of LHD and plotted against the location temperature where the impurity ion exists. The result is shown in Fig. 6.5. It is clear from the figure that the He^{+} and C^{3+} ions are located in outer region of the ergodic layer ($1.06 \leq \rho \leq 1.08$) since the ionization energies are low. The

helium neutral with room temperature existing as the residual gas in the vacuum vessel deeply penetrates into the edge plasma. However, the carbon ions are transferred from the divertor plates along the magnetic field. Therefore, the charge state of carbon ions reflects information of the local electron temperature. As a result, the C^{3+} ions exist outside the radial location of He^{+} ions and distribute in a little wider temperature range compared to the He^{+} ions. On the other hand, the C^{5+} ions are located a little inside the LCFS (ρ=1) because the ionization energy (E_i=490 eV) is sufficiently high. The electron temperature range where the C^{5+} ions are located is further wide, i.e. 200-350eV, reflecting the change of the radial location. From the measurement, we can conclude that the C^{3+} emission is suitable for studying the impurity behavior near X-points.

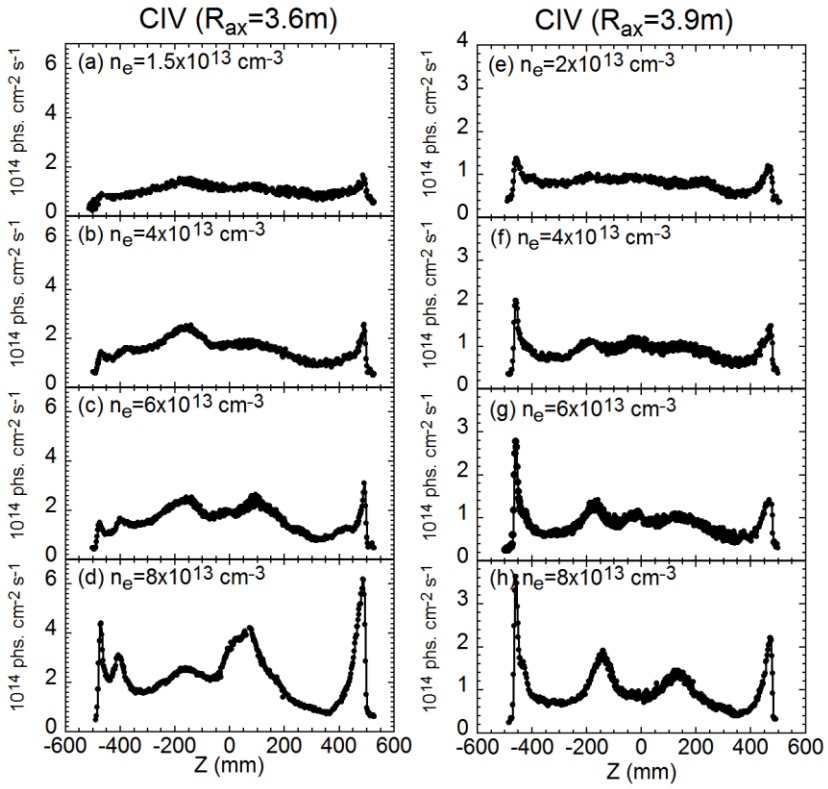

Fig. 6.6 (a)-(d) Vertical profiles of CIV (312.4 Å, $1s^2 3p\ ^2P_{1/2,3/2}$ -$1s^2 2s\ ^2S_{1/2}$, E_i=65 eV) at horizontally elongated plasma cross section at magnetic axis position of R_{ax}=3.6 m and (e)-(h) vertical profiles of CIV (312.4 Å, $1s^2 3p\ ^2P_{1/2,3/2}$ -$1s^2 2s\ ^2S_{1/2}$, E_i=65 eV) at horizontally elongated plasma cross section at magnetic configuration of R_{ax}=3.9 m.

The vertical profiles of CIV at horizontally elongated plasma cross section are shown in Fig. 6.6 at different density ranges for two magnetic configurations of R_{ax}=3.6 and 3.9 m. In the plasma axis position of R_{ax}=3.6 m two ordinary peaks are appeared at around Z=±470 mm, which indicate the radial location of C^{3+} ions in the vicinity of O-points at the top and bottom of the plasma showing an asymmetric intensity profile. On the contrary, the CIV emissions in the region of Z=-200 mm – Z=+200 mm reflects information in the vicinity of inboard and outboard X-points, as shown in Fig. 6.1(a). Here, it should be noticed that the observation chord in the region passes through both the inboard and outboard X-points. In low electron density range less than n_e=1.5x10^{13} cm^{-3} at Fig. 6.6(a), no clear CIV intensity peak appears in the region of Z=-200 mm – Z=+200 mm. With increasing the electron density, two peaks additionally appear at around Z=-150 mm and Z=+100 mm. The two peaks are very clear in high electron density range at n_e=8x10^{13} cm^{-3} at Fig. 6.6(d). A small intensity peak can be also identified at around Z=-400 mm.

The CIV profiles at the plasma axis position of R_{ax}=3.9 m, as plotted in Figs. 6.6(e)-(h), show the result similar to ones at R_{ax}=3.6 m. The behavior of ordinary peaks located at Z=±460 mm in R_{ax}=3.9 m is exactly the same as the case of R_{ax}=3.60 m. However, the CIV intensity at the bottom edge of Z=-460 mm is stronger than that at the top edge of Z=+460 mm. The result shows an opposite asymmetric intensity profile compared to R_{ax}=3.6 m case. Additional two peaks near X-points are also appeared at Z=±150 mm in R_{ax}=3.9 m. We notice that the distance at R_{ax}=3.9 m between the two peaks is a little wider than that at R_{ax}=3.6 m. The small peak appeared near the bottom edge in the case of R_{ax}=3.6m seems to disappear in the case of R_{ax}=3.9 m. It is probably merged into the ordinary peak at the bottom edge. All the CIV profile structures observed here of course reflect non-uniform temperature and density profiles including impurity based on stochastic magnetic field structure in the ergodic layer.

On the other hand, the CVI profile shows an entirely different structure. Since the C^{5+} ion is located a little inside the LCFS (ρ=1), as shown in Fig. 6.5, the CVI emission is basically a function of magnetic flux surfaces. The upper half of CVI vertical profile at

horizontally elongated plasma cross section is plotted in Fig. 6.7 at different density range for two magnetic configurations of R_{ax}=3.6 m and 3.75 m. It is clear from the figure that the profile does not reflect any magnetic field structure in the ergodic layer, in particular near the X-points. No clear change is observed in the CVI profile for both the magnetic configurations of R_{ax}=3.6m and 3.75m, even if the density is increased. The CIV and CVI vertical profiles with completely different structures are then analyzed by simulation code.

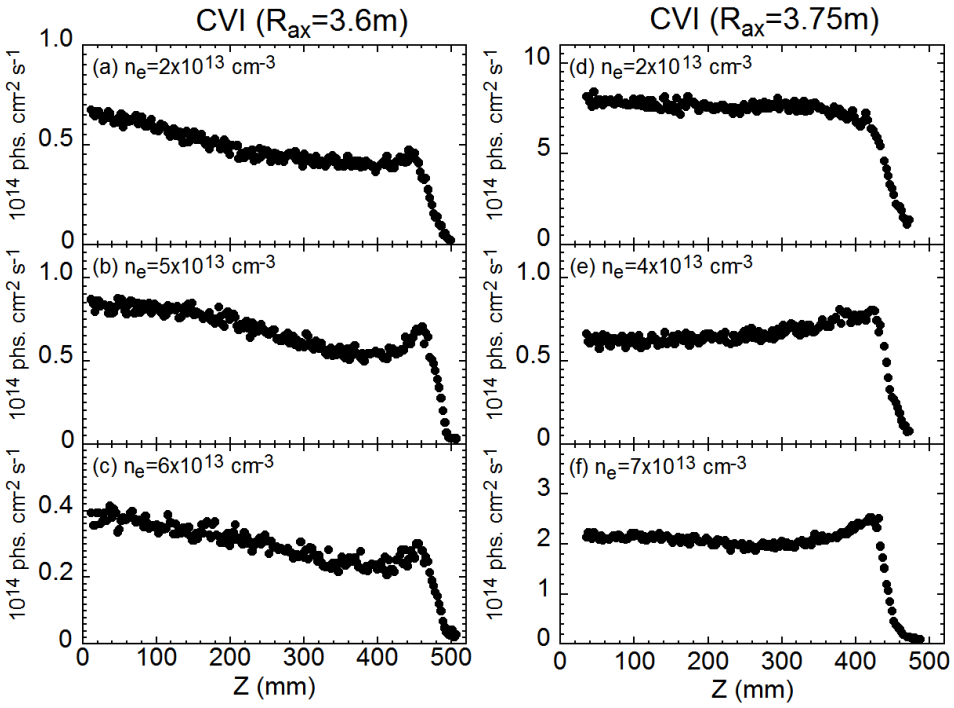

Fig. 6.7 (a)-(c) Vertical profiles of CVI (33.73 Å, 2p $^2P_{1/2,3/2}$ – 1s $^2S_{1/2}$, E_i=490 eV) at horizontally elongated plasma cross section at magnetic axis position of R_{ax}=3.6m and (d)-(f) vertical profiles of CVI (33.73 Å, 2p $^2P_{1/2,3/2}$ – 1s $^2S_{1/2}$, E_i=490 eV) at horizontally elongated plasma cross section at magnetic configuration of R_{ax}=3.75 m.

6.3.2 Three dimensional edge transport code, EMC3-EIRENE

Impurity transport in the ergodic layer has been analyzed using three-dimensional edge transport code, EMC3-EIRENE [11]. The code of EMC3 solves the fluid equations of particle, momentum and energy in steady state. This code is coupled with the neutral transport code, EIRENE, which solves the kinetic model of neural transport and simulates the recycling neutrals from divertor plates as well as interaction with bulk plasma, e.g., ionization, recombination, charge exchange and so on. The density and energy flux at the LCFS are used as the boundary conditions for particle and energy transport, while the Bohm condition is imposed at the divertor plate.

In the fluid model of EMC3, the momentum balance equation of impurity ions along the magnetic field line is given as

$$m_z \frac{\partial V_{z//}}{\partial t} = -\frac{1}{n_z}\frac{\partial T_i n_z}{\partial s} + m_z \frac{V_{i//} - V_{z//}}{\tau_s} + ZeE_{//} + 0.71\mathrm{Z}^2 \frac{\partial T_e}{\partial s} + 2.6\mathrm{Z}^2 \frac{\partial T_i}{\partial s} \ , \qquad (6.1)$$

where z and i denote the impurity with charge state Z and the bulk plasma ion, respectively. The notation of s is the coordinate along the magnetic field line. The variables of $V_{i//}$, $V_{z//}$, τ_s and $E_{//}$ denote the parallel velocities of background ion and impurity, impurity-ion collision time and parallel electric field, respectively. In this equation, the temperature of impurity ion, T_z, and the temperature of bulk plasma ion, T_i, is assumed to be the same. The terms on the right hand side of Eq. (6.1) represent the impurity pressure gradient force, the friction force exerted by the background parallel plasma flow, electrostatic force, electron and ion thermal forces called temperature gradient force. It has been proved that the dominant terms in the equation are the friction force at the second term and the ion thermal force at the fifth term. For the steady condition, therefore, the equation can be rewritten by

$$0 = m_z \frac{V_{i//} - V_{z//}}{\tau_s} + 2.6\mathrm{Z}^2 \frac{\partial T_i}{\partial s} \ . \qquad (6.2)$$

The parallel impurity velocity is then given by

$$V_{z//} = V_{i//} + 2.6Z^2 \frac{\tau_s}{m_z} \frac{\partial T_i}{\partial s} \quad . \tag{6.3}$$

The flow of the bulk plasma ions, $V_{i//}$, is usually directed towards the downstream, i.e., from plasma edge to diverter plates. On the contrary, the temperature gradient, $\frac{\partial T_i}{\partial s}$, is directed towards the upstream, i.e., from the divertor plates to the plasma edge. Therefore, the resulting impurity velocity, $V_{z//}$, is a consequence of the competition between the two terms of friction and ion thermal forces at right hand side.

In the direction perpendicular to the magnetic field lines, the impurity is assumed to diffuse with a spatially constant diffusion coefficient which is the same for all charge states and the bulk plasma ions.

6.3.3 Comparison with 3-D simulation on vertical profiles of CIV and CVI

Two-dimensional distribution of magnetic field connection length, L_c, is plotted in Fig. 6.8(a) for R_{ax}=3.6 m magnetic configuration. In the figure the L_c length is distinguished in different color. The bright and dark color means longer and shorter connection lengths in the ergodic layer, respectively. We understand well from the figure that stochastic magnetic field lines in the ergodic layer consist of magnetic field connection lengths from 10 to 10^4 m. The edge plasma in a region having longer magnetic field connection lengths, e.g., $L_c \geq 10^3$ m, behaves like core plasma with magnetic surface. Therefore we usually define the normalized plasma radius even in the ergodic layer as the extension of the magnetic surface in the core plasma. In this case the defined normalized plasma radius exceeds unity, e.g., ρ=1.1. We also notice that the magnetic field connection length ranges at L_c<100 m in most area near X-point.

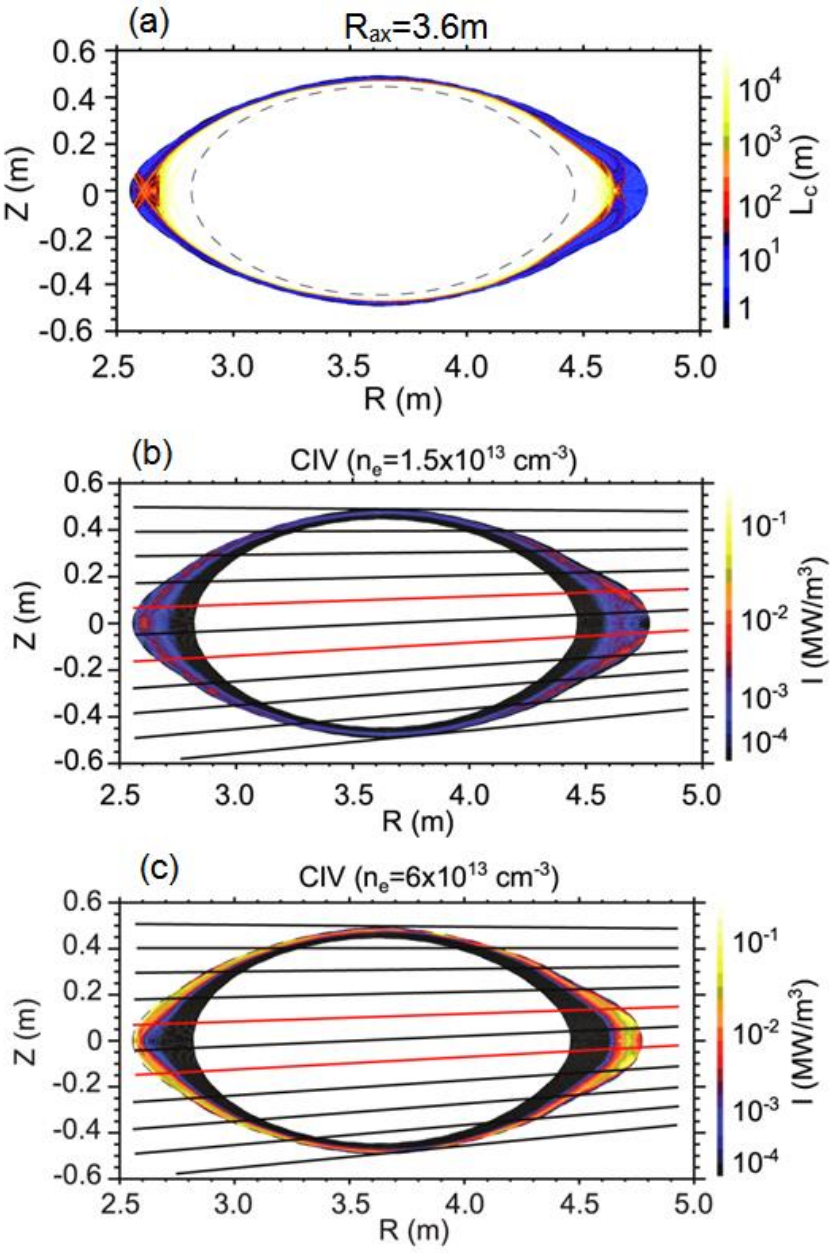

Fig. 6.8 Two-dimensional distributions of (a) connection length of magnetic field lines, L_c, (b) CIV intensity at n_e=1.5x10^{13} cm^{-3} and (c) CIV intensity at n_e=6x10^{13} cm^{-3}. Solid lines in (b) and (c) indicate the observation chord of EUV spectrometer in each interval of ΔZ=100 mm from Z=-500 mm to Z=500 mm.

CIV distribution in the ergodic layer simulated with EMC3-EIRENE is shown in Figs. 6.8 (b) and (c) at different densities of 1.5 and 6.0×10^{13} cm^{-3}, respectively. Here, the density is denoted at LCFS. In the figure the CIV intensity is expressed in different color. In the low electron density, the thermal force, i.e., the second term in the right side of Eq. (6.2), is dominant because the ion temperature in the edge plasma boundary outside the ergodic layer is relatively high. Then, it pushes the carbon ions to the upstream. As a result, the CIV is located a little inside the ergodic layer and the distribution is nearly uniform, as seen in Fig. 6.8 (b). In high electron density, the friction force between carbon and bulk ions, i.e. the second term at the right side of Eq. (6.2), becomes strong because the ion temperature in the edge plasma boundary is low. The change in the force balance along the magnetic field turns the impurity ions in the edge boundary and finally pushes the carbon ions to the downstream. Since the CIV is located in the edge boundary outside the ergodic layer where the magnetic field lines are short, the two-dimensional distribution is extremely non-uniform.

The impurity screening effect appeared at high density range is also observed in magnetic configuration of R_{ax}=3.9 m. The two-dimensional distribution of magnetic field connect length is shown in Fig. 6.9(a). The ergodic layer at R_{ax}=3.9 m is much thicker than that at R_{ax}=3.6 m (also see Fig. 6.8(a)). In the low electron density of $n_e=2x10^{13}$ cm^{-3}, the CIV is widely distributed in the ergodic layer. In the high electron density of $n_e=8x10^{13}$ cm^{-3}, however, the CIV is only distributed in a limited poloidal location near X-points of the ergodic layer where the connection length of magnetic field lines is relatively small.

On the other hand, the CVI poloidal distribution is much different from the CIV because of its high ionization energy (E_i=490 eV). The two-dimensional distribution of CVI at magnetic configuration of R_{ax}=3.6 m is plotted in Fig. 6.10. The CVI is emitted near LCFS in both the low and high electron densities. In addition, the CVI distribution is poloidally uniform. The poloidally uniform CVI distribution is also observed at magnetic

configuration of R_{ax}=3.9 m. Therefore, it means that the ergodic layer near LCFS can behave exactly like the core plasma with magnetic surfaces.

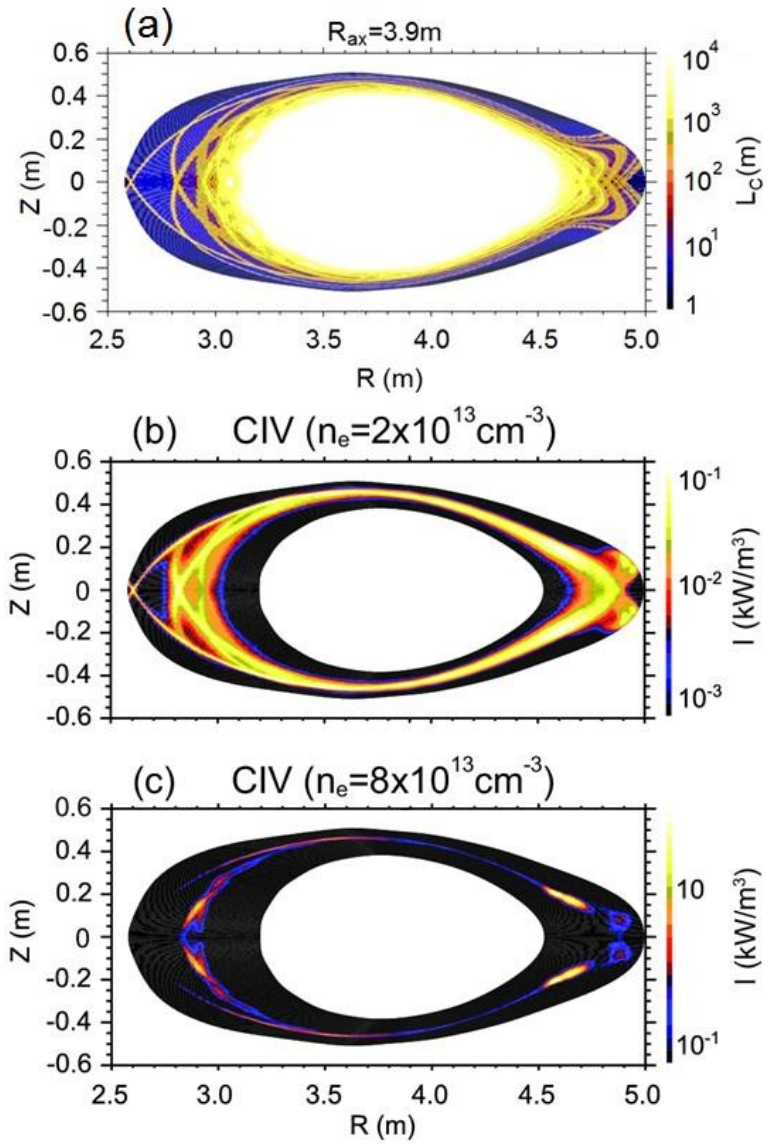

Fig. 6.9 Two-dimensional distributions of (a) connection length of magnetic field lines, L_c, (b) CIV intensity at n_e=2x10^{13} cm^{-3} and (c) CIV intensity at n_e=8x10^{13} cm^{-3} at magnetic configuration R_{ax}=3.9 m.

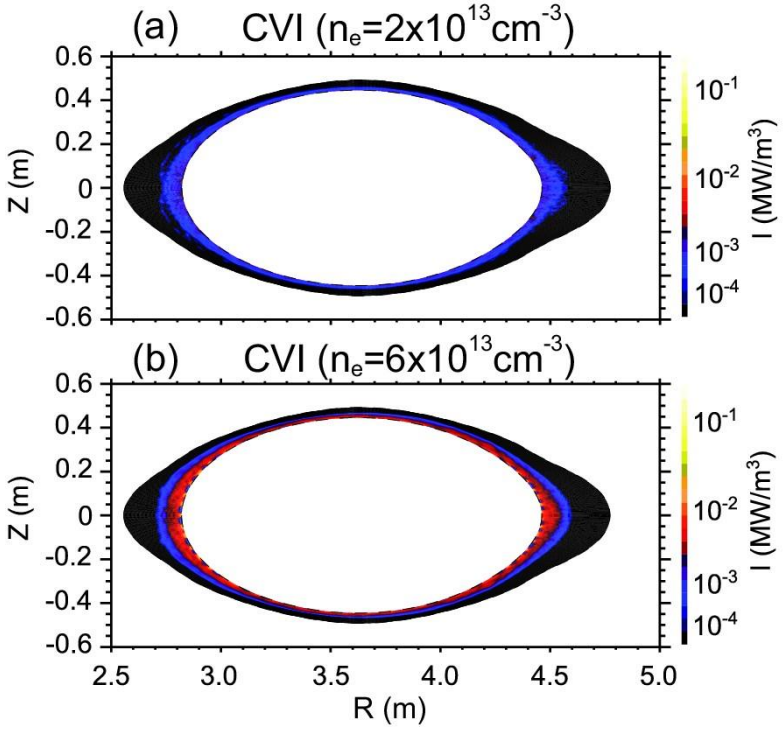

Fig. 6.10 Two-dimensional distributions of (a) CVI intensity at n_e=2x10^{13} cm^{-3} and (b) CVI intensity at n_e=6x10^{13} cm^{-3} at magnetic configuration R_{ax}=3.6 m.

Vertical profiles of carbon ions are calculated from three-dimensional carbon density distribution obtained from the simulation code. Observation chords of the space-resolved EUV spectrometer are considered in the calculation. Typical results from R_{ax}=3.6 m magnetic configuration are plotted in Figs. 6.11 (a) and (b) at different densities of 1.6 and 6.0×10^{13} cm^{-3}, respectively. The vertical profiles of CII, CIII, CV and CVI are also shown in the figures in addition to CIV. The line emissions of CII (E_i=24 eV), CIII (E_i=48 eV) and CIV (E_i=64 eV) are located in the edge boundary of ergodic layer due to their low ionization energies. Then, the vertical intensity profiles near X-point, i.e., the range of Z=-200 mm to Z=+200 mm, reflect a complicated magnetic field structure. On the contrary, the CV (E_i=392 eV) and CVI (E_i=490 eV) are located near LCFS (ρ=1) due to their high

ionization energies. The vertical profiles of CV and CVI seem to have no relation with three-dimensional magnetic field structure in the ergodic layer. In particular, it becomes clear at high electron density range shown in Fig. 6.11 (b), in which the vertical profiles of CV and CVI in the vicinity of X-point are nearly flat. In the working wavelength range of space-resolved EUV spectrometer (30-650 Å), the line CII emission does not exist and CIII and CV emissions are very weak. Therefore, in the present study on the impurity behavior in ergodic layer, strong line emissions of CIV (312.4 Å, $1s^2 3p\ ^2P_{1/2,3/2} - 1s^2 2s\ ^2S_{1/2}$) and CVI (33.73 Å, $2p\ ^2P_{1/2,3/2} - 1s\ ^2S_{1/2}$) are mainly used for the carbon ions.

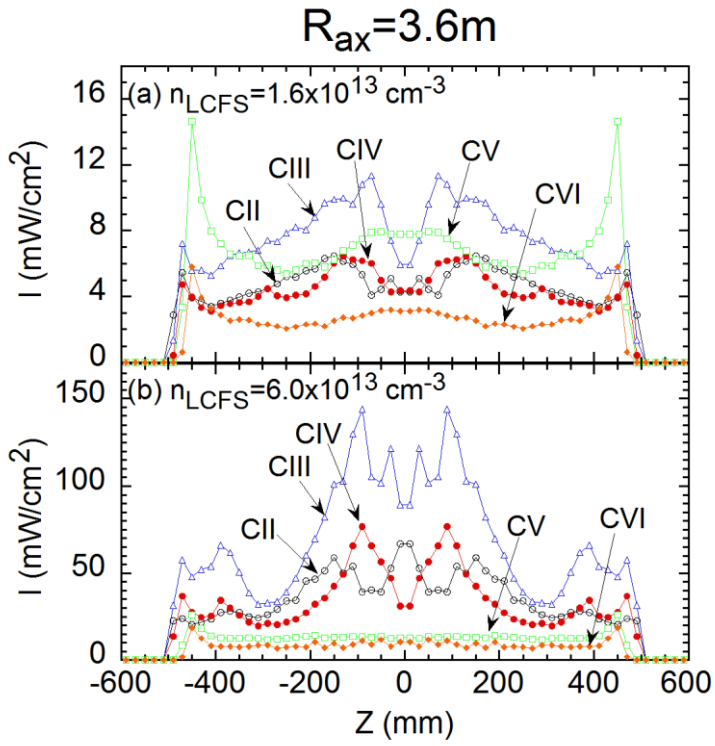

Fig. 6.11 Simulated vertical profiles of CII, CIII, CIV, CV and CVI intensities at horizontally elongated plasma cross section for magnetic axis position of R_{ax}=3.6 m.

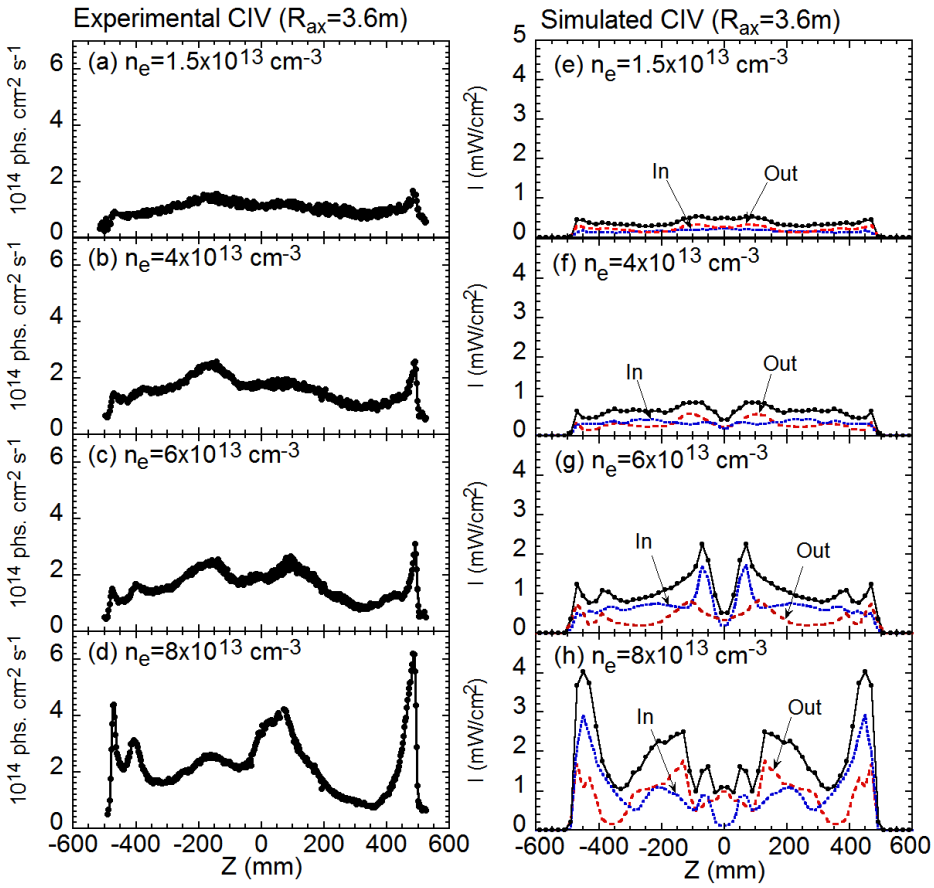

Fig. 6.12 (a)-(d) Measured vertical profiles of CIV (312.4 Å, $1s^2 3p\ ^2P_{1/2,3/2}$ -$1s^2 2s\ ^2S_{1/2}$, E_i=65 eV) and (e)-(h) simulated vertical profile of CIV in horizontally elongated plasma cross section at different electron densities for R_{ax}=3.6 m. The notations of "In" and "Out" indicate vertical profile of CIV emitted from inboard (R_{ax}<3.6 m) and outboard (R_{ax}>3.6 m) sides in the ergodic layer, respectively.

The vertical profiles of CIV measured at horizontally elongated plasma cross section in R_{ax}=3.6 m is compared with the simulation. The result is shown in Fig. 6.12 for four different density ranges. It seems that the simulation can well explain the measurement, in particular, in the viewpoint of the density effect. In low electron density of $1.5x10^{13}$ cm^{-3}, the vertical profile of CIV is relatively flat as shown in Figs. 6.12(a) and

(e). With increasing the electron density, two peaks appear at Z~-150 mm and Z~+100 mm for measurement and Z=-80~-150 mm and Z=+80~+150 mm for simulation. In the figures the notations of "In" and "Out" indicate the vertical profiles of CIV calculated by only considering the left (2.5≤Z≤3.6 m) and right half (3.6≤Z≤4.8 m) of two-dimensional emission distribution shown in Fig. 6.8, respectively. In the low electron density, the CIV line emissions from outboard X-point mainly contributes to the two peak intensities, as seen in Fig. 6.8(b) and Figs. 6.12(e) and (f). When the electron density is increased to n_e=6x10^{13} cm^{-3}, the intensity of two peaks is dominant at inboard X-point, as seen in Fig. 6.8(c) and Fig. 6.12(g). However, the intensity of two peaks is dominant again at the outboard X-point, when the electron density further increases to n_e=8x10^{13} cm^{-3}, as seen in Fig. 6.12(h). In the simulation the CIV intensity is sensitive to the presence of island in the edge boundary region. When the density increases, the radial location of CIV changes a little. When the CIV radial location overlaps with a small island in the edge boundary region, the CIV intensity is changed. Then, the dominant CIV intensity region is changeable between the inboard and outboard X-points. At present, however, it is not easy to certificate experimentally the intensity difference between the inboard and outboard X-points due to the lack of data. Another small peak experimentally identified at Z=-400 mm in Figs. 6.12(c) and (d) can be found in the simulation, i.e., Z=±370 mm in Fig. 6.12(g). However, it is also disappeared as shown in Fig. 6.12(h), when the electron density increases to n_e=8x10^{13} cm^{-3}.

The CIV profile structure is also simulated at magnetic configuration of R_{ax}=3.9 m to compare with the measurement shown in Figs. 6.6(e)-(h). The result is plotted in Fig. 6.13 with experimental result. Additional two peaks near X-point are located at Z=±150 mm for measurement as seen in Fig. 6.13(d) and Z=±170 mm for simulation as seen in Figs. 6.13(f-h). The simulation can also explain the experimental result as well as the R_{ax}=3.6 m case. In the simulation at high electron density rages of Figs. 6.13(g) and (h), however, the intensity of additional two peaks is much stronger than that of ordinary two peaks at Z=±450 mm, whereas the intensity of ordinary two peaks is stronger than that of

additional two peaks in the experiment. The reason is probably originated in the electron temperature distribution near X-points calculated in the simulation. The explanation of experimental results by the edge simulation code tends to be difficult when the magnetic axis position shifted outwardly, in which the ergodic layer is thicker and the magnetic field in the ergodic layer is more complicated. A small peak at around Z=±400 mm near ordinary peaks is not also observed in the simulation as well as the measurement.

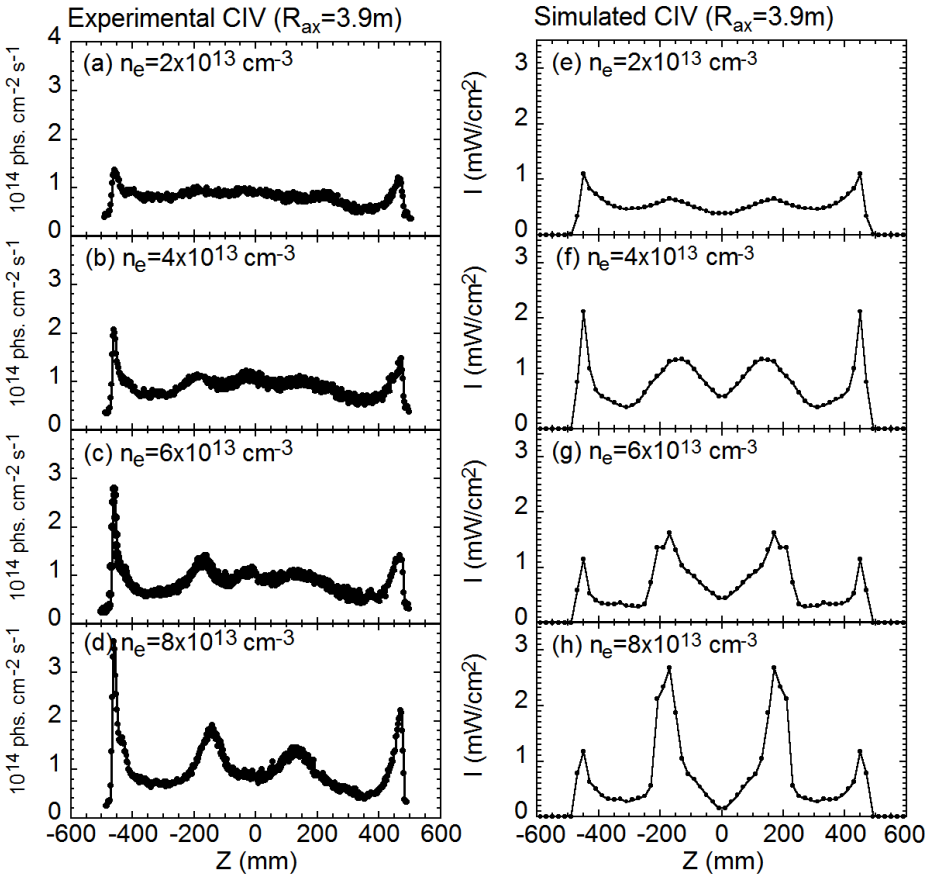

Fig. 6.13 (a)-(d) Measured vertical profiles of CIV (312.4 Å, $1s^2 3p\ ^2P_{1/2,3/2}$ -$1s^2 2s\ ^2S_{1/2}$, E_i=65 eV) and (e)-(h) simulated vertical profile of CIV intensity in horizontally elongated plasma cross section at different electron densities for R_{ax}=3.9 m.

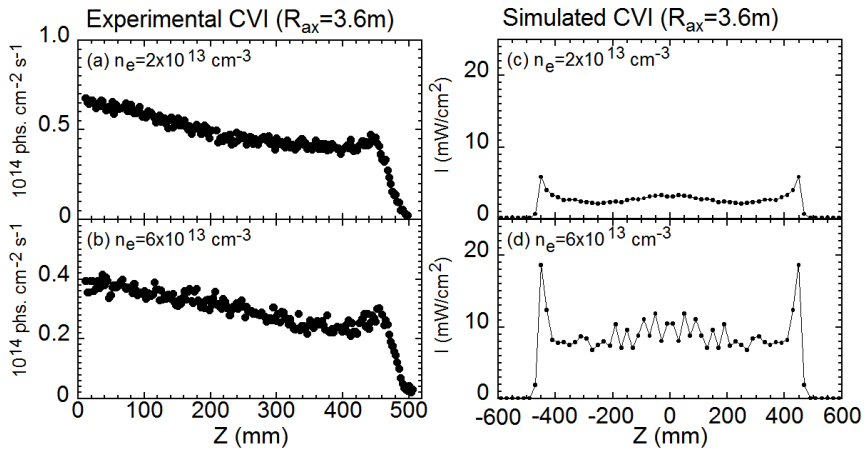

Fig. 6.14 (a)-(b) Measured vertical profiles of CVI (33.4 Å, E_i=392 eV) and (c)-(d) simulated vertical profile of CVI intensity in horizontally elongated plasma cross section at different electron densities for R_{ax}=3.6 m.

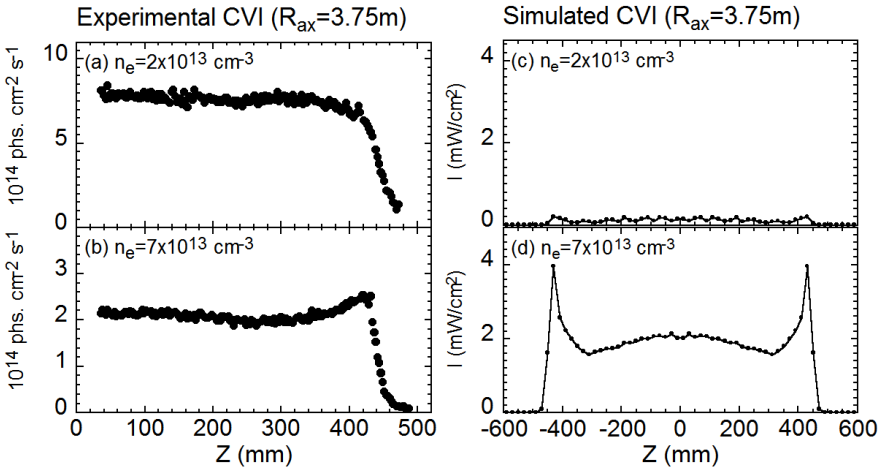

Fig. 6.15 (a)-(b) Measured vertical profiles of CVI (33.4 Å, E_i=392 eV) and (c)-(d) simulated vertical profile of CVI intensity in horizontally elongated plasma cross section at different electron densities for R_{ax}=3.75 m.

Next, the CVI vertical profile located near LCFS is compared with the simulation. The result for R_{ax}=3.6 m magnetic configuration is shown in Fig. 6.14. Any additional peaks near X-points are not also seen in the simulation, while the two ordinary peaks at Z=±450 mm are much sharp in the simulation. The comparison is also made for R_{ax}=3.9 m magnetic configuration, as shown in Fig. 6.15. Although the result is basically similar to the case of R_{ax}=3.6 m, the ordinary edge peak intensity is further strong in high electron density range of $7x10^{13}$ cm^{-3}. However, both the CIV intensities at ordinary edge peaks and near X-points are extremely weak when the density decreases to $2x10^{13}$ cm^{-3} shown in Fig. 6.15(c). The reason is now unclear.

6.4 Two-dimensional distribution of impurity line emissions in the vicinity of X-point

6.4.1 Two-dimensional distribution of impurity line emissions

The two-dimensional distribution of impurity line emissions has been observed by scanning the observation chord of space-resolved EUV spectrometer horizontally (Y direction in Fig. 6.16) during stable discharges. In LHD the elliptical plasma cross section rotates along the magnetic axis five times in one toroidal turn. It means the X-point position also rotates along the magnetic axis as a function of toroidal angle, as illustrated in Fig. 6.16. In the horizontally elongated plasma cross section ($\varphi=0^o$) the observation chord passes through both the inboard and outboard X-points, as shown in Fig. 1. If the observation chord is moved from $\varphi=0^o$, e.g. $\varphi=-2^o$ and $\varphi=+1^o$ in Fig. 6.16, the observation chords can selectively pass through either of the inboard or outboard X-points. Therefore, the impurity behavior can be separately studied against the inboard and outboard X-points based on the two-dimensional measurement.

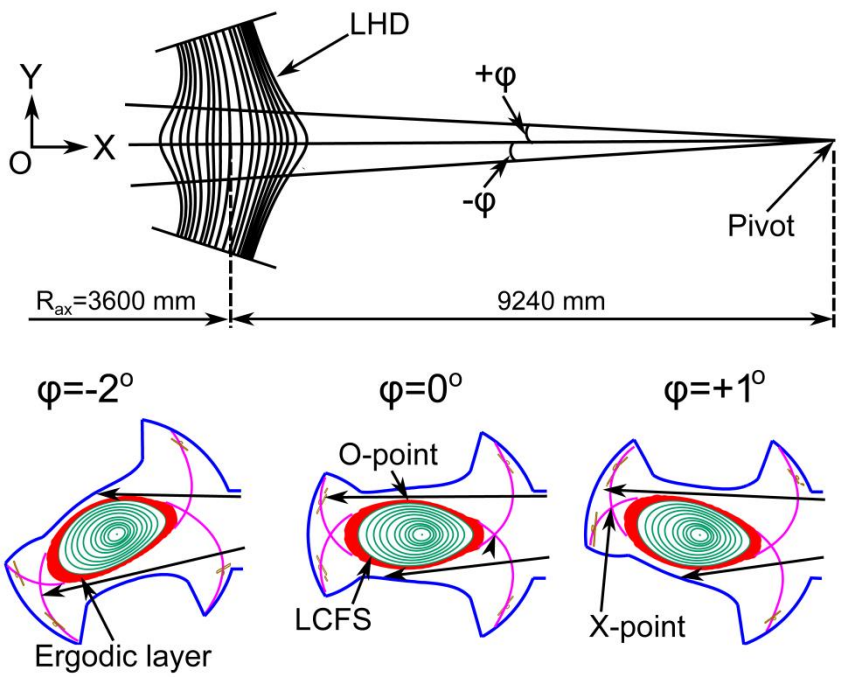

Fig. 6.16 Cross sections of LHD plasma at toroidal angles of $\varphi=-2^{o}$, $\varphi=0^{o}$ and $\varphi=+1^{o}$. Two arrows in the bottom three figures indicate the observation range of space-resolved EUV spectrometer. The toroidal angle is defined as an angle from X-axis at the pivot of spectrometer.

The two-dimensional distribution of impurity line emissions are observed at different magnetic configurations. The result on R_{ax}=3.6 m is shown in Fig. 6.17 for different impurities of (a) HeII, (b) CIV (c) FeXV and (d) CVI. The line emissions of HeII (E_i=54 eV) and CIV (E_i=65 eV) are located at the edge boundary of ergodic layer and FeXV (E_i=457 eV) and CVI (E_i=490 eV) are located around LCFS (ρ=1). Seeing Fig. 6.17, we clearly notice that the HeII and CIV emissions from inboard X-point is stronger than that from outboard X-point. A similar tendency can be also seen for FeXV and CVI emissions. Therefore, the impurity is enhanced at inboard X-point in R_{ax}=3.6 m magnetic configuration.

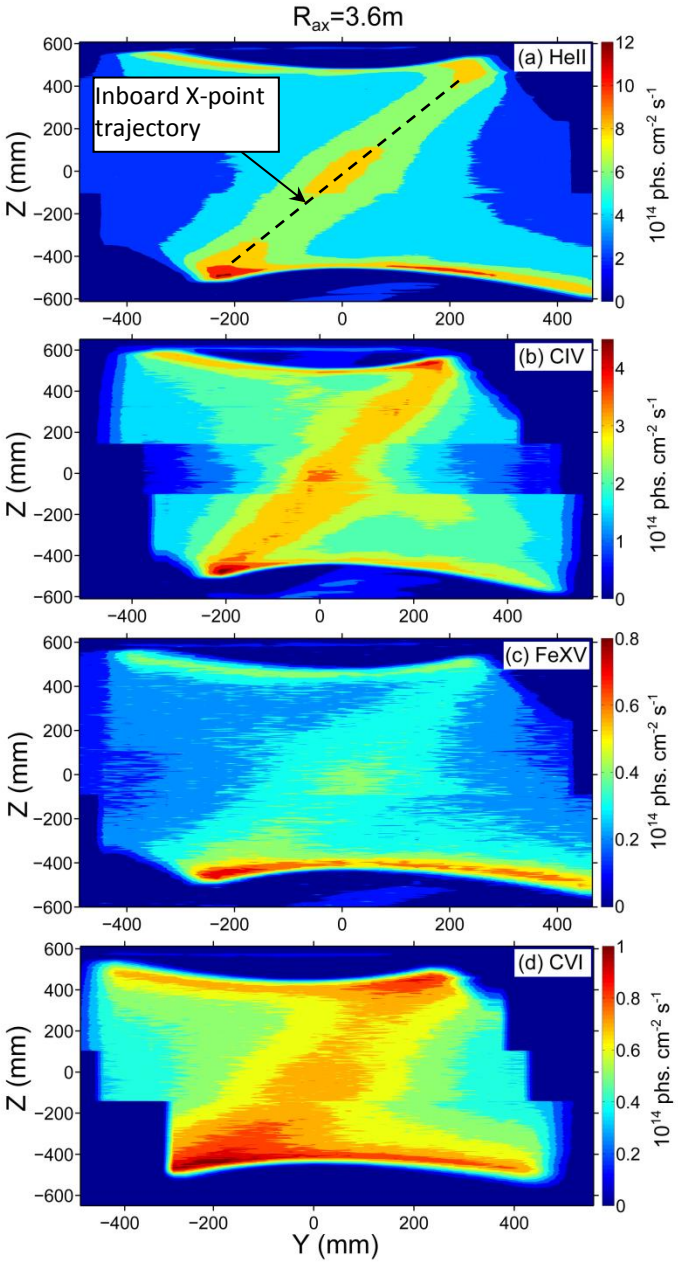

Fig. 6.17 Two-dimensional distributions of (a) HeII (303.78 Å, 2p $^2P_{1/2,3/2}$ - 1s $^2S_{1/2}$, E_i=54 eV), (b) CIV (312.4 Å, 1s^{2}3p $^2P_{1/2,3/2}$ - 1s^{2}2s $^2S_{1/2}$, E_i=65 eV), (c) FeXV (284.15 Å, 3s3p $^1P_1$ - 3s^2 $^1S_0$, E_i=457 eV) and (d) CVI (33.73 Å, 2p $^2P_{1/2,3/2}$ - 1s $^2S_{1/2}$, E_i=490 eV) at magnetic axis position of R_{ax}=3.6 m.

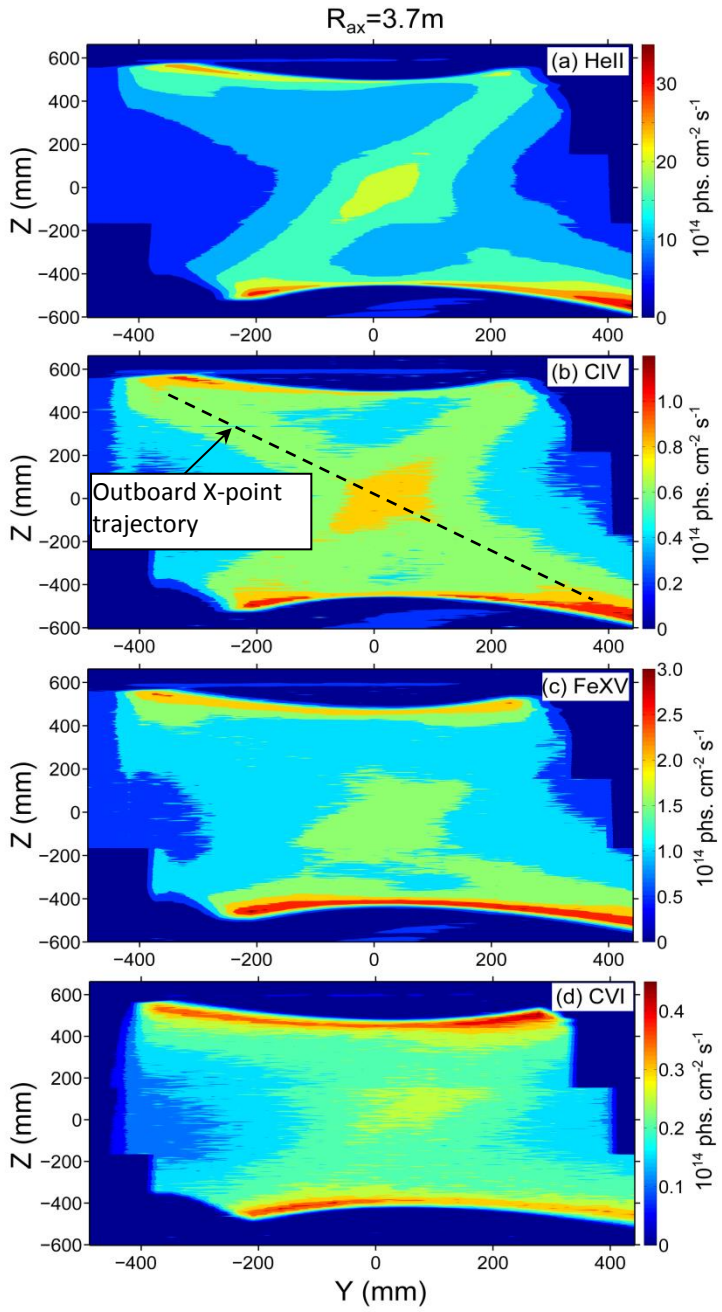

Fig. 6.18 Two-dimensional distributions of (a) HeII (303.78 Å, 2p $^2P_{1/2,3/2}$ -1s $^2S_{1/2}$, E_i=54 eV), (b) CIV (312.4 Å, $1s^2$3p $^2P_{1/2,3/2}$ -$1s^2$2s $^2S_{1/2}$, E_i=65 eV) (c) FeXV (284.15 Å, 3s3p $^1P_1$ - $3s^2$ $^1S_0$, E_i=457 eV) and (d) CVI (33.73 Å, 2p $^2P_{1/2,3/2}$ – 1s $^2S_{1/2}$, E_i=490 eV) at magnetic axis position of R_{ax}=3.7 m.

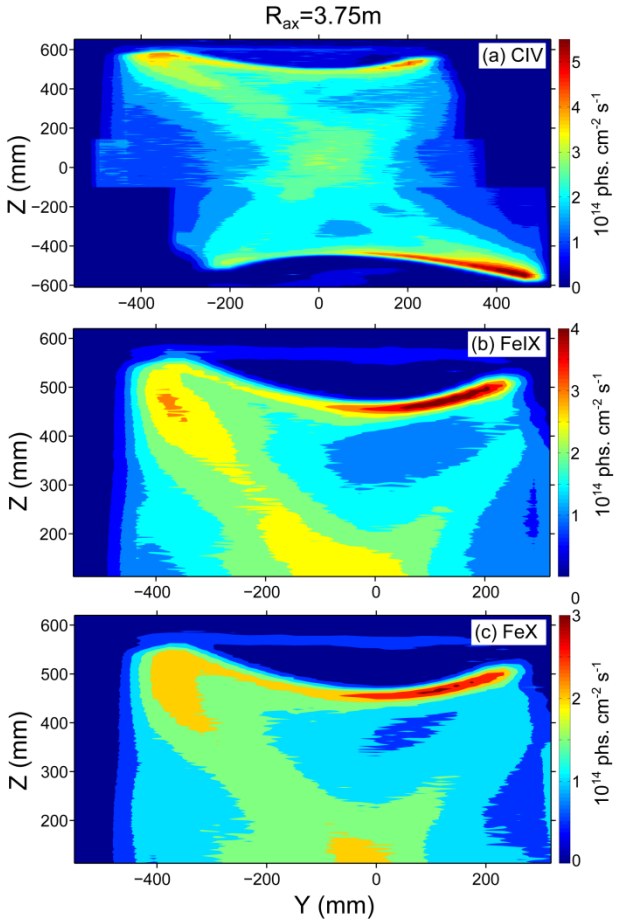

Fig. 6.19 Two-dimensional distribution of (a) CIV (312.4 Å, $1s^2 3p\ ^2P_{1/2,3/2}$ -$1s^2 2s\ ^2S_{1/2}$, E_i=65 eV) and (b) FeIX (171.1 Å, $3s^2 3p^5 3d\ ^1P_1$ – $3s^2 3p^6\ ^1S_0$, E_i=234 eV) and (c) FeX (174.5 Å, $3s^2 3p^4(^3P) 3d\ ^2D_{5/2}$ – $3s^2 3p^5\ ^2P_{3/2}$, E_i=262 eV) at magnetic axis position of R_{ax}=3.75 m.

When the magnetic axis position is shifted, the impurity behavior near X-points is clearly changes. The two-dimensional distribution for R_{ax}=3.7 m configuration is shown in Fig. 6.18 for the same impurities as Fig. 6.17. The strong trajectory from inboard X-point observed in R_{ax}=3.6 m configuration seems to disappear and the impurity emission near X-point is strong at horizontally elongated plasma cross section of Y=0 mm. The result on R_{ax}=3.75 m configuration is shown in Fig. 6.19 for impurity emissions of (a) CIV, (b) FeIX and (c) FeX. In the figure only upper half distribution is plotted for FeIX and FeX

due to the lack of data set. Seeing the figure we notice immediately that the strong impurity line trajectory near X-points is inversed reflecting the outboard X-point trajectory. From these results we conclude that the impurity near X-point changes against the magnetic axis position. When the magnetic axis position is shifted outwardly, the magnetic field line reaching the divertor plate expands from inboard side to outboard side. Therefore, magnetic field lines passing through the vicinity of outboard X-point increases in outwardly shifted magnetic configuration such as R_{ax}=3.75 m. As a result, the change of the trajectory in the impurity emission from inboard to outboard X-point strongly suggests that the impurity source is located at the divertor plate.

In the two-dimensional distribution asymmetric impurity emission is also observed at the top and bottom edge. In particular, it is clear for FeXV in Figs. 6.17(c) and 6.18(c). At present the reason is unclear. However, it shows us an interesting phenomenon on the impurity transport in the ergodic layer. It remains as the future subject.

6.4.2 Analysis of measured 2-D impurity distribution with 3-D simulation code

The two-dimensional distribution of impurity line emissions is simulated by the 3-D EMC3-EIRENE code. The result at R_{ax}=3.60m is plotted in Fig. 6.20. The trapezoidal area denoted with dashed line in Fig. 6.20(a) indicates the projection of LHD port by which the observation range of the present space-resolved EUV spectroscopy is mainly limited. The horizontally elongated plasma cross section is defined at the angle of $\varphi=18^{o}$, which corresponds to the position of Y=0 mm. The inboard and outboard X-points trajectory can be clearly seen in the 2-D distribution of HeII, as shown in Fig. 6.20(a), while the HeII emission along the inboard X-point trajectory is relatively strong. In the measurement shown in Fig. 6.17(a), however, the inboard X-point trajectory is selectively enhanced for the HeII emission. In case of the CIV and CVI, the emission along the outboard X-point trajectory seems to be relatively strong. It simply gives an opposite result compared to the measurement shown in Fig. 6.17(b) and (d).

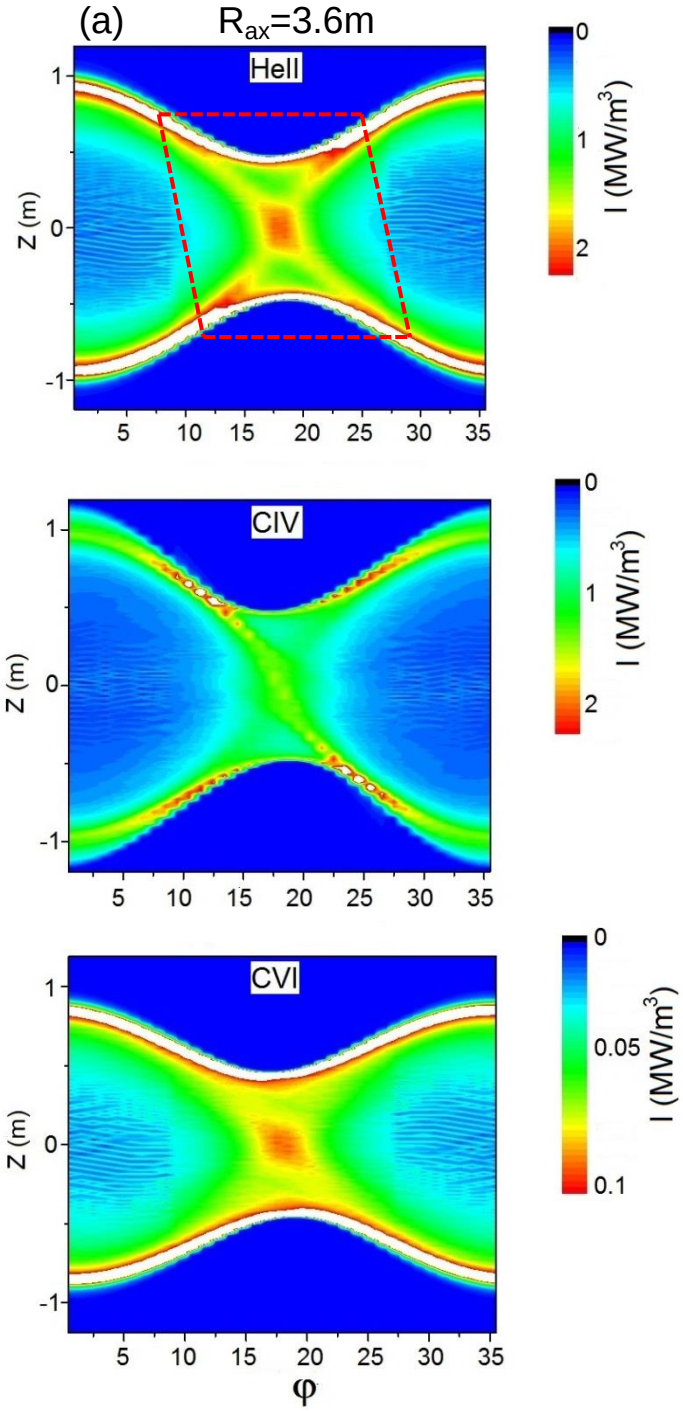

Fig. 6.20 3-D simulation on two-dimensional distributions of (a) HeII (303.78 Å, 2p $^2P_{1/2,3/2}$ - 1s $^2S_{1/2}$, E_i=54 eV), (b) CIV (312.4 Å, 1s^{2}3p $^2P_{1/2,3/2}$ - 1s^{2}2s $^2S_{1/2}$, E_i=65 eV), and (c) CVI (33.73 Å, 2p $^2P_{1/2,3/2}$ - 1s $^2S_{1/2}$, E_i=490 eV) at magnetic axis position of R_{ax}=3.6m. The trapezoidal area denoted with dashed line indicates the projection of LHD port.

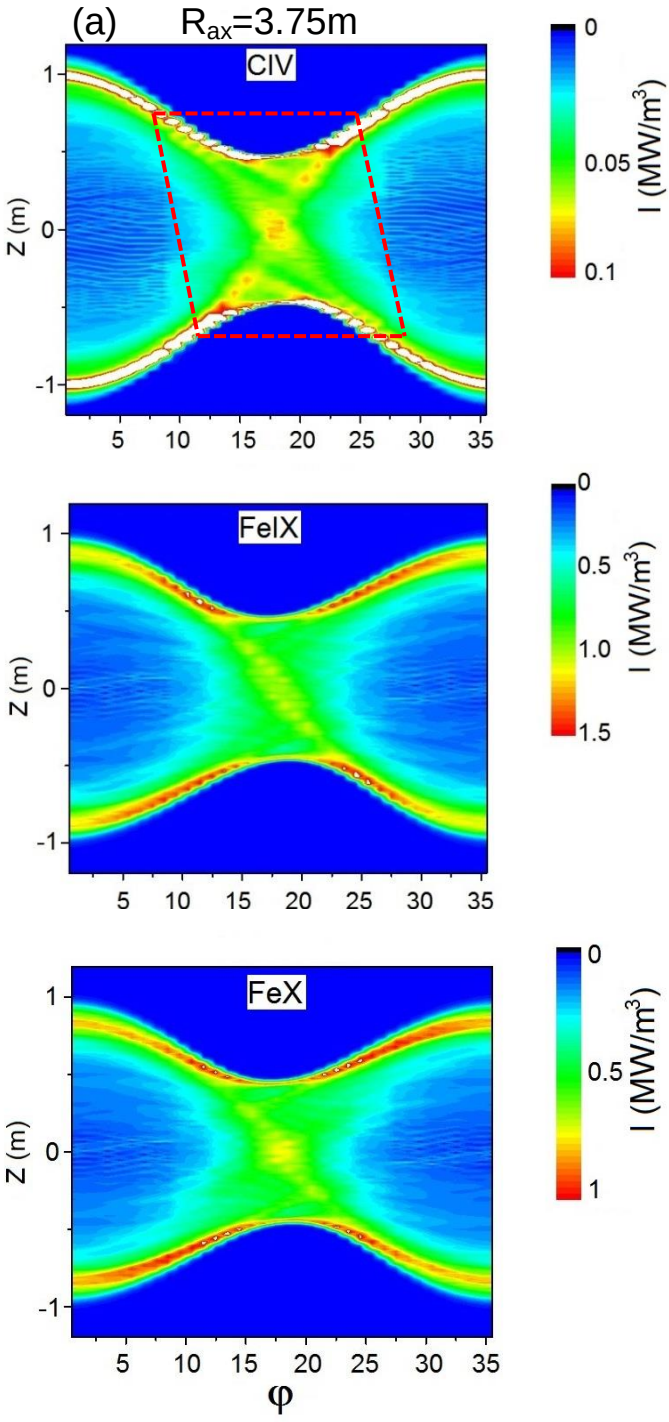

Fig. 6.21 3-D simulation on two-dimensional distribution of (a) CIV (312.4 Å, $1s^2 3p\ ^2P_{1/2,3/2}$ - $1s^2 2s\ ^2S_{1/2}$, E_i=65 eV) and (b) FeIX (171.1 Å, $3s^2 3p^5 3d\ ^1P_1$ – $3s^2 3p^6\ ^1S_0$, E_i=234 eV) and (c) FeX (174.5 Å, $3s^2 3p^4(^3P)3d\ ^2D_{5/2}$ – $3s^2 3p^5\ ^2P_{3/2}$, E_i=262 eV) at magnetic axis position of R_{ax}=3.75 m.

The result of 2-D simulation at magnetic configuration of R_{ax}=3.75 m is shown in Fig. 6.21. In the CIV 2-D distribution, the X-point trajectory blurs for both the distributions from the measurement (Fig. 6.19(a)) and the simulation (Fig. 6.21(a)). On the contrary, the emissions of FeIX and FeX are clearly enhanced at the outboard X-point trajectory as shown in Figs. 21(b) and (c), respectively. When the result is compared with the measurement shown in Figs. 6.19(b) and (c), we understand that the simulation shows a good agreement with the measurement.

Through the present 2-D measurement, it is shown that the present 3-D simulation code can basically explain the experimental result, although a small discrepancy is observed for the 2-D distribution of CIV. In discharges with R_{ax}=3.6 m configuration a strong particle recycling is usually observed at the inboard side. An increased neutral density at the inboard side can enlarge the density gradient and enhance the friction force along magnetic fields at the inboard side of horizontally elongated plasma cross section. As a result, the impurity transport at the inboard side may be modified due to the localized neutral density, showing stronger impurity screening.

6.5 Summary

The CIV vertical profiles near X-point are studied at horizontally elongated plasma cross section with magnetic field structure in the ergodic layer. In low-density range less than $2x10^{13}$ cm^{-3}, the CIV profile near X-point is almost flat. When the density increases, two peaks newly begin to appear near X-points in addition to ordinary edge peaks, whereas such peaks do not appear in the profile of CVI located near LCFS. Those additional peaks become very clear at high-density range of $n_e \geq 8x10^{13}$ cm^{-3}. This phenomenon can be observed at several magnetic axis positions. The vertical profile of CIV is analyzed using three-dimensional edge transport code. In the low-density case, the C^{3+} ions move upstream and widely expand in the ergodic layer due to dominant thermal force, which leads to the flat CIV profile. With increasing the density, the friction force becomes dominant and the impurity ions start to move downstream. The C^{3+} ions stay in the

vicinity of the X-point, where magnetic field lines are directly connected to divertor plates. Thus, the two peaks near X-point are clearly formed with increase in the C^{3+} density. This is a clear experimental certification on the presence of the impurity screening in the ergodic layer of LHD.

The two-dimensional distributions of impurity line emissions are observed for different plasma axis positions. It is found that the impurity emission becomes strong along the poloidal trajectory of X-points and the poloidal trace is moved from inboard X-point trajectory to outboard X-point trajectory when the plasma axis is changed from 3.60 m to 3.75 m. When the magnetic axis position is shifted outwardly, the dominant fraction of magnetic field lines connecting to the divertor plate moves from inboard side to outboard side. The change of the poloidal trajectory of X-points in the impurity emission strongly suggests that the impurity source is located at the divertor plate. The 3-D simulation with EMC3-EIRENE code can well explain the 2-D distribution of impurity line emissions, while the 2-D CIV distribution at magnetic configuration of R_{ax}=3.6 m indicates a small discrepancy between the simulation and measurement. An increased neutral density at the inboard side can enlarge the density gradient and enhance the friction force along magnetic fields at the inboard side of horizontally elongated plasma cross section. Therefore, the impurity transport at the inboard side may be modified due to the localized neutral density, showing stronger impurity screening.

References

[1] J. Wesson, Tokamaks, 4th edition, Oxford University press, (2012).

[2] P.C. Stangeby, The Plasma Boundary of Magnetic Fusion Devices. Series: Series in Plasma Physics, vol. 7, 2000.

[3] M.Kobayashi, et.al. Nucl. Fusion **53**, 033011 (2013).

[4] N. Ohyabu, et.al. Nucl. Fusion **34**, 387 (1994).

[5] M.B. Chowdhuri, et. al. Phys. Plasmas **16**, 062502 (2009).

[6] M. Kobayashi, et. al. Plasma Fusion Res. **3**, S1005 (2008).

[7] C.F Dong, et. al. Phys. Plasmas **18**, 082511 (2011).

[8] S. Masuzaki, et. al. Nucl. Fusion **42**, 750 (2002).

[9] T. Morisaki, et. al. J. Nucl. Mater. **313**, 548 (2003).

[10] K. Narihara, et. al. Rev. Sci. Instrum. **72**, 1122 (2001).

[11] M. Kobayashi, et. al. Contrib. Plasma Phys. **48**, 255 (2008).

Chapter 7

Summary

A space-resolved extreme ultraviolet (EUV) spectrometer has been upgraded to study the impurity transport in the ergodic layer at plasma edge of large helical device (LHD) by observing the two-dimensional distribution of impurity line emissions. The ergodic layer composing of stochastic magnetic field lines maintains a low-temperature ($10 \leq T_e \leq 500$ eV) and relatively high-density ($n_e < 10^{13}$ cm^{-3}) plasma with three-dimensional structure. The space-resolved EUV spectrometer is basically consisted of a space-resolved slit placed in front of an entrance slit, a gold-coated varied-line-spacing (VLS) holographic grating (1200 grooves/mm) and a back-illuminated charge-coupled device (CCD) with 1024 x 255 pixels (26.6 μm/pixel). The two-dimensional measurement became possible by adding two stepping motors with the EUV spectrometer system to scan the observation chord horizontally and vertically. Since the EUV spectrometer observes the LHD plasma with 50 cm long image in the vertical direction, the measurement at three different vertical angles is required to record the full vertical plasma image. The spatial resolution in the vertical direction is determined by a vertical width of the spatial resolution slit. Since the spatial resolution slit of 0.2 mm in width is usually used, the EUV spectrometer system possesses a sufficient spatial resolution of 10 mm which roughly corresponds to one hundredth of the full vertical length at horizontally elongated plasma cross section of the LHD plasma. The two-dimensional distribution of impurity line emissions can be observed by scanning the horizontal angle of the EUV spectrometer with a constant speed during a relatively long stable discharge at a fixed vertical angle. Therefore, the spatial

resolution in the horizontal direction is a function of the scanning speed in addition to the original spatial resolution of 75 mm determined by the grating size and the focal length. Since the scanning speed is usually set to 3 mm/s, the horizontal spatial resolution is 90 mm at major radius of R=3.6 m. Although the horizontal observation range is limited by the rectangular spectrometer port and diamond LHD port, the upgraded EUV spectrometer system secures a sufficient image area with vertical and horizontal lengths of 1.2x0.8 m^2 to study the impurity transport in the ergodic layer. Furthermore, the wavelength range of the EUV spectrometer for measuring impurity line emissions has been also extended from 50-500 Å to 30-650 Å by adding the second stage, which enables to expand the stroke for the CCD movement in the wavelength dispersion direction from 45 mm to 75 mm. As a result, the radial profile of several line emissions such as CV at 40.3 Å, CVI at 33.7 Å and OV at 629.7 Å can be newly measured after the improvement of the spectrometer system. For the positional calibration of the observation chords a toroidal slit with one meter long was installed between the spectrometer and LHD post. The toroidal slit has a rectangular-corrugated edge with a variety of opening sections of which the width is periodically changed from 2 mm to 9 mm. When the toroidal slit is closed remaining the opening sections of the rectangular edge, the resultant vertical intensity profile of line emissions reflects a projection of the opening sections. Thus, the vertical position of observation chords can be accurately calibrated by considering the geometrical relation among the space-resolved slit, the opening section of the rectangular edge and the LHD plasma. The horizontal position is also calibrated basically with the same method. The uncertainties in the vertical and horizontal positions are estimated to be 4 mm and 10 mm, respectively. The intensity of line emissions is absolutely calibrated by comparing the bremsstrahlung continuum between visible and EUV ranges in high-density discharges of LHD, since the absolute value of the visible bremsstrahlung intensity is already known by use of integrated sphere as the standard lamp.

Vertical profiles of edge impurity line emissions of HeII and CIV have been measured at different toroidal locations of LHD by changing the horizontal angle of the EUV spectrometer shot by shot to observe the edge impurity distribution at different

poloidal positions. The radial location of HeII with ionization energy of E_i=54.4 eV reflects the penetration depth of neutral helium and the radial location of CIV with E_i=64.5 eV expresses the index of plasma edge boundary in the ergodic layer of LHD. The result indicates that the radial location of HeII is positioned at inner side compared to that of CIV, whereas the ionization energy of HeII is smaller than that of CIV. It is found that the distance between HeII and CIV radial positions is nearly constant, i.e., 4 mm, not depending on poloidal positions of the elliptical LHD plasma. The penetration depth of helium is analyzed for the comparison with the measurement. The analysis shows a good agreement with the measurement when the room temperature of 300 K is assumed for the neutral helium energy. It suggests that the neutral helium mainly enters the plasma as the residual gas in the vacuum vessel, but not as the recycling particle from the vacuum vessel or divertor plates. The full vertical profile of HeII is also measured at horizontally elongated plasma cross section to compare the intensity between the top and bottom O-points. The result shows an asymmetric profile indicating that the HeII intensity at the bottom O-point is two times stronger than that at the top O-point. This asymmetric intensity profile can be also seen in the CV vertical profile, while it is not seen in the vertical profile of CVI locating inside the last closed flux surface (LCFS). The reason still remains an open question at present.

Two-dimensional measurement of electron temperature in the ergodic layer is of crucial importance to study the transport in the edge plasma of helical devices. However, there was no diagnostics to measure such the two-dimensional edge temperature distribution in the fusion research. In the present study a diagnostic method based on the intensity ratio between two line emissions is attempted to measure the two-dimensional electron temperature distribution in the ergodic layer of LHD. For the purpose the line intensity ratio of Li-like CIV and NeVIII has been adopted in the two-dimensional EUV spectroscopy, since the C^{3+} (E_i=64.5 eV) and Ne^{7+} (E_i=239 eV) ions are located at edge boundary and deep inside near LCFS of the ergodic layer, respectively. The use of such Li-like ions in the intensity ratio measurement exhibits an important advantage that a pair of two spectral lines is closely emitted in an adjacent wavelength. The two spectral lines

can be then measured in the same CCD position. Since the intensity ratio is recorded as a function of time in a single discharge, any uncertainties based on the shot-to-shot reproducibility error in plasma discharges can be avoided from the temperature analysis. The CIV line intensity ratio of 2p-3d (384 Å) to 2p-3s (420 Å), of which the wavelengths are close, is calculated from ADAS and CHIANTI atomic codes. The result shows that the ratio is sufficiently sensitive to the electron temperature but entirely insensitive to the electron density. The vertical profile of electron temperature at the edge boundary of ergodic layer measured from the CIV line ratio ranges in 13-16 eV in the vicinity of X-point except for the plasma edge near O-point. Since the edge boundary at O-point near helical coils is connected to the divertor plate with short magnetic field lines around 10 m, the CIV temperature at O-point can be correlated with the temperature on the divertor plate. The electron temperature on divertor plates measured by Langmuir probe ranges around 10 eV. Therefore, the temperature from the CIV intensity ratio shows a good consistency with the divertor temperature. The line intensity ratio of NeVIII 3p-2s (88.08 Å+88.12 Å) to 3s-2p (102.9 Å+103.9 Å) is used to measure the electron temperature at the deep inside of ergodic layer in neutral beam injection (NBI) discharges. The vertical electron temperature distribution evaluated from ADAS ranges in 100-130 eV, while that from CHIANTI shows higher temperature, i.e., 120-230 eV. The electron temperature measured with Thomson scattering diagnostic shows 120 eV at LCFS, while it is 110 eV for ADAS and 170 eV for CHIANTI at LCFS. The electron temperature profile is also simulated with three-dimensional edge transport code, EMC3-EIRENE, and the result indicates the electron temperature of 100 eV at LCFS. As a result, the ADAS code with the reasonable electron temperature was selected for the analysis. The two-dimensional electron temperature distribution in the ergodic layer is measured at upper half of LHD plasmas using the NeVIII intensity ratio in electron cyclotron resonance (ECH) discharges. The electron temperature profile analyzed against different horizontal angles. The result indicates that the electron temperature from NeVIII intensity ratio in the ergodic layer does not show any large non-uniformity in the most part of LHD plasma. However, the electron temperature at the top plasma edge shows a higher temperature of 210-220 eV in all

toroidal locations, whereas the electron temperature in the vicinity of X-point shows lower temperature around 150-180 eV. Although further detailed analysis is necessary for understanding the difference in the electron temperature, the observed relatively flat temperature profile is in a good agreement with result from the three-dimensional simulation code, EMC3-EIRENE.

The CIV vertical profiles near X-point are studied at horizontally elongated plasma cross section with magnetic field structure in the ergodic layer. In low-density range less than $2x10^{13}$ cm^{-3}, the CIV profile near X-point is almost flat. When the density increases, two peaks newly begin to appear near X-points in addition to ordinary edge peaks, whereas such peaks do not appear in the profile of CVI located near LCFS. Those additional peaks become very clear at high-density range of $n_e \geq 8x10^{13}$ cm^{-3}. This phenomenon can be observed at several magnetic axis positions. The vertical profile of CIV is analyzed using three-dimensional edge transport code. In the low-density case, the C^{3+} ions move upstream and widely expand in the ergodic layer due to dominant thermal force, which leads to the flat CIV profile. With increasing the density, the friction force becomes dominant and the impurity ions start to move downstream. The C^{3+} ions stay in the vicinity of the X-point, where magnetic field lines are directly connected to divertor plates. Thus, the two peaks near X-point are clearly formed with increase in the C^{3+} density. The two-dimensional distributions of impurity line emissions are observed for different plasma axis positions. It is found that the impurity emission becomes strong along the poloidal trajectory of X-points and the poloidal trace is moved from inboard X-point trajectory to outboard X-point trajectory when the plasma axis is changed from 3.60 m to 3.75 m. When the magnetic axis position is shifted outwardly, the magnetic field line reaching the divertor plate expands from inboard side to outboard side. The change of the poloidal trajectory of X-points in the impurity emission strongly suggests that the impurity source is located at the divertor plate.

Acknowledgements

The doctoral thesis is completed through the study of plasma spectroscopy in the Large Helical Device (LHD) at National Institute for Fusion Science (NIFS), Toki, Japan.

First and foremost, I would like to express my deepest and most sincere thanks to my supervisor, Prof. Shigeru MORITA, for his patient guidance and tireless support during my whole PhD period. He has always encouraged me and continuously taught me the scientific and physical writing during the three years with patience to successfully finish the PhD thesis. He has provided me many opportunities to participate in the domestic and overseas meetings and conferences. I also gratefully appreciate him for his help in my daily life in Japan.

I am deeply grateful to Prof. Motoshi GOTO for his sincere help and technical support in the LHD experiment. During the three years, he has served me an excellent data acquisition system on several spectrometers to analyze the spectroscopic data for PhD thesis. I also appreciate him for his help in my daily life in Japan.

I express my most gratitude to Dr. Masahiro KOBAYASHI. He has operated three-dimensional edge simulation code for me to analyze the impurity behavior in the ergodic layer and provided me a lot of simulation data which were extremely helpful to complete the PhD thesis. Without his help, I could not finish my PhD thesis.

I would also like to extend my appreciation to Prof. Izumi MURAKAMI. She has supported me by calculating the atomic data to evaluate the electron temperature in the ergodic layer which is one of the most important parts in my PhD thesis. I am also gratefully thankful for her excellent lecture on the atomic physics.

Great thanks also go to Dr. Tetsutarou OISHI for his fruitful discussions on the experiment and sincere help in my daily life.

I would also like to express my great thanks to my life tutor, Dr. Jyotishankar MISHRA for his help in my daily life and improvement of my English conversation.

Special thanks are given to Dr. Akiyoshi MURAKAMI and Dr. Kunihiro OGAWA for their lots of help in my office life and daily life.

I would like to express my great thanks to the LHD experimental group for their technical supports, and the Graduate University for Advanced Studies (SOKENDAI) and NIFS for financial supports during the three years for my PhD study.

I sincerely thank to my friends in Japan, Dr. Chunfeng DONG, Dr. Tingfeng MING, Dr. Hao WANG, Mr. Xiaodi DU, Mr. Haishan ZHOU, Mr. Xianli HUANG and Ms. Haiying FU and to my friends in China who have already returned from Japan to China, Dr. Pengfei ZHENG, Dr. Yanfen LI, Dr. Xiaobing DING and Dr. Wei CHEN for their encouragements. It could leave my unforgettable memory in Japan.

I would also like to give my deeply thanks to Prof. Xiang GAO and Prof. Yinxian JIE in Institute of Plasma Physics, Chinese Academy of Sciences (ASIPP), Hefei, China, for their supports and encouragements in my master and PhD periods.

Finally, I would like to dedicate the present thesis to my parents, my brothers and brother's family for their warm-heated supports and continuous encouragements to finish my PhD thesis. Their love is the motivation in my study and my life.

Publications

(1) “Two-dimensional measurement of edge impurity emissions using space-resolved extreme ultraviolet spectrometer in Large Helical Device ”
E. H. Wang, S. Morita, M. Goto and C. F. Dong
Review of Scientific Instruments **83**, 043503 (2012).

(2) “Vertical profiles and radial locations of He II and C IV line emissions observed at different toroidal angles in LHD”
E. H. Wang, S. Morita, M. Goto, M. Kobayashi and C. F. Dong
Plasma and Fusion Research **7**, 2402059 (2012).

(3) “Radial profile measurement of electron temperature in edge stochastic magnetic field layer of LHD using intensity ratio of EUV line emissions”
E. H. Wang, S. Morita, M. Kobayashi, I. Murakami, M. Goto and C. F. Dong
Review of Scientific Instruments **83**, 10E509 (2012).

(4) “Observation of two-dimensional distribution of impurity line emissions using space-resolved EUV spectrometer in LHD”
E. H. Wang, S. Morita, M. Goto and C. F. Dong
Plasma Science and Technology **15**, 106 (2013).

(5) “Two-dimensional distribution of electron temperature in ergodic layer of LHD measured from line intensity ratio of CIV and NeVIII”
E. H Wang, S. Morita, C. F. Dong, M. Goto, I. Murakami and T. Oishi
To be published in Plasma and Fusion Research **8**, (2013)